Minimal Phagocyte

A bottom-up synthetic biology approach to studying phagocytosis

Van de Cauter, L.

DOI
10.4233/uuid:113f828d-faa4-4f99-8b76-74b7e6203134

Publication date
2024

Document Version
Final published version

Citation (APA)
Van de Cauter, L. (2024). *Minimal Phagocyte: A bottom-up synthetic biology approach to studying phagocytosis*. [Dissertation (TU Delft), Delft University of Technology]. https://doi.org/10.4233/uuid:113f828d-faa4-4f99-8b76-74b7e6203134

Important note
To cite this publication, please use the final published version (if applicable).
Please check the document version above.

MINIMAL PHAGOCYTE

A bottom-up synthetic biology approach to studying phagocytosis

MINIMAL PHAGOCYTE

A bottom-up synthetic biology approach to studying phagocytosis

Dissertation

for the purpose of obtaining the degree of doctor
at Delft University of Technology
by the authority of the Rector Magnificus,
prof. dr. ir. T.H.J.J. van der Hagen,
Chair of the Board for Doctorates,
to be defended publicly on Monday 8th of July 2024 at 15:00 o'clock

by

Lori VAN DE CAUTER

Master of Science in Biochemistry and Biotechnology, University of Leuven, Belgium
born in Leuven, Belgium

This dissertation has been approved by the promotors.

Composition of the doctoral committee:

Rector Magnificus,	chairperson
Prof. dr. G.H. Koenderink,	Delft University of Technology, promotor
Prof. dr. ir. S.J. Tans,	Delft University of Technology, promotor
Dr. K.A. Ganzinger,	AMOLF, external advisor
Independent members:	
Prof. dr. K.P. Adamala,	University of Minnesota, USA
Prof. dr. A.P. Liu,	University of Michigan, USA
Prof. dr. C. Dekker,	Delft University of Technology
Dr. D. Vorselen,	Wageningen University & Research
Dr. L. Laan,	Delft University of Technology
Prof. dr. ir. S.J.J. Brouns,	Delft University of Technology, reserve member

The work described in this dissertation was performed at the research institute AMOLF, located at Science Park 104, 1098 XG Amsterdam, The Netherlands. This work was financially supported by the Netherlands Organisation for Scientific Research (NWO).

Printed by: Gildeprint

ISBN 978-94-92323-74-3

An electronic version of this dissertation is available at http://repository.tudelft.nl/ and http://www.amolf.nl/. Printed copies can be obtained by request via e-mail to library@amolf.nl.

Summary

Within the intricate landscape of immunology, the captivating cellular process of engulfing external objects, known as phagocytosis, has sparked scientific interest for several decades. This essential process, how for example macrophages devour and engulf bacteria, not only fuels the imagination, but also represents our first line of defense against these pathogens. While phagocytosis is often recognized for its significance in the human immune system, its scope extends well beyond immunity. The process is for example also an essential feeding mechanism in unicellular organisms and plays a key role in maintaining tissue homeostasis by clearing apoptotic cells. Considering more than ten billion cells undergo apoptosis in a healthy human every day, it quickly becomes clear why phagocytosis is a fundamental biological process. The wide diversity in cells performing phagocytosis and the objects targeted for phagocytosis calls for a diversified set of mechanisms, signalling pathways, and receptors. Despite this diversity, all phagocytotic process converge on the common outcome of particle engulfment, hinting at an overlap in membrane reshaping processes. While our understanding of the process has reached unprecedented clarity, a wide knowledge gap persists. Especially the detailed roles of the cytoskeleton in phagocytosis remain an area of ambiguity. The inherent complexity and underlying redundancy of the process make studying the basic physical principles underlying cytoskeletal remodelling challenging to achieve in living cells. Therefore, aiming to understand the role of the cytoskeleton and the minimal requirements for initiating phagocytosis, this thesis presents a bottom-up synthetic biology approach to studying phagocytosis - the 'minimal phagocyte'.

As the 'container' for this synthetic, cell-like entity, we envision giant unilamellar vesicles (GUVs), given they provide a close mimic to biological cells and are therefore also often used as model membrane systems in biophysics. **Part II** of this thesis focuses on the fabrication of these GUVs. Given their widespread use, a plethora of different methods for their production exist, ranging from relatively straightforward bulk techniques to sophisticated microfluidic assembly lines. However, there is no one-size-fits-all method and reliable GUV fabrication still remains a major experimental hurdle in the field. A promising method that is increasingly being used for complex reconstitutions is continuous droplet interface crossing encapsulation (cDICE). In **Chapter 3**, we show that by tightly controlling environmental conditions and tuning the lipid-in-oil dispersion, it is possible to significantly improve the reproducibility of high-quality GUV formation

in cDICE as well as increase the encapsulation efficiency. Furthermore, we demonstrate efficient encapsulation for a range of biological systems, including actin, a key participant in phagocytosis.

Despite the method's wide applicability, the underlying physical principles governing the formation of GUVs in cDICE and related methods remain poorly understood. To gain a deeper understanding of GUV formation in cDICE, we developed a high-speed microscopy setup that allows us to visualize GUV formation in real time, detailed in **Chapter 4**. We show a complex droplet formation process at the capillary orifice, generating both larger droplets and, likely, GUV-sized satellite droplets. Further results, combined with theoretical modeling of the system's fluid dynamics, hint at a size-selective transfer of droplets through the oil-water interface, resulting in distinct final GUV sizes. Finally, we show that proteins in the inner solution affect GUV formation by increasing viscosity and altering lipid adsorption kinetics. These findings explain the widely observed variable yield and encapsulation efficiency when encapsulating more complex solute mixtures. While these findings lead to a better understanding of GUV formation processes in cDICE, the results are, by extension, applicable to emulsion-based methods in general. Ultimately, these insights will aid the development of more reliable and efficient methods for GUV production.

In **Chapter 5** we zoom out from cDICE and provide an extensive overview of the different GUV fabrication methods available in synthetic biology today. We discuss the state-of-the-art in various GUV production methods, considering their compatibility with specific membrane and encapsulation requirements, and address often-overlooked operational requirements such as reproducibility and ease of use. This chapter aims to be a refence work for researchers aiding them in making a well-informed decision regarding the most suitable method for their particular application.

While Part II focuses on the fabrication of GUVs, which make up the 'container' of our 'minimal phagocyte', **Part III** focuses on the remaining components needed to develop the proposed experimental platform for bottom-up study of phagocytosis. **Chapter 6** introduces a specialized toolbox containing all elements needed to strip this complex phagocytic process to its minimal set of components. In particular, our aim was to reconsitute spatially directed actin polymerization to promote membrane wrapping around a particle. We highlight the essential components necessary for such a system, including a membrane-spanning peptide, DBCO-labelled VCA, microfluidic GUV traps, and external beads. As a first step towards integrating these various building blocks into a single unit, we conducted a proof-of-principle assay, showing peptide clustering. Together, these results form a solid starting point for further integration of the aforementioned building blocks comprising the 'minimal phagocyte'. It serves as a framework for development of a valuable experimental platform offering legion opportunities to further elucidate the hitherto unknown roles of the cytoskeleton in phagocytosis. Ultimately, this approach will shed light on unresolved biophysical questions, providing fundamental insights into the mechanics of phagocytosis, and potentially even answer the question: What is minimally needed to initiate phagocytosis?

In the **Epilogue**, I reflect on the progress made in this thesis, both in expanding on existing GUV research and in introducing a novel, bottom-up synthetic biology approach to studying phagocytosis. Looking forward, the focus on reproducibility of GUV formation, particularly through the lens of cDICE, aims to make GUVs into a more robust tool for synthetic cell work. On the other hand, the presented results establish the groundwork for an experimental platform dedicated to studying phagocytosis, with the aim to further unravel the intricate complexities of this fascinating immunological process, thereby furthering our understanding of the world, one small step at a time.

Samenvatting

In de wereld van de immunologie staat fagocytose, het proces waarmee cellen externe objecten omsluiten, bekend als een uiterst fascinerend proces. Het heeft dan ook al decennialang de interesse gewekt van wetenschappelijk onderzoek. Het idee dat macrofagen bacteriën achtervolgen en ze vervolgens "opeten" spreekt niet alleen erg tot de verbeelding, maar is daarnaast ook essentieel in onze eerste verdedigingslinie tegen deze micro-organismen. Hoewel fagocytose dus een cruciale rol speelt in het menselijk immuunsysteem, vervult het ook een hele reeks andere functies. Zo stelt dit proces eencellige organismen in staat om voedsel op te nemen en fungeert het als een mechanisme voor het handhaven van cellulaire homeostase door apoptotische cellen op te ruimen. Gezien het feit dat meer dan tien miljoen cellen dagelijks apoptose ondergaan in ons lichaam, is het duidelijk dat fagocytose door de evolutie heen is uitgegroeid tot een fundamenteel biologisch proces.

De grote diversiteit aan cellen die fagocytose uitvoeren en aan objecten die het doelwit vormen vereist een verscheidenheid aan mechanismen, signaalwegen en receptoren om dit proces te regelen. Toch is de uitkomst van het proces altijd hetzelfde: volledige opname van het externe object door de cel. Dit suggereert dat reorganisatie van het celmembraan, noodzakelijk voor de cel om het object te omsluiten, ten grondslag ligt aan dit proces. Hoewel onze kennis vandaag de dag groter is dan ooit tevoren, blijft een gedetailleerd beeld, met name wat betreft de rol van het cytoskelet, uit. De intrinsieke complexiteit en onderliggende redundantie van fagocytose maken het uitdagend om het proces in levende cellen te bestuderen, wat op zijn beurt het begrijpen van de mechanismen en fysische principes die ten grondslag liggen aan de remodellering van het cytoskelet, bemoeilijkt.

Dit proefschrift heeft als doel een antwoord te bieden op deze tot nu toe onbeantwoorde fundamentele vragen over de rol van het cytoskelet in fagocytose en poogt daarnaast de minimale set componenten te identificeren die nodig zijn voor het initiëren van fagocytose. Hiervoor introduceren we de 'minimale fagocyt', een synthetisch-biologische, bottom-up benadering voor de studie van fagocytose.

Als de 'container' voor deze kunstmatige 'minimale fagocyt' zijn zogeheten *giant unilamellar vesicles* (GUVs), de synthetische tegenhanger van biologische cellen, een logische keuze. Deze GUVs zijn daarnaast intrinsiek compatibel met biologie, wat verklaart

waarom ze veelvuldig worden gebruikt als membraansysteem in de biofysica. In **Deel II** van deze thesis gaan we dieper in op hoe deze GUVs te produceren. Daar deze modelsystemen voor een scala aan toepassingen worden gebruikt, bestaan er verschillende methoden om ze te produceren, variërend van relatief eenvoudige bulktechnieken tot geavanceerde microfluïdische systemen. Tot op heden is er echter geen universele methode beschikbaar en blijft het reproduceerbaar produceren van GUVs een uitdaging. Een methode die de laatste jaren aan populariteit heeft gewonnen en als veelbelovend wordt beschouwd, is *continuous droplet interface crossing encapsulation* (cDICE). In **Hoofdstuk 3** tonen we aan dat door het zorgvuldig afstemmen van de omgevingscondities en het aanpassen van de samenstelling van de gebruikte lipide-in-olie dispersie, we kunnen zorgen voor reproduceerbare productie van kwalitatief hoogwaardige GUVs. Daarnaast laten we ook zien dat het mogelijk is hiermee de efficiëntie van het omsluiten van de inhoud aanzienlijk te verbeteren. Tot slot laten we zien dat de geoptimaliseerde methode goed werkt voor het produceren van GUVs met verschillende biologische systemen als inhoud, van een synthetische celcortex tot een artificieel eiwitsysteem.

Hoewel de methode dus breed toepasbaar is, begrijpen we de onderliggende fysische principes van GUV vorming in cDICE nog niet volledig, wat verdere optimalisatie belemmert. Om dit verder uit te zoeken, hebben we in **Hoofdstuk 4** een microscoop ontwikkeld die ons in staat stelt GUV productie in realtime te bestuderen. We tonen aan dat in de eerste stap van het proces, druppelvorming bij de capillaire opening, zowel grotere als kleinere druppels vormen worden gevormd via complexe processen. Theoretische modellering van de vloeistofdynamica van het systeem suggereert dat er vervolgens een selectie op grootte plaatsvindt bij het olie-water grensvlak, een noodzakelijke stap om GUV vorming te voltooien. Ten slotte laten we zien dat het omsluiten van complexe biologische systemen, zoals eiwitten, de vorming van GUVs beïnvloedt, hetgeen eerder geobserveerde variabele resultaten bij GUV productie met verschillende biologische systemen kan verklaren. Hoewel onze resultaten specifiek van toepassing zijn op GUV productie in cDICE, zijn ze ook relevant voor andere, vergelijkbare GUV-productie methoden. Deze resultaten zullen uiteindelijk dan ook bijdragen aan de ontwikkeling van betrouwbaardere en efficiëntere methoden voor GUV productie.

In **Hoofdstuk 5** verbreden we onze blik van cDICE en bieden we een uitgebreid overzicht van alle verschillende GUV fabricagemethoden die momenteel gebruikt worden in synthetische biologie. We bespreken de laatste resultaten van deze methoden, met specifieke aandacht voor hun compatibiliteit met specifieke membraan eigenschappen en hun toepasbaarheid voor het omsluiten van verschillende biologische systemen. Daarnaast richten we ons op vaak over het hoofd geziene operationele vereisten, zoals reproduceerbaarheid en gebruiksgemak. Dit hoofdstuk dient bijgevolg als naslagwerk voor onderzoekers en helpt hen een weloverwogen beslissing te nemen over welke methode het meest geschikt is voor hun specifieke toepassing.

Waar Deel II zich toespitste op het creëren van GUVs als de unit van de 'minimale fagocyt', richt **Deel III** zich op de overige onderdelen die nodig zijn voor het experimentele platform om fagocytose te bestuderen. In **Hoofdstuk 6** introduceer ik een

gespecialiseerde toolbox met alle benodigde elementen om het complexe fagocytaire proces na te bootsen met slechts die onderdelen die essentieel zijn. Dit minimale systeem beoogt actine-polymerisatie te lokaliseren op specifieke plekken op de GUV, wat de stimulatie van membraanwikkeling rond een extern deeltje mogelijk maakt. Hiervoor presenteren we onder andere een membraanoverspannend peptide, DBCO-gelabeld VCA, een microfluidisch systeem, en artificiële beads. Als een eerste stap naar verdere integratie van deze bouwstenen, laten we zien hoe dit peptide clustert. Samen vormen deze resultaten een solide basis voor om te komen tot de 'minimale fagocyt'. We zien dit dan ook in de toekomst uitgroeien tot een waardevol experimenteel platform, met talloze mogelijkheden om de rol van het cytoskelet in fagocytose te onderzoeken. Hierdoor zal deze nieuwe bottom-up benadering licht werpen op nog onopgeloste biofysische vraagstukken, fundamentele inzichten bieden in de mechanica van fagocytose, en misschien ooit een antwoord kunnen bieden op de vraag: Wat is nu echt de minimale set van componenten nodig voor fagocytose?

In de **Epiloog** reflecteer ik op de vooruitgang die geboekt werd in deze thesis, zowel wat betreft het verdiepen van het bestaande GUV onderzoek, als de introductie van een unieke bottom-up synthetische benadering voor de studie van fagocytose. Ik verwacht dat de focus in de toekomst voornamelijk zal liggen op verdere verbeteringen in de reproduceerbaarheid van GUV productie, met als ultiem doel het ontwikkelen van een robuust instrument voor synthetisch celwerk. Aan de andere kant leggen de gepresenteerde resultaten het fundament voor een experimenteel platform dat is gewijd aan het bestuderen van fagocytose, met als doel de ingewikkelde complexiteiten van dit fascinerende immunologische proces verder te ontrafelen en zo stap voor stap onze kennis van de wereld een beetje te vergroten.

Contents

Part I

Prologue

CHAPTER 1

The dynamic world of phagocytosis

1883, a private laboratory along the coast of Messina, Sicily:

> *"One day when the whole family had gone to a circus to see some extraordinary performing apes, I remained alone with my microscope, observing the life in the mobile cells of a transparent starfish larva, when a new thought suddenly flashed across my brain. It struck me that similar cells might serve in the defence of the organism against intruders. Feeling that there was in this something of surpassing interest, I felt so excited that I began striding up and down the room and even went to the seashore in order to collect my thoughts."*
>
> - Elie Metchnikoff [1]

The concept of phagocytosis emerged from this mere fleeting thought, struck upon Metchnikoff when he was mindlessly looking through his microscope. Immediately after, he tested his hypothesis by introducing rose thorns to transparent starfish larvae. When he then observed mobile cells surrounding the thorns, he first postulated the now widely known defensive function of cells, so akin to eating. Vividly describing these 'devouring cells', the term 'phagocyte' emerged, derived from the ancient Greek "$\phi\alpha\gamma\varepsilon\tilde{\iota}\nu$" (to eat) and "$\kappa\acute{\upsilon}\tau o\varsigma$" (cell). [1–3]

In 1908, the pioneering work of Metchnikoff was recognized when he and Paul Ehrlich were jointly awarded the Nobel Prize "in recognition of their work on immunity" [4], marking a paradigm shift in our understanding of how host cells defend against pathogens through innate and adaptive immunity [3]. This pivotal moment is often seen as the starting point for the field of immunology.

Anno 2024, our understanding of phagocytosis, including its roles, mechanisms, functions, and key players, has reached unprecedented clarity. A significant body of research continues to focus on this vital process, deemed crucial in the context of understanding and curing human disease. This chapter gives a brief overview of the principles of phagocytosis and its lingering unknowns, with a particular emphasis on the pivotal roles played by the actin cytoskeleton, and as such provides context to the following experimental chapters.

1.1 Understanding the basics

Phagocytosis is a cellular process characterized by the ingestion of particles larger than 0.5 µm, including bacteria, parasites, and fungi. As such, it is most recognized for playing a key role in our immune response to pathogens, effectively clearing microorganisms from the site of infection. So-called 'professional phagocytes', *i.e.* leukocytes including macrophages, neutrophils, and dendritic cells, are the primary cells involved in this process.[5–7] Phagocytosis is highly evolutionarily conserved and is for example also used as a feeding mechanisms in unicellular organisms, yet has evolved to play a crucial role in both the innate and adaptive immune responses. While phagocytosis is prominently recognized for its role in immune defence, it also serves another crucial function – the clearance of apoptotic cells. Knowing more than ten billion cells undergo apoptosis in a healthy human per day, the need for effective clearing of apoptotic corpses becomes evident.[6,8] This task is carried out by 'professional phagocytes' as well as by 'non-professional phagocytes' such as fibroblasts and epithelial cells.[9]

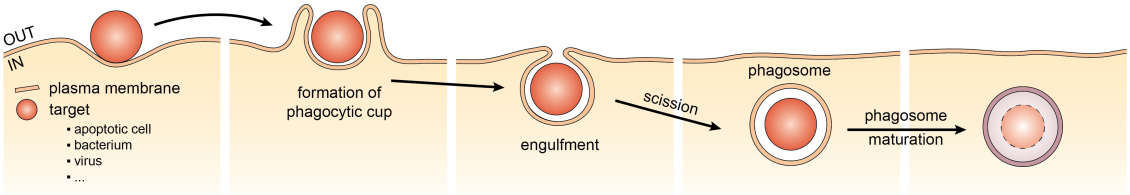

Figure 1.1 | Phagocytosis is a stepwise process in which particles larger than 0.5 µm are engulfed. Upon receptor-mediated recognition of an external target, a downstream signaling cascade is induced, driving cytoskeletal rearrangements. These, in turn, lead to the formation of a phagocytic cup surrounding the external object. The phagocytic cup then extends to fully wrap the external object, after which membrane fusion finalizes engulfment of the target. Following scission of the phagosome, the contents are degraded and processed in a process known as phagosome maturation. Figure adapted from Stuart *et al.*[10].

Generally, phagocytosis can be described as a stepwise process (Figure 1.1).[5,11,12] Characteristic to phagocytosis is the receptor-mediated recognition of the target, the initial step of the process.[13] In this, phagocytosis distinguishes itself from macropinocytosis, a related endocytic process by which cells engulf bulk extracellular fluid.[14] Upon clustering of the receptors, a myriad of signalling cascades will be activated and, in turn, drive cytoskeletal reorganisation. This will lead to the formation of a so-called phagocytic cup, membrane protrusions surrounding the external object.[15] Next, the cup will extend to fully wrap the external object. Finally, after membrane fusion, a membrane-bound

vacuole is formed, the phagosome. After scission from the plasma membrane, this phagosome still resembles the cellular membrane in membrane composition and the extracellular medium in its lumen.[5] During phagosome maturation, the final step of phagocytosis, the engulfed microorganisms or apoptotic bodies are stepwise degraded through fusion with endosomes and lysosomes.[16,17]

It is clear that a very diverse set of objects serve as the targets of phagocytosis. Phagocytes, therefore, not only need to discriminate 'self' from 'non-self', but also distinguish 'healthy' from 'non-healthy' to maintain cellular homeostasis.[5,12] Despite this heterogeneity and the diverse nature of phagocytosis, a set of underlying similarities can be identified. In all cases, to wrap the membrane around the particle and eventually engulf it, spatiotemporally coordinated signalling triggering cytoskeletal reorganisation and membrane rearrangements are required.

1.2 The dynamic actin cytoskeleton

In phagocytes, as in most animal cells, a thin layer of actin cortex underlies the plasma membrane, providing the cell with mechanical strength and mobility. This cellular cortex is made up of a dense network of actin filaments, many regulatory proteins, and myosins.[18,19] Via its close association with the membrane, the dynamics of the actin cytoskeleton are a main driver of phagocytosis.

Actin filaments (filamentous actin, or F-actin) are composed of monomeric actin (globular actin, or G-actin) that assembles into dynamic polymers through a treadmilling mechanism (Figure 1.2a).[20,21] New monomers are added in an ATP-dependent fashion to the barbed end of the filaments, while depolymerization happens at the pointed end.[20,21] *In vivo*, countless actin-binding proteins make this into a highly dynamic network characterized by high turnover rates.[22,23] Nucleators, such as the Arp2/3 complex (Figure 1.2b) and the formin mDia1 (Figure 1.2c), play crucial roles in promoting F-actin.[24]

The Arp 2/3 complex, a seven-protein complex, is able to bind the side of an existing actin filament to nucleate a new filament, thereby forming branched filaments (Figure 1.2b).[25,26] It is activated by nucleation promoting factors (NPFs), including Wiskott-Aldrich syndrome family proteins such as WASP and N-WASP.[27,28] Activation is mediated through their VCA (verprolin, central, acidic) domain which stabilizes at the branching site.[29] NPFs are bound to and regulated by the plasma membrane and activated through downstream signaling processes.[30]

Formins, like mDia1, nucleate actin filaments at the barbed end, promoting polymerization from that end (Figure 1.2c).[24,31] Activation occurs through membrane-associated factors such as the Rho family of GTPases. By carefully balancing Arp2/3 and mDia1, it is possible for the cell to tune the resulting structure of F-actin assemblies, leading either to a more branched network (via Arp2/3) or rather to a linear array of filaments (via mDia1).[32]

A myriad of other actin-binding proteins further regulate the actin cytoskeleton.[33] Examples include severing proteins, such as gelsolin and cofilin, which break down

filaments and effectively free up actin monomers[34]; profilin, which enhances the overall polymerization rate[35]; or coronins, serving various functions[36]. Finally, molecular motor proteins like myosin also play a key role as they provide contractility.[37,38] Myosin II, for example, can move across actin filaments and slide two filaments across each other in opposite directions, thereby generating force.[39] A resting cell, rather than a static entity, thus contains a dynamic actin cytoskeleton that is constantly rearranged by a large set of proteins.

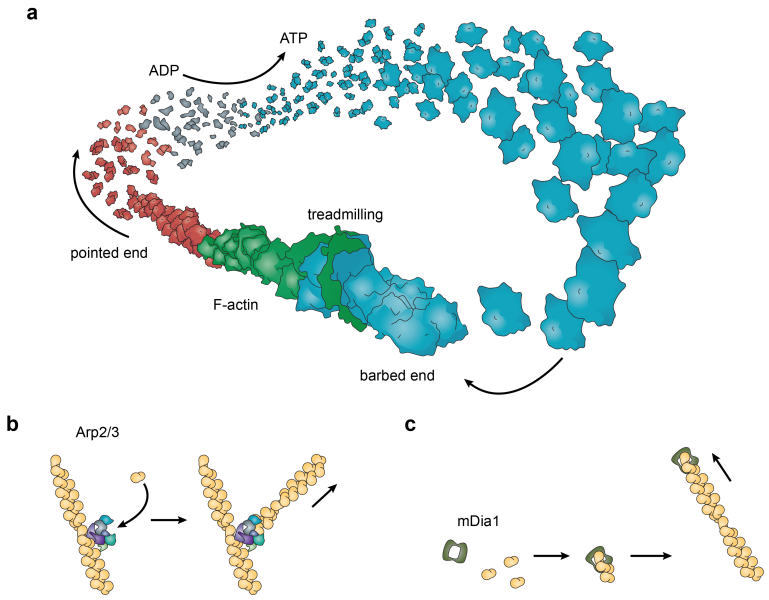

Figure 1.2 | Actin filaments and nucleators. (a) The actin cortex consists of actin filaments that are assembled via a treadmilling mechanism. The filaments grow from the barbed end, where monomeric actin is added in an ATP-dependent manner, while depolymerization occurs at the pointed end. (b) The Arp2/3 complex nucleates branched filaments by binding to the side of an existing actin filament. (c) The formin mDia1 nucleates actin filaments at the barbed end, promoting polymerization from that end. Figure adapted from Pak *et al.*[40].

1.3 Surveilling the cellular environment

The dynamic nature of the actin cytoskeleton of phagocytes proves beneficial when probing the cellular environment for potential targets. Active immune surveillance is needed, as relying solely on encounters through Brownian diffusion is inefficient. Phagocytes effectively scout the cellular environment using membrane ruffles - membrane protrusions of several microns in size.[41,42] These membrane ruffles are driven by local cytoskeletal rearrangements driven by Arp2/3, leading to the formation of branched structures.[41] Membrane ruffles increase the likelihood of encountering potential targets and often serve as the initial point of contact between the phagocyte and its target. Exposure to soluble cytokines or other agonists induce priming of the cell, triggering

membrane ruffling and cytoskeletal changes.[6,43] However, these membrane ruffles are not only important for immune surveillance, but also serve a crucial role in receptor diffusion.[44]

1.4 Receptor-mediated recognition

As mentioned before, phagocytosis is characterized by receptor-mediated recognition. Given the wide variety of objects targeted for phagocytosis, it is unsurprising that a wide variety of receptors is involved.[12] External objects can be detected directly, through surface markers like pathogen-associated molecular patterns (PAMPs), which are found on microorganisms like bacteria and fungi.[6] Toll-like receptors (TLRs) and G protein-coupled receptors (GPCRs) play a role here, although they alone are not sufficient to trigger phagocytosis. C-type lectin receptors, capable of binding carbohydrates, are another group of receptors involved in phagocytosis; an important example is dectin-1, which binds fungal polysaccharides.[45]

In addition to direct detection, external objects can also be indirectly detected through a process called opsonisation. This involves the deposition of immunoglobins, opsonins, on the surface of the targets to be engulfed.[6] Fc receptors (FcR), recognizing the Fc region of immunoglobins, are an important family of opsonin receptors. The Fcγ receptor, which bind to Fc portion of immunoglobulin G, is the best understood model of phagocytic receptors and is the most widely studied receptor in context of phagocytosis.[46]

Another family of receptors are integrins, which can bind directly to ligands as well as to opsonised targets. Integrins are activated by an 'inside-out' mechanism via different pathways involving FcγR, TLRs, and GPCRs. Following activation, their ligand affinity increases due to conformational changes, thereby priming phagocytes.[12,47] Integrins are also thought to serve as mechanosensors.[48] As the deformability of the variety of objects encountered by phagocytes spans a wide range (several kPa for apoptotic bodies to hundreds of MPa for bacteria)[49–52], they could play an additional role in discriminating between 'self' and 'non-self'.[8]

Apart from dectin-1 and FcγR, none of the phagocytic receptors are fully known to be sufficient to trigger phagocytosis on their own. However, many other phagocytic receptors have not been formally tested to determine their sufficiency. Often, multiple receptors are concurrently activated, leading to a complex downstream signaling pathway that is synergistic in nature. Adding to this complexity, microorganisms have developed multiple mechanisms to inhibit receptor binding and escape phagocytosis.[5]

For apoptotic bodies, different recognition mechanisms come into play.[53] A combination of 'find me' and 'eat me' signals governs phagocytosis in this context.[54] Apoptotic cells secrete soluble 'find me' signals, chemoattractants released to recruit phagocytes.[55] Additionally, they display 'eat me' signals, distinguishing them from their healthy counterparts, which exhibit 'don't eat me' signals.[5] The most widely recognized marker for apoptosis is the occurrence of the lipid phosphatidylserine (PS) on the outer leaflet of the plasma membrane, whereas in healthy cells, it is mainly localised to the inner leaflet of plasma membrane.[56]

To provide tight control over the immune response and trigger phagocytosis only when a target is actually encountered, phagocytes make use of receptor clustering.[12] Given the abundance of soluble immunoglobins in the cellular environment, clustering provides a means of discriminating between bound and unbound opsonins.[6] However, this process of receptor clustering known to be a highly complex and intricate phenomenon *in vivo*.

1.5 Receptor clustering

In vivo, the mobility of receptors is constrained by several factors, hampering clustering. In particular, the actin meshwork beneath the plasma membrane acts as a 'fence', while transmembrane proteins tethered to the actin cytoskeleton serve as diffusion barriers, or 'pickets'.[41,44,57,58] This 'picket fence' mechanism significantly reduces the lateral diffusion rate of receptors. While beneficial in countering premature activation, it potentially hinders sufficiently fast clustering upon target encounter. To facilitate this clustering, diffusion must not be a rate-limiting step.

When probing the cellular environment using membrane ruffles, only a brief contact between cell and target needs to be sufficient to drive phagocytosis. Given the importance of receptor clustering, many factors play a role here: geometry, size, and distribution of ligands on phagocytic targets, and surface density of receptors, lateral mobility of receptors, affinity, and avidity of receptors in phagocytes. Their respective roles have not yet been fully elucidated.[41,44,57,58]

Once the cell has been activated, F-actin is disrupted in areas where ruffling is occurring, increasing the local diffusion of receptors. This is crucial as it elevates the number of receptor encounters, effectively enhancing the chances of receptor clustering upon target encounter.[41,57]

1.6 Signaling pathways and pseudopod formation

Following dynamic probing of the environment by membrane ruffles (Figure 1.3a), an initial receptor-mediated contact with a target disrupts the actin cytoskeleton, enhancing lateral mobility of receptors and leading to receptor clustering (Figure 1.3b). This, in turn, will activate a downstream signaling cascade leading to spatiotemporally coordinated actin remodeling, forming pseudopods that drive particle engulfment (Figure 1.3b).[41]

Clustering of receptors activates a complex downstream signaling cascade with many different biological players. We here only outline the most important ones that directly impact cytoskeletal remodeling. Activation of Src-family kinases (SFK) results in activation of Cdc42, Rac1, and Rac2, which in turn activate NFPs such as WASP, N-WASP and WAVE. As mentioned before, these promote the Arp2/3 complex and drive branching of the actin cytoskeleton, supporting pseudopod formation. RhoGTPases are often involved too, leading to the activation of formins. Arp2/3-mediated pseudopod formation is sustained at the leading edge of the phagocytic cup, where mDia elongates the filaments. At the base of the phagocytic cup, severing proteins are actively deconstructing the actin network, stopping polymerization and freeing up actin monomers.[8,41,42,59]

Through complex spatiotemporal patterns, involving integrin adhesions sustaining receptor engagement and active force generation through the actin cytoskeleton, pseudopod formation is effectively driven forward (Figure 1.3c). Altogether, this is thought to be a mechanosensitive process, the complex details of which remain to be elucidated.[59]

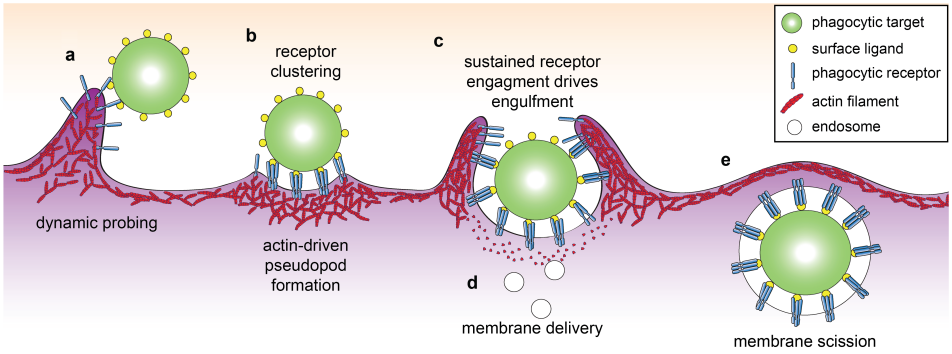

Figure 1.3 | The actin cytoskeleton in phagocytosis. (a) Dynamic probing of the cellular environment via Arp2/3-mediated membrane ruffles. Recognition of targets leads to local disruption of cortical F-actin, increasing the lateral mobility of receptors. (b) Following receptor clustering, downstream signaling pathways drive Arp2/3- and mDia-mediated pseudopods leading to engulfment of the target. (c) Progressive receptor interaction along the surface of the target and dynamic actin cytoskeletal rearrangements drive full engulfment of the target. (d) At the base of the phagocytic cup, actin is disassembled in order for endomembrane delivery to sustain the growth of the cup. (e) Membrane scission, supported by active forces from the actin cytoskeleton, completes phagosome formation. Figure adapted from Jaumouillé *et al.*[6].

Lipids, particularly phosphatidylinositol-4,5-bisphosphate (PIP2), also play a critical role in the signaling cascade. Through phosphorylation by phosphatidylinositol 3-kinase (PI3K), PIP2 is converted to phosphatidylinositol (3,4,5)-trisphosphate (PIP3). These lipids and their dynamic changes are thought to contribute to actin remodeling via regulatory proteins, thus serving as another key player in phagocytic cup formation.[6,41,58] FERM domain proteins, such as ezrin, radixin and moesin, interact with PIP2 for example, giving the cell spatial control of contractility and control over strength of anchoring to the cytoskeleton.[57] PIP2 furthermore enhances the activity of regulatory proteins (e.g. WASP), while PIP3 recruits myosin X.[60] Additionally, PIP2 interacts with profilin, increasing the overall actin polymerization rate. Complex dynamics underlie lipid diffusion, such as the observed disappearance of PIP2 at the base of the cup, supporting actin disassembly. Interestingly, it has been shown that these dynamic changes in lipid compositions are solely restricted to the phagocytic cup, possibly due to the existence of a diffusion barrier, forming an isolated part of the membrane and triggering local signaling.[61]

Evidently, engulfing larger particles requires a substantial amount of extra membrane area. Initially, this membrane is derived from the cellular plasma membrane, but this is later replenished with additional membrane from intracellular organelles, such as endosomes, lysosomes, or others (Figure 1.3d).[62] These membranes are added at the

base of the phagocytic cup via SNARE-mediated processes.[5] For this to occur, the actin cytoskeleton is actively disassembled at the base of the phagocytic cup.[41]

When the target is eventually completely surrounded, the membranes fuse to achieve complete engulfment of the particle. It is known that dynamin and myosin II, as well as forces from the actin cytoskeleton, are involved in this process.[59] After scission of the membrane-bound vacuole (Figure 1.3e), the phagosome matures, and phagocytosis is completed.[5,11,12]

1.7 The unknowns of phagocytosis

Insights into the mechanisms underlying phagocytosis have primarily emerged from cellular studies. Despite significant advancements, a comprehensive understanding remains elusive. It is evident that remodeling of the actin cytoskeleton is the main driver of the process, as it not only plays a crucial role in the formation of the pseudopods that shape the membrane invaginations engulfing the target, but also dictates receptor mobility, a key factor for receptor clustering - a key step in phagocytosis. However, the details of the spatiotemporal coordination of cytoskeletal remodeling and the individual roles of cytoskeletal proteins, remain areas of ambiguity. Furthermore, the roles of myosins[63] and microtubules[64], a second major component of the cytoskeleton alongside actin[65], are not well defined.

Studies on model cell lines initially provided a valuable approach for studying isolated receptors within the cellular context.[5] More recently, these studies have been complemented by mechanical studies on phagocytes within engineered microenvironments, offering a means of elucidating further physical details.[59] Despite this substantial progress in our understanding, a large knowledge gap persists, attributed to the intricate complexity, large heterogeneity, and vast redundancy inherent in phagocytosis. Exploring alternative approaches may provide a fresh perspective, potentially bridging existing gaps and advancing our comprehension of this intriguing cellular process.

1.8 A bottom-up approach to studying phagocytosis

While cellular research might help to grasp larger concepts, biology often proves to be too convoluted to elucidate intricate details. With over 20,000 human genes and up to four million proteins per cubic micron in living cells, the biological context is so vastly complex that our understanding remains limited. Bottom-up synthetic biology aims to address this complexity by taking a reductionist approach and building things up from the ground, adding complexity along the way.[66]

A prime example of bottom-up synthetic biology is the recent efforts to design and build an artificial cell. Using Richard Feynman's famous words, "What I cannot create, I do not understand", as a design principle, the Dutch research consortium BaSyC ('Building a Synthetic Cell') was established in 2015 to join nationwide efforts in building a synthetic cell (Figure 1.4).[67] Imagining a synthetic cell as a lifelike entity capable of autonomous growth, information transfer, and division, it is clear a long road lies ahead. However, by breaking the artificial cell down to its individual building blocks, studying them in

isolation, and rebuilding cellular functions from the bottom up, this approach allows for a detailed understanding of the intricate details underpinning cellular life. In doing so, it provides mechanistic insights into the most basic unit of life - the cell.

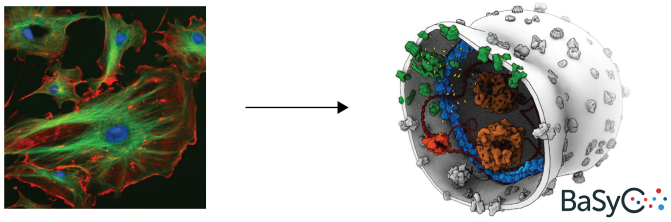

Figure 1.4 | BaSyC – Building a synthetic cell. The aim of the BaSyC consortium is to build an artificial cell from the bottom up, containing the different molecular building blocks of cellular life. Left: a microscopy image of endothelial cells with a fluorescently labeled nucleus (blue), tubulin (green), and F-actin (red). Right: artist's impression of a synthetic cell by Graham Johnson depicting the cell division machinery (blue), DNA processing components (orange/red), and cell fueling parts (green).

Reflecting on phagocytosis, one cannot help but consider a similar approach. Imagine peeling away layers of complexity, revealing only those elements essential for initiating cytoskeletal rearrangements and driving membrane remodeling for target engulfment. Such a strategic simplification could not only reduce complexity, remove cellular crosstalk and redundancy, but simultaneously also enhance our control over the process (Figure 1.5a). Consequently, such an approach enables a focused study of the fundamental mechanics underlying phagocytosis, a process inherently too complex *in vivo*.

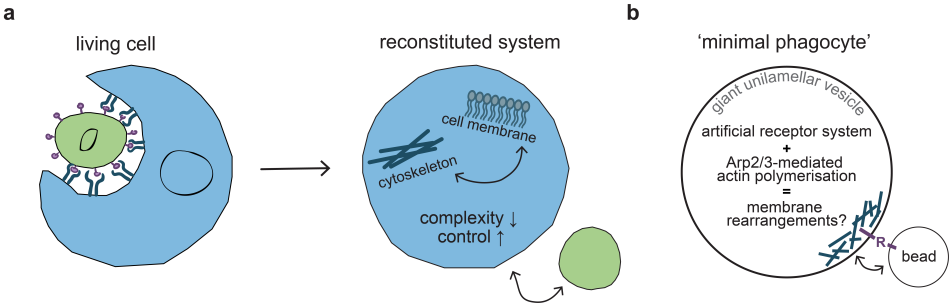

Figure 1.5 | Studying phagocytosis in a bottom-up synthetic biology way. (a) Reconstituting phagocytosis in a minimal way allows us to reduce the complexity of the process while enhancing our control. This, in turn, facilitates the study of elementary details of the interactions between the cellular membrane and cytoskeleton, as well as the interactions between the cell and the external target of phagocytosis. (b) Conceptual representation of a 'minimal phagocyte': a synthetic, cell-like entity designed for reconstituting phagocytosis. This artificial system includes an artificial receptor system mimicking phagocytic receptors, and a minimal actin cytoskeleton, replacing the cellular cortex. Such 'minimal phagocyte' provides a platform for investigating fundamental questions regarding the essential components and mechanisms underlying phagocytic processes.

We can conceptualize a 'minimal phagocyte' (Figure 1.5b): a synthetic, cell-like entity, containing an artificial receptor system that mimics phagocytic receptors and a minimal actin cytoskeleton, replacing the complex cellular cortex. Such a system would facilitate addressing fundamental questions, such as whether Arp2/3-mediated actin polymerization is sufficient or merely necessary alongside formin-mediated actin polymerization and opens the door to addressing the most fundamental question: *What is the minimal set of components needed to initiate phagocytosis?*

CHAPTER 2

Outline of this thesis

In this **Prologue**, I introduced the process of phagocytosis, explained its profound biological relevance, and gave a brief overview of the molecular mechanisms underlying it. Despite the vast body of research dedicated to phagocytosis over the years, numerous questions still remain today. The basic biophysical principles and underlying mechanisms regarding cytoskeletal reorganization and membrane rearrangements, underpinning all forms of phagocytosis, remain to be fully elucidated. I argued that an *in vitro*, bottom-up synthetic biology approach could offer valuable insights. By removing phagocytosis from its cellular context, complexity is reduced while experimental control in increased. This provides a platform to answer basic questions, such as identifying the minimal set of components needed for phagocytosis or pinpointing the roles of cytoskeletal components in the process. Such a reductionist approach could go hand in hand with existing cellular research, leading to a synergistic understanding in the future. Throughout the remainder of this thesis, I will gradually outline the steps toward such bottom-up synthetic biology approach to studying phagocytosis.

Part II focuses on the bottom-up fabrication of giant unilamellar vesicles (GUVs), which serve as our model membrane system of choice. **Chapter 3** details an optimized method for GUV fabrication called continuous droplet interface crossing encapsulation, or cDICE. By tightly controlling environmental conditions and tuning the lipid-in-oil dispersion, we show that it is possible to significantly improve the reproducibility of high-quality GUV formation and encapsulation efficiency. Additionally, we demonstrate efficient encapsulation of various biological systems, showcasing the method's wide applicability. Moving to **Chapter 4**, we delve deeper into cDICE to gain a better mechanistic understanding of GUV formation. Visualizing GUV formation in real-time using a custom-built high-speed microscope, we show a complex droplet formation process at the capillary

orifice, generating both larger droplets and, likely, GUV-sized satellite droplets. Further results, combined with theoretical modeling of the system's fluid dynamics, hint at a size-selective transfer of droplets through the oil-water interface resulting in distinct final GUV sizes. Finally, we show that proteins in the inner solution affect GUV formation by increasing viscosity and altering lipid adsorption kinetics. These finding not only lead to a better understanding of GUV formation processes in cDICE but, by extension, in emulsion-based methods in general. Ultimately, this will aid the development of more reliable and efficient methods for GUV production. Concluding Part II in **Chapter 5**, we provide an extensive overview of different GUV production methods in synthetic biology today. While well-studied swelling-based methods offer a broad range of lipid compositions, they come at the expense of limited encapsulation efficiency. Emulsion-based methods on the other hand, excel at encapsulation but are only effective with a limited set of membrane compositions and may entrap residual additives in the lipid bilayer. We discuss the state-of-the-art in various GUV production methods, considering their compatibility with specific membrane and encapsulation requirements, and address often-overlooked operational requirements such as reproducibility and ease of use. This comprehensive overview enables researchers to make an informed choise of the method most suited for their particular application.

In **Part III**, I lay the groundwork for an experimental platform for a bottom-up synthetic biology approach to study phagocytosis, termed the 'minimal phagocyte'. **Chapter 6** introduces a specialized toolbox containing all elements needed to strip this complex phagocytic process to its minimal set of components. Having explored and optimized GUV formation in Part II, we here systematically explore the other components needed. We successfully incorporate two membrane-spanning peptides into the GUV membrane, designed to enable the localization of actin polymerization. To induce this localized actin polymerization, we explore the binding of streptavidin-coated beads and DBCO-labelled VCA to this membrane-spanning peptide from the outside and the luminal side, respectively. Furthermore, we replicate a microfluidic GUV trapping protocol, enabling time-resolved and parallel studies of single GUVs. Finally, we present an initial experiment toward the integration of different components, marking a crucial step toward spatially triggering actin polymerization and highlighting the future potential of our approach.

In the **Epilogue**, I bring this thesis to a close by, on the one hand, reviewing the progress made, while on the other hand, focusing on uncovering potential avenues for future research and contextualizing the results in a broader sense.

Part II

Bottom-up fabrication of giant unilamellar vesicles

CHAPTER 3

Optimized cDICE for efficient reconstitution of biological systems in giant unilamellar vesicles

▸ Giant unilamellar vesicles (GUVs) are often used to mimic biological membranes in reconstitution experiments. They are also widely used in research on synthetic cells, as they provide a mechanically responsive reaction compartment that allows for controlled exchange of reactants with the environment. However, while many methods exist to encapsulate functional biomolecules in GUVs, there is no one-size-fits-all solution and reliable GUV fabrication still remains a major experimental hurdle in the field. Here, we show that defect-free GUVs containing complex biochemical systems can be generated by optimizing a double-emulsion method for GUV formation called continuous droplet interface crossing encapsulation (cDICE). By tightly controlling environmental conditions and tuning the lipid-in-oil dispersion, we show that it is possible to significantly improve the reproducibility of high-quality GUV formation as well as the encapsulation efficiency. We demonstrate efficient encapsulation for a range of biological systems including a minimal actin cytoskeleton, membrane-anchored DNA nanostructures, and a functional PURE (protein synthesis using recombinant elements) system. Our optimized cDICE method displays promising potential to become a standard method in biophysics and bottom-up synthetic biology.

Published as: L. Van de Cauter, F. Fanalista, L. van Buren, N. De Franceschi, E. Godino, S. Bouw, C. Danelon, C. Dekker, G. H. Koenderink, and K. A. Ganzinger, "Optimized cDICE for Efficient Reconstitution of Biological Systems in Giant Unilamellar Vesicles", *ACS Synthetic Biology*, vol. 10, no. 7, pp. 1690–1702, 2021.

3.1 Introduction

Cellular life is enabled by countless interacting molecules and biochemical reactions with a high degree of interconnectivity and redundancy. Reconstituting cell biological processes using only their minimal functional units from the bottom-up is therefore very helpful to study cellular mechanisms on a molecular and mechanistic level.[66,68,69] The field of bottom-up synthetic biology has gained a lot of traction over the past decade, an evolution synchronized with the emergence of several different consortia worldwide to lead the journey toward functional reconstitution of all basic cellular functions, culminating in the creation of a minimal synthetic cell.[67,70–72]

In this synthetic cell community, giant unilamellar vesicles (GUVs) are widely used as cell-sized, lipid bilayer-enclosed reaction compartments that can be visualized by real-time microscopy and directly manipulated using biophysical tools.[73–76] Using GUVs as a basis for a functional synthetic cell requires encapsulation of different biological modules in a precise stoichiometry, consisting of a variety of biomolecules ranging in size and charge. However, state-of-the-art GUV fabrication methods are still far from ideal in establishing complex reconstituted systems. On the one hand, easy-to-implement and high-yield methods, such as natural swelling,[77] electroformation,[78–81] and gel-assisted swelling,[82–85] offer poor control over encapsulation efficiency and stoichiometry, and inconveniently contain the same solution on the in- and outside. On the other hand, emulsion-based techniques, in which GUVs are generated from water-in-oil droplets crossing an oil-water interface (using gravity, centrifugation, microfluidic devices, or microfluidic jetting[86–92]), offer more control over GUV content and size monodispersity, but at the cost of being less reliable and more technologically advanced, and therefore less accessible.

A promising method that is increasingly being used for complex reconstitutions is continuous droplet interface crossing encapsulation (cDICE). This double-emulsion based technique relies on the continuous transfer of capillary-generated water-in-oil droplets across an oil–water interface using centrifugal force.[93] Requiring only easy-to-operate laboratory instrumentation, cDICE can in principle provide high yields while being less technologically demanding than microfluidic-based approaches and allowing for more control over size and encapsulated content than swelling methods.[93,94] However, despite promising first outcomes, using cDICE for protein encapsulation has remained difficult, beyond a few specific cases.[95–98] At least in part, this is likely due to our lack in understanding of the physical process of vesicle formation and of which parameters are essential to control tightly for the method to work robustly. Significant lab-to-lab variability and constant adaptations to the protocol devised by various laboratories[93–95,98] have also made it hard to reproduce results across different institutions, leading to the technique being far from accessible.

Here, we aimed to gain a better understanding of the parameters influencing both vesicle formation and encapsulation efficiency in cDICE, allowing us to design an accessible, robust, and reproducible workflow for different encapsulation needs. We show that control of environmental conditions is crucial for reliable formation of defect-free GUVs

(*i.e.*, the vesicular membrane is uniform at optical length-scales and does not contain visible lipid pockets) at high yields. Furthermore, we demonstrate different approaches for enhancing the encapsulation efficiency of cDICE by changing the composition of the lipid-in-oil dispersion. We thus provide future users with a detailed protocol for GUV fabrication and a toolbox that can form a firm basis for further experiment-specific optimization. By reproducing key experiments across multiple laboratories in different locations and encapsulating a large variety of biological systems, from the encapsulation of purified proteins to the PURE *in vitro* transcription-translation system, membrane-anchored DNA origami, and bacteria, we show robustness and versatility of the method. Overall, we demonstrate that our improved cDICE protocol shows great promise for a wide range of complex reconstitution processes in the future, overcoming a major hurdle on the route toward functional synthetic cells.

3.2 Results

3.2.1 Environmental control is essential for producing defect-free GUVs with cDICE

To improve the robustness of the cDICE method, we sought to systematically screen various experimental parameters that might influence GUV formation in cDICE. A typical cDICE setup (Figure 3.1a) consists of a rotating chamber containing two concentric fluid layers: an inner, lower-density lipid-containing oil phase and an outer, aqueous layer. The aqueous solution to be encapsulated is injected into the lipid-in-oil layer through a capillary, leading to the formation of water-in-oil droplets at the capillary orifice. As these droplets travel outward and traverse the interface of the oil with the outer aqueous phase, a bilayer is formed, yielding GUVs, collected in the outer layer of the system (Figure 3.1a). GUV formation is thus dependent on the properties of all phases and on other experimental parameters, such as rotation speed and capillary size.[93] When we sought to enhance the consistency of vesicle production in this inherently sensitive experimental system, the first striking improvement was made by using a chloroform-based lipid-in-oil dispersion[98] as oil phase and preparing it in a humidity-free environment, *i.e.*, inside a glovebox. Without the use of a glovebox, GUVs were generated but the sample contained a lot of residual membrane material, such as free tubes and fluorescent aggregates, and the vast majority of GUVs showed visible fluorescent pockets or budding membrane structures (Figure 3.1b). In contrast, when the lipid-in-oil dispersion was prepared in a glovebox, samples were much cleaner with most GUVs having quasi-spherical shapes without visible lipid pockets or budding membrane structures (Figure 3.1c).

In line with this observation, preparation of the lipid-in-oil dispersion inside a glovebox also affected its macroscopic appearance: oil dispersions prepared in a humidity-free environment were transparent, while preparations outside a glovebox yielded visibly opaque dispersions, as quantified by turbidity measurements (A_{350} = 0.10 ± 0.05 *vs* 0.42 ± 0.10, Figure 3.5). Furthermore, we analyzed the lipid adsorption kinetics of the different oil dispersions using pendant drop measurements,[99] where a drop of aqueous solution is suspended in a lipid-in-oil mixture, mimicking the process happening at the orifice of the cDICE capillary. Without humidity control, interfacial tension decreased much faster (Figure 3.6), indicating faster adsorption of lipids to the oil–water interface.

In combination with the adverse effect on vesicle quality, our experiments suggest that presence of water in the lipid-in-oil dispersion interferes with vesicle formation and bilayer quality via changing the microscopic organization of the lipids and their adsorptive behavior.

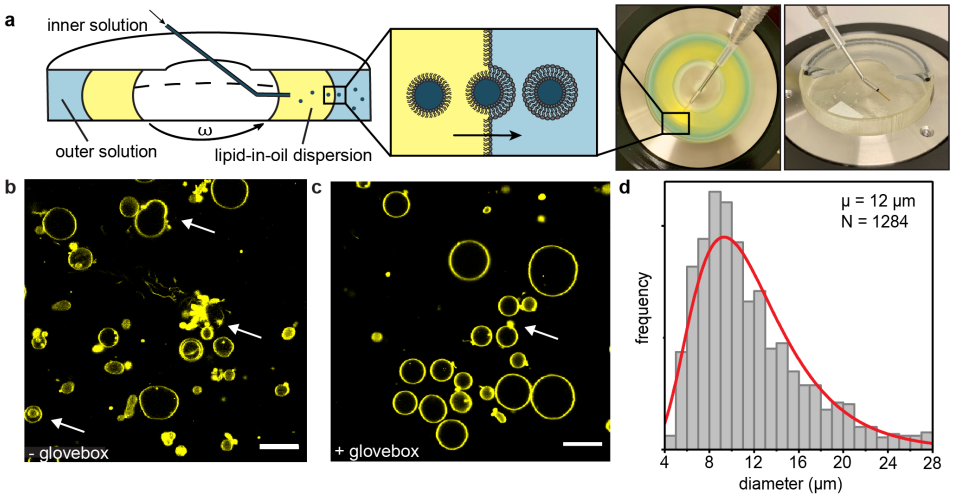

Figure 3.1 | General overview of the cDICE technique and influence of environmental conditions. (a) Cross-sectional schematic of the cDICE method. The center image displays the 3D printed rotation chamber, with the different fluid layers colored differently for illustration purposes. The rightmost image displays the custom-built spinning device that accommodates the 3D printed rotation chamber. The capillary is inserted using an adjustable magnetic base to allow spatial flexibility upon insertion. During experiments, this setup is connected to a syringe and syringe pump. (b) Representative field of view of GUVs formed using a chloroform-based lipid-in-oil dispersion prepared outside of the glovebox. ATTO 655 DOPE was used as a membrane stain and images were taken using confocal microscopy. Most GUVs contain artifacts in the lipid membrane, and examples are indicated with arrows. Scale bar indicates 20 μm. (c) Representative field of view of GUVs formed using the final protocol including the use of a glovebox. ATTO 655 DOPE was used as a membrane stain and images were taken using confocal microscopy. Most GUVs are spherical and possess a clean membrane, and only a small population of GUVs still shows artifacts, as indicated with an arrow. Scale bar indicates 20 μm. (d) Size distribution of GUVs made of DOPC lipids, obtained by the optimized protocol. The distribution is fitted to a log-normal function (red curve).

It is well-known that humidity values change throughout the year, reaching highest values in summer. This seasonal dependency in daily relative humidity can be as large as several tens in percentage,[100] equivalent to the range of 40-75% that we observed in the lab. Given the importance of humidity in preparation of the lipid-in-oil dispersion, we extended environmental control to regulating humidity in the room where the cDICE experiments were performed by using a dehumidifier. Indeed, dehumidification down to 30-40% resulted in smaller variability between lipid adsorption kinetics as measured in pendant drop experiments (Figure 3.5), indicating a more reproducible adsorption behavior. In line with the lower variability found in lipid adsorption rates, dehumidifi-

cation also proved to be essential for reliable production of clean vesicles throughout the year. Taken together, using a glovebox for preparation of the lipid-in-oil dispersion and storage of its components, and performing cDICE experiments in a continuously dehumidified room, resulted in a robust formation of clean GUVs.

In the original cDICE paper,[93] as well as in other follow-up studies,[94,95,101,102] injection capillaries were pulled from glass tubes to final orifice diameters of a maximum of 20 µm. Since we found these narrow glass capillaries to be a significant source of experimental variation and problems due to easy clogging of the orifice, we instead used commercially available fused silica capillary tubing with larger diameters (25, 50, and 100 µm) to allow for more consistent results, as previously used by Litschel *et al.*[98] We found that using all three capillary sizes, our chloroform-based lipid-in-oil dispersion and optimized workflow led to high yields of GUVs with a mean diameter of 12 µm and coefficient of variation of 47% for a capillary size of 100 µm and rotation speed of 1900 rpm (Figure 3.1d). The size distributions of the GUVs did not significantly change across the different capillary sizes (Figure 3.7) and they were broader than the ones previously obtained for smaller orifice sizes.[93] However, the lack of control over GUV size is compensated by a much-improved reliability of encapsulation and GUV formation due to avoidance of clogging, in particular for 100 µm fused silica capillaries. Other capillary materials were also successfully used, *i.e.*, 100 µm PEEK capillary tubing. Changes in rotation speed (1000-2900 rpm) also did not alter the size distributions for the different orifice diameters (Figure 3.7). No precise control of rotation speed is thus needed in order to get robust GUV formation, with size distributions in an ideal range for bottom-up reconstitution of eukaryotic cells. In terms of yield, the absolute number of GUVs obtained using the optimized cDICE protocol is dependent on total encapsulation volume, flow rate, and characteristics of the used biological agents. From the average number of GUVs visible per field of view, we estimate the absolute number of GUVs to reach well over 1000 vesicles in a typical experiment (100 µL of inner aqueous solution and a flow rate of 25 µL min^{-1}).

3.2.2 Unilamellarity of cDICE-produced GUVs

Many reconstitution experiments require unilamellar lipid membranes, as this determines permeability and mechanical properties of the GUV and is needed for insertion of transmembrane proteins, including pore proteins, into the bilayer. Therefore, we next aimed to investigate if our GUV membranes were unilamellar by monitoring insertion of alpha-hemolysin, a protein that assembles a heptameric pore structure in the lipid membranes with a diameter of 14 Å, through which small molecules can pass and which is highly sensitive to the thickness of lipid bilayers.[103,104] As a tracer, we encapsulated 5 µM of the fluorescent dye Alexa Fluor 488 (643 Da) and we immobilized the GUVs within a polyisocyanide hydrogel[105] to aid long-term imaging.[106] After that, alpha-hemolysin was added to the chamber and fluorescent imaging was immediately started. Within minutes following alpha-hemolysin addition, all GUVs observed started to lose their fluorescent content and all had lost 50% of their content after ~20 min (Figure 3.2a, top row; Figure 3.2b, red curve). In stark contrast, when only alpha-hemolysin buffer was added to the GUVs as a control, fluorescent molecules were clearly retained within all

GUVs (Figure 3.2a, bottom row; Figure 3.2b, blue curve). This indicated that loss of GUV content was due to pore formation and hence membrane unilamellarity. Furthermore, individual GUV membrane intensities normalized by the population's mean membrane intensity are consistently distributed around unity, indicating a homogeneous lamellarity over the GUV population (Figure 3.2c). Taken together, our results clearly show that the cDICE method produces unilamellar GUVs.

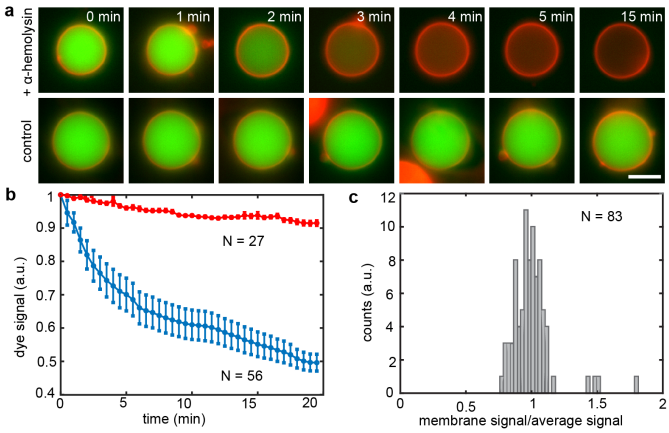

Figure 3.2 | Incorporation of alpha-hemolysin pore protein demonstrates unilamellarity of GUV membrane. (a) Fluorescence microscopy images of single GUVs prepared using a chloroform-based lipid-in-oil dispersion showing different membrane permeability in presence (top row) or absence (bottom row) of alpha-hemolysin. When the pore protein is added to the lipid membrane (red, rhodamine-PE membrane stain), the encapsulated fluorescent dye (green, Alexa Fluor 488) is released in the outer environment within a few minutes. When only alpha-hemolysin buffer is added as a control instead, fluorescent molecules are retained within the GUV volume. Scale bar indicates 5 µm. (b) Quantitative analysis of GUV fluorescent content loss over time. In presence of alpha-hemolysin (blue curve), Alexa Fluor 488 signal intensity decreases down to 50% of the initial value within the first 20 min, while in absence of pores (red curve) only a minor decrease (<10%), likely due to photobleaching, is detected. (c) Histogram showing GUV membrane fluorescence intensities compared to the overall GUV population.

3.2.3 Improvement of encapsulation efficiency

To allow for complex reconstitution experiments, it is essential to have control over the encapsulation of functional biomolecules in the right stoichiometric ratios. We probed the encapsulation efficiency of our improved cDICE protocol by encapsulation of the cytoskeletal protein actin, a broadly used protein in the synthetic biology field. [107] While all experiments using our optimized cDICE protocol resulted in successful encapsulation of monomeric actin in GUVs at high vesicle yields, automated analysis of actin fluorescence at the equatorial plane of the GUV from confocal fluorescence imaging surprisingly revealed a substantial fraction of GUVs with very low actin content, indicating that many of the formed vesicles were seemingly empty (23%, Figure 3.3a, Figure 3.8a). We tested if the encapsulation efficiency could be improved by using different lipid-in-oil mixtures. We reasoned that the encapsulation efficiency may depend on the lipid adsorp-

tion kinetics, as it has been reported earlier that the dispersion method of lipids had a strong effect on their adsorptive behavior. [108] Therefore, we investigated the effect of lipid dispersion strategy on adsorption kinetics, GUV formation, and encapsulation efficiency for three lipid mixtures: lipids in chloroform dispersed as aggregates in a 80:20 mixture of silicon and mineral oil as mentioned above, a similar dispersion of lipid aggregates but using decane instead of chloroform, and a lipid–chloroform solution in mineral oil only. Chloroform and decane serve as good solvents for the lipids, while the lipids do not dissolve in the oils. This way, we aimed to produce different lipid-in-oil dispersions with various aggregation states, with the mineral oil dispersion having smallest aggregate size, and both chloroform- and decane-based lipid dispersions having larger aggregate sizes. [108]

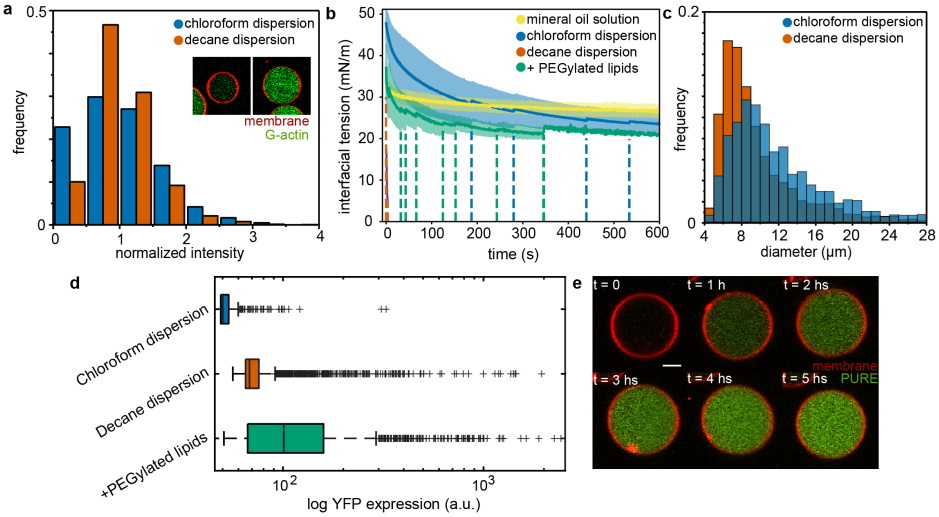

Figure 3.3 | Improved encapsulation by tuning of the lipid-in-oil dispersion. (a) Encapsulation efficiency of G-actin using a chloroform-based lipid dispersion (blue) and decane-based lipid dispersion (orange). The first bin represents GUVs with very low fluorescence intensity, and represents 23% of the population for the chloroform-based lipid dispersion and only 10% for the decane-based lipid dispersion. (b) Interfacial tension decrease measured for a pendant droplet of G-buffer in different lipid-in-oil mixtures. Solid lines show averaged data with standard deviation for a lipid–chloroform solution in mineral oil only (yellow, n = 9), dispersed lipid aggregates using chloroform (blue, n = 13), or decane (orange, n = 7) in silicone oil:mineral oil 80:20 and a chloroform-based lipid-in-oil dispersion with 0.01 mol % of PEGylated lipids (green, n = 9). The dashed lines indicate individual events where the droplet fell off, which gave rise to apparent jumps in the averaged curves. When using the decane-based dispersion, all droplets detached within seconds. (c) Size distribution of GUVs made using a chloroform-based lipid dispersion (blue) and decane-based lipid dispersion (orange). (d) Box plots of the YFP expression after 5 h of incubation in GUVs obtained using dispersed lipid aggregates using chloroform (blue), decane (orange), and a chloroform-based lipid-in-oil dispersion with 0.01 mol % of PEGylated lipids (green). The boxes represent IQR (25th–75th percentiles), the center line indicates the median and the whiskers extend to the maximum and minimum value excluding outliers. Outliers are individually indicated using plus symbols. (e) Time-lapse images of YFP expression in a single GUV using a chloroform-based lipid-in-oil dispersion with 0.01 mol % of PEGylated lipids. Scale bar indicates 5 μm.

First, we confirmed the aggregation state of the lipids by absorbance measurements. Indeed, the mineral oil dispersion was much less turbid (A_{350} = 0.03 ± 0.01) than the chloroform- or decane-based dispersion (A_{350} = 0.10 ± 0.05 and A_{350} = 0.20 ± 0.12 respectively, Figure 3.5), indicating that the latter two have a higher propensity to form aggregates. Pendant drop measurements showed that dispersing lipids as aggregates using chloroform resulted in fast lipid adsorption (Figure 3.3b, blue curve), indicating fast monolayer formation. The decane-based lipid dispersion resulted in even faster adsorption, with all droplets detaching within several seconds (Figure 3.3b, orange curve). In contrast, lipids dispersed in mineral oil exhibited a slower and smaller decrease of interfacial tension (Figure 3.3b, yellow curve), meaning slow adsorption of lipids to the oil–water interface and a small coverage of the final interface. In line with the idea that faster stabilization of the oil–water interface by faster lipid adsorption leads to more robust monolayer formation, we observed no GUV formation when using lipids dispersed in mineral oil, whereas experiments using lipids dispersed as aggregates in a 80:20 mixture of silicon and mineral oil using chloroform or decane gave large GUV yields (Figure 3.8).

We then tested if the fast-adsorbing decane mixture could improve the encapsulation efficiency of cDICE. In stark contrast to the encapsulation of G-actin using chloroform as an organic solvent, using a decane-based lipid dispersion resulted in a significant decrease of the fraction of seemingly empty vesicles (10% *vs* 23%, Figure 3.3a, Figure 3.8). Although large differences in both adsorption kinetics and encapsulation efficiency can be observed between decane- and chloroform-based lipid-in-oil dispersions, they yield GUVs similar in size distribution, size polydispersity, and visual membrane cleanliness (Figure 3.3c, Figure 3.8). We also note that the lipid adsorption behavior of the chloroform-based dispersion is highly variable, much more so than for decane-based lipid dispersions or lipids dispersed in mineral oil only (Figure 3.3b). Since the lipid dispersions are metastable mixtures and chloroform readily evaporates under ambient conditions, changes to their composition happen on time scales similar to the experimental runtime. Indeed, time-dependent absorbance measurements indicated a rapid change in oil turbidity, indicative of an increase in aggregate size, on the time scale of minutes, confirming the intrinsic instability of chloroform-based lipid dispersions (Figure 3.9).

Efficient encapsulation is particularly important for reconstitution of cell-free gene expression reactions (*in vitro* transcription–translation systems) within GUVs, as the relative stoichiometry of their components has to be rather closely retained for optimal functioning.[109] Functionality might further be affected by possible hydrophobic interactions of the protein components with organic solvents during encapsulation, although some groups already successfully encapsulated *in vitro* transcription–translation systems with emulsion-droplet transfer-[110–112] and microfluidic-based methods.[113] To our knowledge, functional encapsulation of a cell-free gene expression (e.g. the Protein synthesis Using Recombinant Elements (PURE) system[114] has never been demonstrated for GUVs produced with the cDICE method. We therefore explored if we could encapsulate the PURE system using our improved cDICE protocol. To this end, GUVs encapsulating PURE*frex*2.0, a commercially available PURE system, along with a linear DNA construct

coding for yellow fluorescent protein (YFP), were produced using both a chloroform-based lipid dispersion and a decane-based lipid dispersion. Gene expression in GUVs incubated at 37 °C was monitored by imaging YFP production within the GUV lumen over time. We observed that the different dispersion strategies used for GUV fabrication influenced the level of gene expression: the distribution of luminal fluorescence intensity after 5 h of gene expression employing decane-based lipid aggregates showed improved gene expression levels compared to the encapsulation using chloroform-based lipid aggregates, which barely yielded any YFP expressing GUVs at all. Nevertheless, both gene expression levels and numbers of YFP expressing GUVs were still very low (Figure 3.3d and Figure 3.10a,b).

In addition to the lipid dispersion strategy, the lipid composition of the bilayer membrane can also alter adsorption kinetics and hence improve encapsulation efficiency. In particular, PEGylated lipids, lipids with a flexible poly(ethylene) glycol (PEG) linker, are often proposed to boost robust vesicle formation for various protocols.[82,115–117] We therefore investigated if doping the vesicular membrane with 0.01 mol% 18:0 PEG2000 PE could improve encapsulation of the PURE system when using cDICE. The presence of PEGylated lipids slightly increased the adsorption rate of lipids to the oil–water interface (Figure 3.3b, green curve). Interestingly, doping the membrane with 0.01 mol% PEGylated lipids greatly enhanced expression of the encapsulated PURE system and resulted in the highest gene expression levels and a large population of GUVs expressing YFP (Figure 3.3d, e and Figure 3.10c). These results show that optimization of encapsulation efficiency both via lipid dispersion and lipid composition is crucial to allow for functional reconstitution of complex reactions such as the PURE system in GUVs made using cDICE.

3.2.4 Proof-of-concept experiments illustrate versatility of the optimized workflow

Finally, to investigate the broad applicability of our improved cDICE method, we aimed to reconstitute a wide range of minimal systems inside cDICE-made GUVs (Figure 3.4). First, we encapsulated a minimal, branched actin network. In eukaryotic cells, the actin cortex is the protein machinery responsible for cell division.[118,119] Reconstitution of a functional actin cortex anchored to the inner leaflet of the GUV membrane therefore offers an attractive route to induce GUV constriction, and possibly membrane fission, in synthetic cells. Our minimal actin cortex consisted of actin together with the verpolin homology, cofilin, and acidic domain of the Wiscot-Aldrin Syndrome protein (VCA), the Arp2/3 complex, and profilin. The Arp2/3 complex is an actin nucleator responsible for promoting formation of a branched actin network at the cell membrane.[120,121] VCA was His-tagged to be able to bind to DGS-NTA(Ni) lipids in the membrane.[122,123] Together with Arp2/3, VCA promoted localized nucleation of a branched cortex at the membrane, while profilin was used to prevent actin polymerization in the GUV lumen.[124,125] Actin displayed a clear localization at the GUV membrane (Figure 3.4a,*i*, Figure 3.11a), similarly to what was obtained using other GUV fabrication methods.[126,127] In the absence of membrane anchors and nucleators, actin was uniformly distributed within the GUV volume (Figure 3.4a,*i*).

As a synthetic mimic of the cellular actin cortex, we encapsulated DNA origami nanostructures [128] that are capable of lateral cross-linking at the vesicular membrane. These four-armed DNA assemblies (Figure 3.12) diffuse freely in the lumen of the GUV but were efficiently recruited to the membrane upon co-encapsulation of a cholesterol-oligonucleotide membrane anchor that binds single-stranded DNA sites on the origami ((Figure 3.4a,*ii*, Figure 3.11b)). Here, the monomeric DNA tiles freely diffuse in the membrane plane and form a precortex. We also successfully encapsulated small unilamellar vesicles (SUVs, ~100 nm diameter),[74] mimicking multicompartmental cellular systems (Figure 3.4a,*iii*, Figure 3.11c). In the future, these compartments could be designed to trigger or sustain intravesicular reactions, allowing control over biochemical reactions inside the GUV lumen. [129–131]

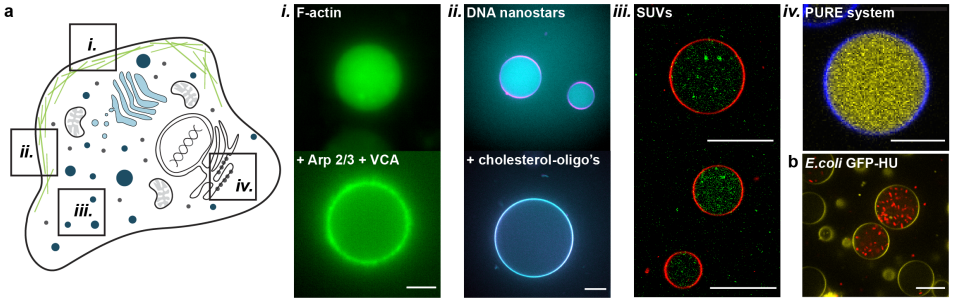

Figure 3.4 | Proof-of-concept experiments showing versatility of cDICE and its applicability for the synthetic cell community. (a) Overview: GUVs as artificial membrane systems to mimic cellular membranes and membrane interactions. (*i*) Reconstitution of a minimal actin cortex inside a GUV, nucleated at the vesicular membrane by the Arp2/3 complex, the C-terminal VCA domain of WASp, and profilin. Scale bar indicates 5 µm. (*ii*) Encapsulation of DNA origami nanostructures, freely diffusing inside the GUV lumen and capable of membrane localization upon addition of 2 µM of cholesterol-oligonucleotides. Scale bar indicates 15 µm. (*iii*) Encapsulation of SUVs inside GUVs to form a multicompartmentalized system. Scale bars indicate 20 µm. (*iv*) Encapsulation of PURE*frex*2.0 and DNA encoding for YFP. Scale bar indicates 10 µm. (b) Encapsulation of GFP-HU expressing *E. coli* bacteria. A large number of bacteria could be observed inside the GUV lumen, clearly viable as evident from their motility. Scale bar indicates 20 µm.

Furthermore, as mentioned above, our cDICE method can be used to encapsulate a functional *in vitro* transcription–translation system (the PURE system), provided PEGylated lipids are included in the lipid mixture (Figure 3.4a,*iv*). The broad applicability of cDICE is further demonstrated by the successful encapsulation of objects that are large compared to the GUV size, *i.e.*, entire *E. coli* bacteria (Figure 3.4b, Figure 3.11d). Cylindrical in shape, with a length of approximately 3 µm and a diameter of 1 µm, [132] these are several orders of magnitude larger than even many DNA origami structures. The bacteria were clearly mobile inside the GUVs (Figure 3.13), showing that the cDICE process does not significantly affect their viability. Encapsulating live bacteria inside synthetic cells could be a promising route to combine "the best of both worlds", e.g. photosynthetic cyanobacteria could be repurposed as "chloroplasts" for the synthetic cell, similar to a recent study which included chloroplasts isolated from plant cells. [133]

Overall, the improved cDICE method is shown to be capable of encapsulating a variety of functional minimal systems related to cell mechanics, cell metabolism, and gene expression, all required for the generation of a synthetic cell.

3.3 Discussion

A good understanding of the parameters influencing the GUV formation process in cDICE is crucial, especially for design of reconstitution experiments beyond first proof-of-concept experiments. Here, we showed that tight control over the lipid-in-oil mixture is key to successful and reproducible GUV formation. We found that membrane quality, which affects mechanical measurements and quantitative fluorescence analysis, was strongly improved by environmental control over preparation and handling of the lipid-in-oil dispersion, notably handling the lipid dispersion in a humidity-free environment (*i.e.*, a glovebox) and decreasing humidity to 30% during vesicle formation. We hypothesize that air humidity affects bilayer formation by changing the microscopic aggregation state of the lipid-in-oil mixture, and thereby the lipid adsorption behavior. Partial hydration of lipids could possibly lead to the formation of larger lipid aggregates, such as reverse micelles or lamellar structures, hindering proper mono- and bilayer formation. Yet, fully understanding the microscopic mechanics of this thermodynamically unstable, multicomponent system remains difficult. [134,135] Importantly, we also demonstrated the unilamellarity of the formed GUVs by correct insertion of alpha-hemolysin to allow pore formation. Although the appearance of the GUV membranes was visibly improved upon environmental control, a common concern remains the possible presence of residual oil traces in the membrane. However, it was shown in previous work that cDICE-formed GUVs are unlikely to have large traces of oil persisting in the membrane. [93,94] It is unknown whether transmembrane proteins are affected by the presence of residual oil in vesicular membranes but interestingly, recent work indicates that it does not significantly alter the static, mechanical membrane properties of the GUVs compared to electroformed GUVs. [136–138] Altogether, this makes vesicle formation with the improved protocol compatible with reconstitution experiments requiring clean unilamellar membranes, such as studies involving membrane mechanics or membrane permeability.

Furthermore, we showed that the dispersion state of the lipids is crucial for efficient GUV formation using cDICE. As other existing protocols show, many different lipid-in-oil mixtures can be used for GUV formation. [93–95,98,108] In particular, Claudet *et al.* [108] found lipids dispersed as aggregates in an oil phase to promote more efficient bilayer formation. We provide experimental evidence that indeed the lipid bulk aggregated state strongly influences adsorption kinetics and thereby vesicle formation, supporting and explaining the observations of Claudet *et al.* [108] Our tensiometry findings also indicate that not solely adsorption speed is of importance for proper bilayer formation, but the structure and content of the lipid aggregates is equally important for mono- and bilayer formation. Hence, having lipids dispersed as aggregates alongside humidity control is essential for clean GUV formation. This indicates a nontrivial relation between lipid properties, lipid dispersion state, adsorption kinetics and the final membrane quality.

Adsorption speed as measured by pendant drop experiments can therefore not be used as a stand-alone quantity to assess whether a given lipid-in-oil mixture will support GUV formation in cDICE. Future research into the molecular mechanisms of the lipid-in-oil dispersions could involve a systematic characterization of the lipid aggregates species via, for example, dynamic light scattering (DLS) or electron microscopy (EM).

By tuning the lipid-in-oil dispersion with different organic solvents or different types of lipids, the encapsulation efficiency of cDICE could be improved. Faster lipid adsorption when using a decane-based dispersion, as compared to using a chloroform-based dispersion, led to a better G-actin encapsulation. For functional encapsulation of the PURE system on the other hand, the presence of PEGylated lipids proved to be crucial. This cell-free expression system has a complex molecular composition and all the individual components need to be present in order to yield a functional readout. While addition of PEGylated lipids has proven to be very effective for encapsulation of the PURE system with cDICE, it should be noted that PEGylated lipids can have adverse effects on protein functionality and membrane physicochemical behavior, as the polymer chains introduce crowding and steric repulsion of components from the membrane as well as affect the membrane thickness.[139] In this case, our experiments suggest that depending on the encapsulated species, PEGylated lipids can be avoided and high encapsulation efficiencies can be reached instead by changing the solvent.

Our cDICE protocol robustly yields GUVs with an average diameter of 12 µm and coefficient of variation of 47%. This size distribution was robust to changes in rotation speed and capillary diameters from 25–100 µm. This consistency over differences in these two central parameters implies that the workflow we have adopted lies in the jetting regime.[140] A jet at the capillary orifice is broken up into a polydisperse droplet population due to the Rayleigh instability in combination with the centrifugal force applied in cDICE.[140] A high degree of polydispersity can be advantageous for bulk assays to screen multiple conditions in one single experiment,[141,142] but undesirable for other applications. As Abkarian *et al.*[93] showed, decreasing the capillary diameter to values around 10 µm or using an additional inner fluid layer to decrease shear forces are viable strategies to achieve more precise size control. However, using these small orifice sizes poses other problems, including fast clogging of small diameter capillaries, rendering the method much less reliable. Here, we demonstrate that to reproducibly encapsulate viscous solutions containing a high concentration of polymerizing protein, as when encapsulating concentrated actin solutions, it is advantageous to use a larger capillary.

Taken together, we have shown that humidity control is essential for reliable production of clean GUVs with cDICE. Furthermore, we found that the encapsulation of different biological systems can be modulated by tuning the lipid-in-oil dispersion and the membrane composition. As a result, the optimized workflow laid out in this research enables the generation of bespoke GUVs at good yields and with high encapsulation efficiency. We showed that encapsulation was compatible with molecular membrane anchors such as the cholesterol-oligonucleotide anchors used with DNA origami and a minimal actin cortex, while maintaining functionality even for complex systems like the PURE system.

This renders a method that is robust and achieves reproducible results across many months and multiple laboratories. By conducting several proof-of-concept experiments, we were able to demonstrate the versatility of the cDICE method: from reconstitution of an actin cortex, to encapsulation of a cell-free expression system, membrane-anchored DNA nanostructures, and entire *E. coli* bacteria, these experiments open up a portal to generating GUVs with contents of ever-greater complexity. In the future, additional modifications by changing experimental parameters such as capillary size, rotation speed, chamber design, *etc.* can be made to further extend the possibilities of cDICE and perform experiment-specific optimization. This way, cDICE displays promising potential to become a standard method for the synthetic biology, biochemistry, and biophysics communities in the future.

3.4 Methods

3.4.1 Design and fabrication of the spinning device/rotational chambers

The cDICE device was designed and developed in-house at AMOLF. A 15-W Maxon EC32 motor (5 wire version, part number 353399) served as the rotating component of the apparatus, providing a wide range of rotation speeds (from 200 rpm up to 6000 rpm) and allowing precise speed ramps for controlled speeding up and slowing down of rotation. This is especially important to avoid mixing of the solutions after experiments, which would lead to lipid debris in the outer aqueous solution, and to avoid disruption of the formed GUVs. Translucent, cylindrical chambers were designed and printed in-house (Stratasys Objet260 Connex3; Veroclear printing material). The chambers measure 38 mm in diameter, have an inner height of 7.4 mm, and include a circular opening of 15 mm in diameter in the top to allow facile access to the solutions with the capillary. The respective designs for rotation chambers and cDICE device are available on GitHub (https://github.com/GanzingerLab). The other laboratories at TU Delft used similar devices.

3.4.2 General cDICE experimental workflow

Synthetic fused silica capillary tubing (TSP 100/050/025 375, Molex) was employed due to its highly smooth inner surface, allowing a controlled flow of inner aqueous solutions. It was cut to a length of several centimeters using the supplied cutting stone and attached to a short piece of flexible microbore tubing (Microbore Tubing, 0.020" x 0.060" OD, Cole-Parmer GmbH) using two-component epoxy glue (Bison) or instant glue (Pattex). Using a hollow piece of metal, the capillary tubing was then bent so it could be inserted horizontally into the rotational chamber. To inject the solutions, this setup was connected to a 250 µL glass syringe (SGE Gas Tight Syringe, luer lock, Sigma-Aldrich) using a shortened needle as connector (Hamilton Needle, Metal hub, needle size 22 ga. blunt tip, Sigma-Aldrich). PEEK capillary tubing (PEEK tubing, 1/32" OD x 0.10 mm ID, BGB Analytik) was used in experiments when explicitly specified. The encapsulation solutions contained 18.5% v/v OptiPrep™ (density gradient medium with a density of 1.320 g mL^{-1}) to increase the density. Unless specified otherwise, the outer aqueous phase was a solution of glucose in Milli-Q water (concentration adjusted to reach a 10–20 mOsm higher osmolarity compared to the inner aqueous solution).

In a typical experiment, the encapsulation solution was loaded into the syringe setup, rotation was started, 700 µL of outer aqueous solutions was inserted into the rotating chamber, followed by 5.5 mL of the lipid-in-oil dispersion. The capillary was then inserted horizontally in the oil layer, until it was visibly embedded. The solution was injected using a syringe pump (KDS 100 CE, KD Scientific) at a rate of 25 µL min^{-1}, unless specified otherwise. The system was spun for a predetermined time depending on the encapsulation volume. Rotation speed ranged from 1000 to 2700 rpm and the capillary diameter from 25 µm to 100 µm depending on the experiment type, with 1900 rpm and 100 µm being considered the default values. After every experiment, the chamber was tilted and excess oil was removed. The GUVs were then allowed to sink to the bottom of the rotation chamber for 10 min, after which they were harvested using a cut pipet tip and transferred to an observation chamber. Glass coverslips were passivated using 1 mg mL^{-1} beta-casein in Milli-Q water. Room humidity was kept around 30-40% using a dehumidifier (TTK 71 E Dehumidifier, Trotec). The other laboratories used a similar workflow, based on this main protocol.

3.4.3 Preparation of lipid-in-oil dispersions

1,2-Distearoyl-sn-glycero-3-phosphoethanolamine-N-[methoxy(polyethylene glycol)-2000] (18:0 PEG2000 PE), 1,2-dioleoyl-sn-glycero-3-phosphoethanolamine-N-(lissamine rhodamine B sulfonyl (18:1 Liss Rhod PE), 18:1 1,2-dioleoyl-sn-glycero-3-phophocholine (DOPC), 1,2-dioleoyl-sn-glycero-3-[(N-(5-amino-1-carboxypentyl)iminodiacetic acid)-succinyl] (nickel salt) (DGS-NTA(Ni)), and 1,2-dioleoyl-sn-glycer-3-phosphoethanol-amine-N-(lissamine rhodamine B sulfonyl) (rhodamine-PE) were purchased from Avanti Polar Lipids. ATTO 488 and ATTO 655 labeled 1,2-dioleoyl-sn-glycero-3-phosphoethanol-amine (DOPE) were obtained from ATTO-TEC. Stock solutions in chloroform were stored at -20 °C. The lipids were mixed in the desired molar ratio in a 20 mL glass screw neck vial (Fisherbrand EPA Screw Neck Vial, Fisher Scientific and Fisherbrand 24 mm PP Screw Seal, Closed Top, 24–400 Thread, Assembled Septum, Fisher Scientific) to obtain a final concentration of 0.2 mg mL^{-1}. After desiccation using a gentle nitrogen flow, the vial was brought inside a glovebox, where the lipid film was resuspended in 415 µL of chloroform (Uvasol, Sigma-Aldrich) or n-decane (99+%, pure, Acros Organics). A mixture of 5.2 mL silicon oil (viscosity 5 cst (25 °C), Sigma-Aldrich) and 1.3 mL mineral oil (BioReagent, Sigma-Aldrich) was then added dropwise to the lipids while vortexing. For the lipid dispersion in mineral oil, 6.5 mL of mineral oil (BioReagent, Sigma-Aldrich) was used instead. After tightly closing the vial and securing the seal with Parafilm, the lipid-in-oil dispersion was vortexed an additional 2.5 min and sonicated in a bath sonicator for 15 min while keeping the bath temperature below 40 °C. The mixtures were used the same day in experiments.

3.4.4 UV-vis absorbance measurements

Turbidity measurements were performed by UV-vis absorbance using a Denovix DS-11 spectrophotometer. Lipid-in-oil dispersions were prepared as described above and used directly for absorbance measurements. For each measurement, a cuvette (UV cuvette ultramicro, BRAND) was filled with 100 µL of lipid-in-oil dispersion and the absorbance

at 350 nm was measured thrice. Prior to each measurement, a blank was taken using the corresponding oil or oil mix.

3.4.5 Pendant drop measurements

Pendant drop measurements were performed using a DSA 30S drop shape analyzer (Kruss, Germany) and analyzed with the Kruss Advanced software. For each measurement, a lipid-in-oil dispersion containing 100% DOPC was prepared in an identical manner as for cDICE experiments. Directly after vortexing, the mixture was divided over three glass 1.0 mm cuvettes (Hellma Analytics). In each cuvette, a 30 µL droplet containing G-buffer (5 mM tris(hydroxymethyl)aminomethane hydrochloride (Tris-HCl) pH 7.8 and 0.1 mM calcium chloride ($CaCl_2$)) and 18.5% v/v OptiPrep™ was formed with a rate of 5 µL s^{-1} using an automated dosing system from a hanging glass syringe with needle diameter of 1.060 mm (Hamilton). Immediately when the droplet reached its final volume, 100 frames of the droplets shape were first acquired at a frame rate of 5 frames per second after which another 500 frames were taken with 1 frame per second. The droplet contour was automatically detected and fitted with the Young–Laplace equation to yield the interfacial tension. For measurements in dehumidified conditions, a dehumidifier was switched on at least 1 h prior to the measurement. The lipid-in-oil dispersion was continuously mixed during each measurement using a magnetic stirrer. In several experiments, interfacial tension decreased very rapidly causing the droplet to detach before the end of the measurement.

3.4.6 Alpha-hemolysin

DOPC (97.4 mol %), DGS-NTA(Ni) (2.5 mol %), and rhodamine-PE lipids (0.1 mol %) were used for preparation of the lipid-in-oil dispersion as described earlier. GUVs encapsulating F-buffer (20 mM Tris-HCl pH 7.4, 50 mM potassium chloride (KCl), 2 mM magnesium chloride ($MgCl_2$), 0.5 mM adenosine triphosphate (ATP) and 1 mM dithiothreitol (DTT)), 18.5% v/v OptiPrep™, and 5 µM Alexa Fluor 488 (Thermo Fischer) were produced in a 200 mM glucose solution. After production, 50 µL of GUV solution was collected from the bottom of the rotating chamber and deposited on a custom-built observation chamber. Separately, a buffered solution (80 mM Tris pH 7.4 and 240 mM glucose) was mixed with a 4 mg mL^{-1} 4 kDa polyisocyanide hydrogel solution[105] in a 1:1 volume ratio, and 50 µL of the resulting solution was quickly added to the GUVs. The hydrogel was used to immobilize the GUVs, facilitating extended time-lapse imaging. After a few minutes, 2 µL of 12 µM alpha-hemolysin solution (100 mM Tris-HCl pH 7.5, 1 M sodium chloride (NaCl), 7.5 mM desthiobiotin (DTB)) was added to the observation chamber. Fluorescence intensity was analyzed manually using ImageJ and results plotted with MATLAB. Alpha-hemolysin was purified in-house according to Stranges *et al.*[143]

3.4.7 G-actin encapsulation

DOPC and ATTO 655 DOPE were mixed in a 99.9:0.1 molar ratio to prepare the lipid-in-oil dispersion. 100 µL of G-actin (4.4 µM, 9% labeled with Alexa Fluor 488) in G-buffer (5 mM Tris-HCl pH 7.8, 0.1 mM $CaCl_2$, 0.02 mM ATP and 4 mM DTT) and 18.5% v/v OptiPrep™ was encapsulated in every experiment, only varying rotation speed and

capillary size. For a capillary size of 25 µm, the flow rate was lowered to 2.5 µL min^{-1} to reduce the pressure in the capillary setup. The encapsulated volume was reduced to 50 µL in these experiments. GUVs were produced in an outer aqueous solution containing approximately 85 mM glucose in Milli-Q water. G-actin was purchased from Hypermol and Alexa Fluor 488-labeled G-actin was obtained from Invitrogen. All proteins were handled according to instructions provided by the manufacturer. GUVs were imaged in the outer aqueous solution using confocal microscopy, 50 µL of GUV solution was deposited on a custom-made glass coverslip and covered. Microscopy was performed using a Nikon A1R-MP confocal microscope, using a Plan APO IR 60x water immersion objective. The 561 nm (laser power 1.0) and 488 nm (laser power 1.0) laser lines were used in combination with the appropriate emission filters to image the ATTO 655-labeled DOPE membrane and Alexa Fluor 488-labeled G-actin, respectively.

3.4.8 Data analysis of GUV images

GUV size and inner intensity (Figure 3.1d, Figure 3.3a,c, and Figure 3.7) were obtained from Z-stack images that were processed using custom-written Python software. The software performs feature tracking in each frame in three consecutive steps. First, the Canny edge detection algorithm [144] is applied, then filling of the detected edges is achieved by applying the binary hole filling function from the ndimage module of the SciPy package, [145] and next these features in each frame are located using the measure module of the scikit-image package [146] for Python. The located features are linked together in a final step to group points belonging to the same GUV along the frame-axis. The radius of the GUVs was determined from the frame where the detected feature was largest and the inner intensity was also obtained from that respective frame and feature. User-based filtering was applied afterward to discard multilamellar structures, aggregates or similar. The software is available on GitHub (https://github.com/GanzingerLab). The intensity was normalized to the mean of the distribution in Figure 3.3a.

3.4.9 PURE system encapsulation

The codon-optimized construct encoding for *meYFPco-LL-spinach* (enhanced yellow fluorescent protein) described in Van Nies *et al.* [147] was used. The sequence is codon-optimized for expression in the PURE system, and the template includes the T7 promoter and terminator. A linear DNA template was employed to observe fluorescence readout of the level of synthesized protein. The linear DNA construct was obtained by polymerase chain reaction (forward primer: GCGAAATTAATACGACTCACTATAGGGAGACC, reverse primer: AAAAAACCCCTCAAGACCCGTTTAGAGG). Amplification products were checked on a 1% agarose gel and were purified using the Wizard PCR cleanup kit (Promega). DNA concentration and purity were measured using a ND-1000 UV–vis Spectrophotometer (Nanodrop Technologies).

The full sequence of the *meYFPco-LL-spinach* linear construct is as follows:

```
  1 GCGAAATTAA TACGACTCAC TATAGGGAGA CCACAACGGT TTCCCTCTAG
 51 AAATAATTTT GTTTAACTTT AAGAAGGAGA TATACATATG CGGGGTTCTC
101 ATCATCATCA TCATCATGGT ATGGCTAGCA TGACTGGTGG ACAGCAAATG
```

```
 151 GGTCGGGATC TGTACGACGA TGACGATAAG GATCCGATGG TTAGCAAAGG
 201 CGAAGAACTG TTTACGGGCG TGGTGCCGAT TCTGGTGGAA CTGGACGGCG
 251 ACGTGAACGG TCACAAATTC AGCGTTTCGG GCGAAGGTGA AGGCGATGCG
 301 ACCTATGGTA AACTGACGCT GAAATTTATT TGCACCACCG GTAAACTGCC
 351 GGTGCCGTGG CCGACCCTGG TTACCACGTT TGGTTATGGC CTGCAGTGTT
 401 TCGCGCGCTA CCCGGATCAT ATGAAACAAC ACGACTTTTT CAAATCTGCC
 451 ATGCCGGAAG GTTATGTGCA GGAACGTACG ATTTTCTTTA AAGATGACGG
 501 CAACTACAAA ACCCGCGCAG AAGTCAAATT TGAAGGTGAT ACGCTGGTGA
 551 ACCGTATTGA ACTGAAAGGC ATCGATTTCA AAGAAGACGG TAATATCCTG
 601 GGCCATAAAC TGGAATACAA CTACAACTCC CACAACGTTT ACATCATGGC
 651 AGATAAACAG AAAAACGGTA TCAAAGTCAA CTTCAAAATC CGCCATAACA
 701 TCGAAGATGG CTCAGTGCAA CTGGCTGACC ACTACCAGCA AAACACCCCG
 751 ATCGGTGATG GCCCGGTTCT GCTGCCGGAC AATCATTATC TGAGCTACCA
 801 GTCTAAACTG AGTAAAGATC CGAACGAAAA ACGTGACCAC ATGGTCCTGC
 851 TGGAATTTGT GACGGCGGCT GGTATTACGC TGGGCATGGA TGAACTGTAT
 901 AAATGAAAGC TTCCCGGGAA AGTATATATG AGTAAAGATA TCGACGCAAC
 951 TGAATGAAAT GGTGAAGGAC GGGTCCAGGT GTGGCTGCTT CGGCAGTGCA
1001 GCTTGTTGAG TAGAGTGTGA GCTCCGTAAC TAGTCGCGTC GATATCCCCG
1051 GGCTAGCATA ACCCCTTGGG GCCTCTAAAC GGGTCTTGAG GGGTTTTTT
```

DOPC and rhodamine-PE were used in a 99.9:0.1 molar ratio for the lipid-in-oil dispersion, 0.01 mol % of 18:0 PEG2000 PE was used when explicitly mentioned. PURE*frex*2.0 (GeneFrontier Corporation, Japan) was used following storage and handling instructions provided by the supplier. Linear DNA template was added at a concentration of 5 nM. Reactions of 40 µL were assembled in test tubes and supplemented with 5% v/v OptiPrep™ (higher ratios negatively interfered with the PURE reaction) and kept on ice. GUVs were produced in an outer aqueous solution composed of 220 mM glucose in Milli-Q water. The flow rate was kept at 2.5 µL min^{-1} for 8 min in total, given the limited availability of inner aqueous solution. After production, 25 µL of GUV solution was transferred to the observation chamber, together with 25 µL of additional outer aqueous solution composed of 35 mM glucose and 50% v/v PURE buffer. YFP expression was monitored at 37 °C by confocal imaging using a Nikon A1R Laser scanning confocal microscope equipped with an SR Apo TIRF 100x oil-immersion objective. The 561 nm (laser power 5.0) and 488 nm (laser power 20.0) laser lines were used in combination with the appropriate emission filters to image the rhodamine-PE membrane and YFP, respectively. The software NIS (Nikon) was used for image acquisition and the settings were identical for all experiments. Samples were mounted on a temperature-controlled stage maintained at 37 °C during imaging up to 5 h.

Image analysis was carried out in MATLAB version R2020b using the script published by Blanken *et al.*[148] Briefly, the script reads the split-channel tiff files, identifies the GUVs, indexes them, and then stores the indexed variables in the data file. The script uses a sharpening filter on the rhodamine-PE image, the GUV lumen is determined by a flood filling step followed by a binarization phase with a cutoff of 200. An erosion step was conducted to filter segments relative to lipid aggregates and other sources of noise. Any

segments with a circularity of less than 0.5 or greater than 2 have been excluded. For each GUV, average rhodamine-PE intensity, average YFP intensity and YFP intensity variance were determined. The box plots of the YFP intensity in the lumen were also generated in MATLAB version R2020b.

3.4.10 Actin cortex

GUVs were prepared using a mixture of DOPC and DGS-NTA(Ni) lipids in a 50:1 molar ratio. G-actin (4.4 μM, 9% labeled with Alexa Fluor 647), profilin (3.3 μM), Arp2/3 (100 nM), and VCA (0.6 μM) were added to a solution containing F-buffer (20 mM Tris-HCl pH 7.4, 50 mM KCl, 2 mM $MgCl_2$, 0.5 mM ATP and 1 mM DTT) and 18.5% v/v OptiPrep™. To minimize photobleaching, an oxygen-scavenger system [149] (1 mM protocatechuic acid (PCA) and 50 nM protocatechuate-3,4-dioxygenase (PCD)) was also added to the solution. GUVs were produced in an outer aqueous solution containing 200 mM glucose in Milli-Q water. After production, 25 μL of GUV solution was collected from the bottom of the rotating chamber and deposited on a custom-built observation chamber, to which an additional 25 μL of a buffered solution (40 mM Tris pH 7.4 and 125 mM glucose) was added. Unless specified otherwise, all chemicals were purchased from Sigma-Aldrich. All proteins, except VCA, which was purified in-house, [150] were purchased from Hypermol and dissolved according to instructions provided by the manufacturer. G-actin was dialyzed in G-buffer (5 mM Tris-HCl pH 7.8 and 0.1 mM $CaCl_2$) before storage at -80 °C.

3.4.11 DNA origami nanostructures encapsulation

The DNA origami design was adapted from Jeon *et al.* [128] by removing the 3' sequence ("sticky ends") mediating multimerization, thus keeping them monomeric. An additional 12 nt sequence was added at the 5' end to allow binding to the membrane via a cholesterol-oligonucleotide anchor. Nanostructures were folded by thermal annealing (from 95 to 23 °C, -0.5 °C min^{-1}) and used at 1 μM in buffered solution (50 mM Tris pH 7.0, 2 mM $MgCl_2$, and 200 mM sucrose). Right before encapsulation, 2 μM of cholesterol-oligonucleotides were added to this buffer. As an outer aqueous phase, 50 mM Tris pH 7.0, 2 mM $MgCl_2$ and 200 mM glucose was used. Experiments were performed using PEEK capillary tubing.

3.4.12 SUV encapsulation

SUVs were prepared using DOPC and ATTO 488 DOPE in a 99:1 molar ratio. Under gentle nitrogen flow, chloroform was evaporated to obtain a homogeneous lipid film. The lipid film was then desiccated for a minimum of 3 h to remove any remaining solvent traces, after which it was rehydrated in phosphate-buffered saline buffer (PBS buffer) at 4 mg mL^{-1} by vortexing. Afterward the solution was sonicated in aliquots of 20 μL for 2 x 30 min. It was then diluted to 0.5 mg mL^{-1} for further use. DOPC and ATTO 655 DOPE were used in a 99.9:1 molar ratio for the lipid-in-oil dispersion. For encapsulation, the SUVs were diluted 10x in PBS buffer and 18.5% v/v OptiPrep™ was added. The outer aqueous phase consisted of 313 mM glucose in Milli-Q water.

3.4.13 Bacteria encapsulation

DOPC, 18:1 Liss Rhod PE, and 18:0 PEG2000 PE were used in a 98.9:0.1:1 molar ratio for the lipid-in-oil dispersion. A saturated lysogeny broth (LB) culture of *Escherichia coli* expressing green fluorescent protein (GFP-HU) was centrifuged and the pellet resuspended in a buffered solution (50 mM Tris pH 7.5, 5 mM NaCl and 200 mM sucrose) and used for encapsulation. As an outer aqueous phase, 50 mM Tris pH 7.5, 5 mM NaCl and 200 mM glucose was used. Experiments were performed using PEEK capillary tubing.

3.5 Acknowledgements

We thank Paul Kouwer (Radboud University) for the kind gift of the polyisocyanide gel, and Josef Melcr and Siewert-Jan Marrink for useful discussions. We acknowledge financial support by the "BaSyC – Building a Synthetic Cell" Gravitation grant (024.003.019) of The Netherlands Ministry of Education, Culture and Science (OCW) and The Netherlands Organization for Scientific Research (NWO) (G.H.K., C. Dekker, and C. Danelon) and NWO-WISE funding (K.A.G.).

3.6 Appendix

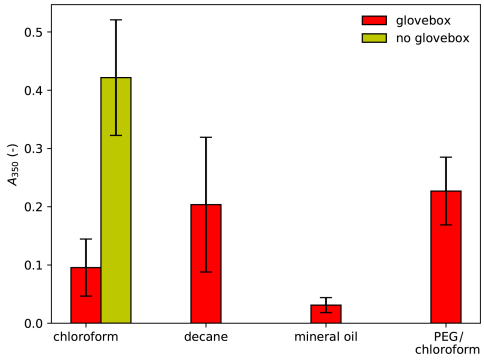

Figure 3.5 | UV-VIS absorbance of different lipid-in-oil mixtures as an indicator of the lipid aggregate size. Absorbance at 350 nm of lipid-in-oil dispersions measured right after preparation. The different lipid-in-oil mixtures consist of: dispersed lipid aggregates using chloroform or decane in silicone oil:mineral oil 80:20, a lipid-chloroform solution in mineral oil only, and a chloroform-based lipid-in-oil dispersion with 0.01 mol% of PEGylated lipids. Red bars indicate dispersions that were prepared in the glovebox. The green bar shows the turbidity of the chloroform-based dispersion prepared outside of the glovebox. Data represents three measurements on at least two individual preparations with standard deviation.

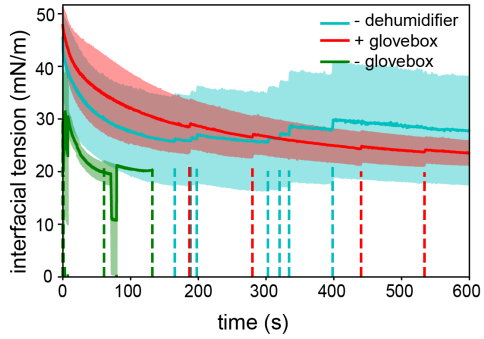

Figure 3.6 | Influence of environmental conditions on lipid adsorption kinetics. Interfacial tension decrease measured for a pendant droplet of G-buffer in different lipid-in-oil mixtures. Solid lines show averaged data with standard deviation for a chloroform-based lipid-in-oil dispersion prepared inside a glovebox with dehumidifier in the experiment room (red, n = 13), outside a glovebox with dehumidifier in the experiment room (green, n = 9), and inside a glovebox without dehumidifier in the experiment room (blue, n = 11). The dashed lines indicate individual events where the droplet fell off, which gave rise to apparent jumps in the averaged curves.

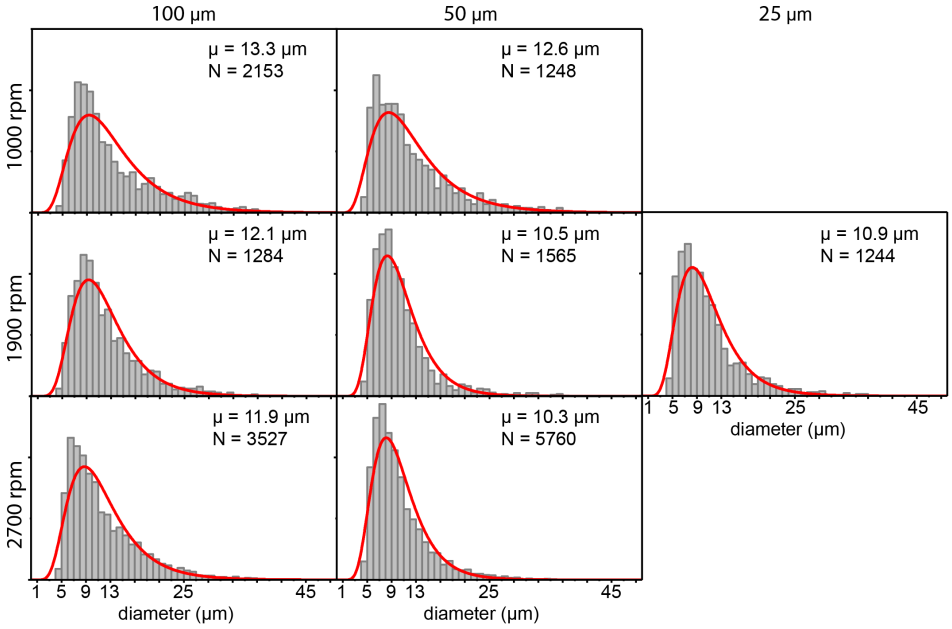

Figure 3.7 | Size distributions for different capillary sizes and rotation speeds. Size distribution of GUVs made of DOPC lipids, using capillary sizes 25 µm, 50 µm, and 100 µm, and rotation speeds 1000 rpm, 1900 rpm, and 2700 rpm. The individual graphs represent pooled data for three experiments. The distributions are fitted to a log-normal function (red curves).

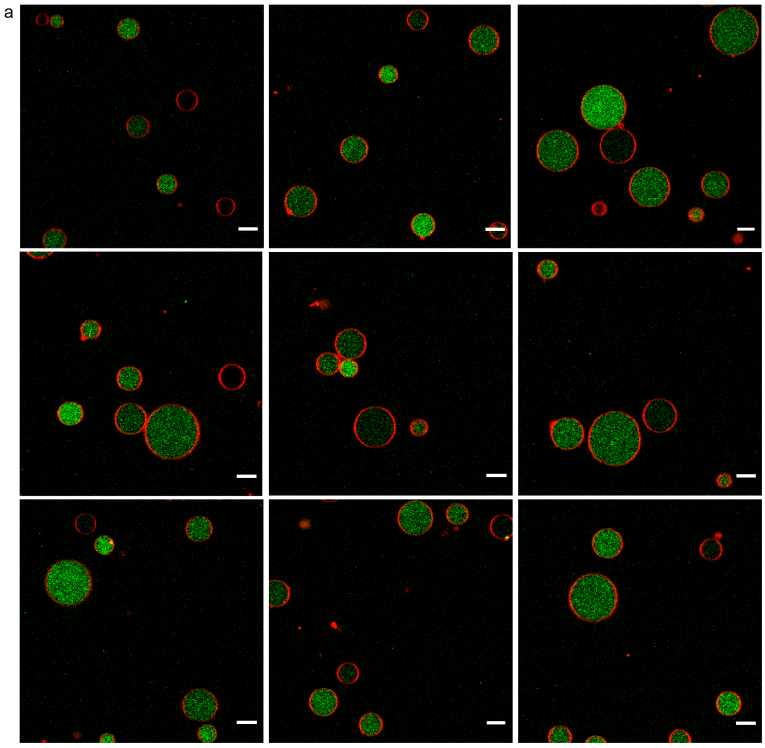
a

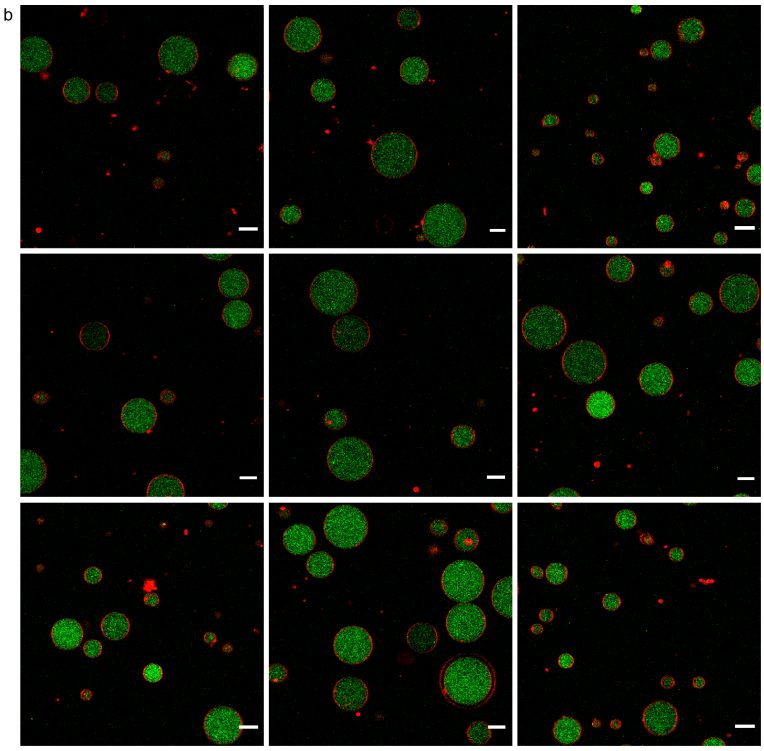

Figure 3.8 | Representative fields of view of GUVs encapsulating G-actin using (a) a chloroform-based lipid-in-oil dispersion and (b) a decane-based lipid-in-oil dispersion. Scale bars indicate 10 µm. Images were acquired with identical imaging settings.

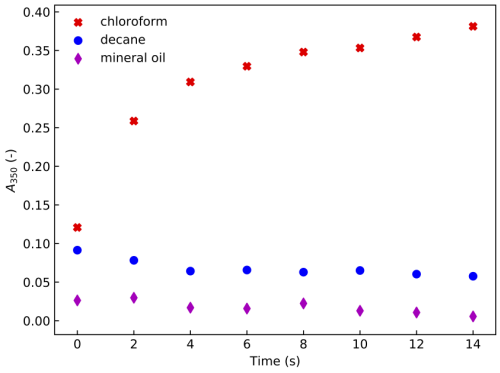

Figure 3.9 | Time traces of UV-VIS absorbance of different lipid-in-oil mixtures. Absorbance at 350 nm of the lipid-in-oil dispersion was measured over ten minutes after opening of the vial. Measured samples include dispersed lipid aggregates using chloroform or decane in silicone oil:mineral oil 80:20 and a lipid-chloroform solution in mineral oil only. All samples were prepared in the glovebox.

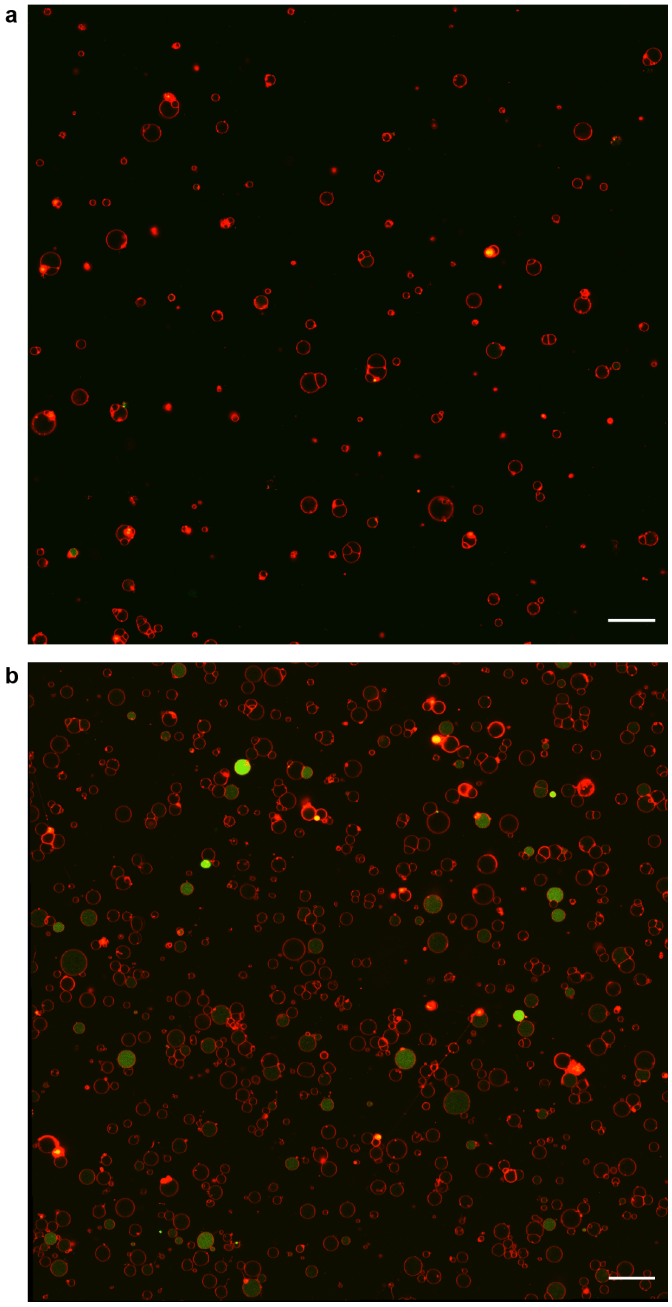
a
b

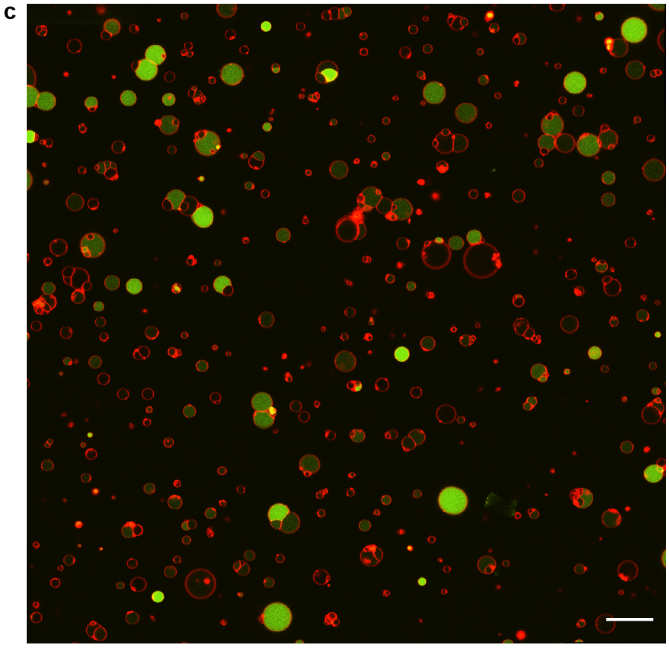

Figure 3.10 | Representative fields of view of GUVs encapsulating the PURE system. (a) Encapsulation of PURE*frex*2.0 and DNA encoding for YFP using a chloroform-based lipid-in-oil dispersion. (b) Encapsulation of PURE*frex*2.0 and DNA encoding for YFP using a decane-based lipid-in-oil dispersion. (c) Encapsulation of PURE*frex*2.0 and DNA encoding for YFP using a chloroform-based lipid-in-oil dispersion and 0.01 mol% PEGylated lipids. All pictures have the same size (scale bars indicate 50 µm) and were acquired with identical imaging settings.

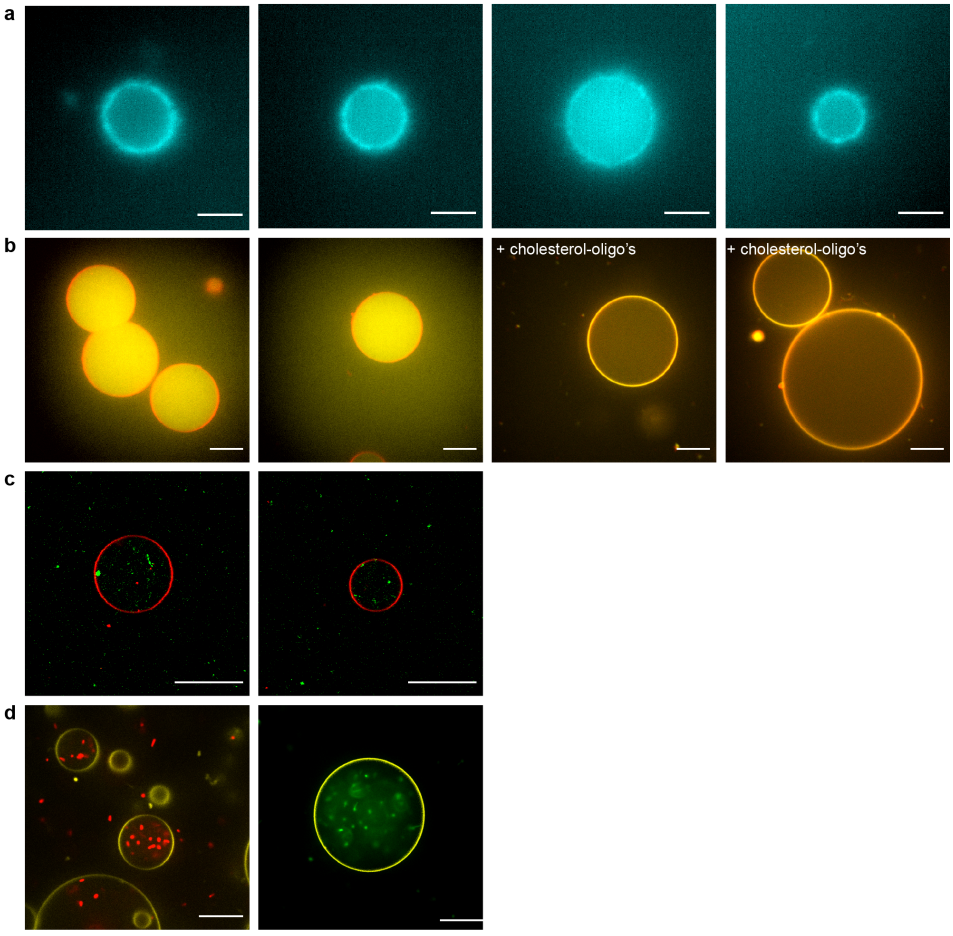

Figure 3.11 | Representative fields of view of proof-of-concept experiments. (a) Reconstitution of a minimal actin cortex inside a GUV, nucleated at the vesicular membrane by the Arp2/3 complex, the C-terminal VCA domain of WASp, and profilin. Scale bar indicates 5 µm (b) Encapsulation of DNA origami nanostructures, freely diffusing inside the GUV lumen and capable of membrane localization upon addition of 2 µM of cholesterol-oligonucleotides. Scale bar indicates 15 µm. (c) Encapsulation of SUVs inside GUVs to form a multicompartmentalized system. Scale bars indicate 20 µm (d) Encapsulation of GFP-HU expressing *E. coli* bacteria. A large number of bacteria could be observed inside the GUV lumen, clearly viable as evident from their motility. Scale bar indicates 20 µm.

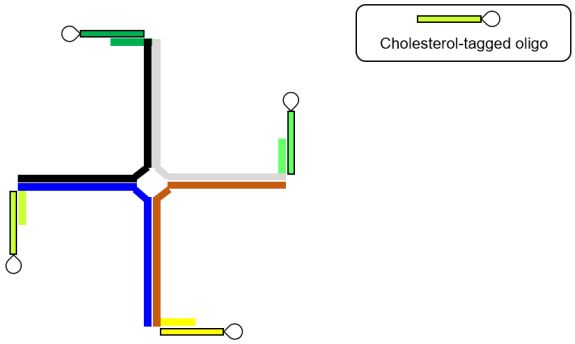

Figure 3.12 | Schematic of a single DNA nanostructure. The DNA nanostructure consists of four single-stranded DNA oligonucleotides (grey, black, blue, and brown) that hybridize forming a cross-like shape. They all have a complementary hybridization sequence for the cholesterol-oligonucleotide at their 5' end.

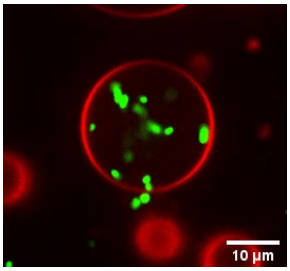

Figure 3.13 | Time-lapse movie of GFP-HU expressing *E. coli* bacteria encapsulated in a GUV. The GFP-HU expressing *E. coli* bacteria (green) are clearly mobile inside the GUV (red), indicating their viability. The time per frame is 1 sec, and the movie is displayed in real time.

CHAPTER 4

High-speed imaging of giant unilamellar vesicle formation in cDICE

▸ Giant unilamellar vesicles (GUVs) are widely used as *in vitro* model membranes in biophysics and as cell-sized containers in synthetic biology. Despite their ubiquitous use, there is no one-size-fits-all method for their production. Numerous methods have been developed to meet the demanding requirements of reproducibility, reliability, and high yield, while simultaneously achieving robust encapsulation. Emulsion-based methods are often praised for their apparent simplicity and good yields; hence, methods like continuous droplet interface crossing encapsulation (cDICE) that make use of this principle, have gained popularity. However, the underlying physical principles governing the formation of GUVs in cDICE and related methods remain poorly understood. To this end, we have developed a high-speed microscopy setup that allows us to visualize GUV formation in cDICE in real-time. Our experiments reveal a complex droplet formation process occurring at the capillary orifice, generating both larger droplets and, likely, GUV-sized satellite droplets. Based on our observations and scaling arguments from fluid dynamics, we find that the transfer of these droplets through the oil-water interface exhibits a size-selectiveness toward GUV-sized droplets. Finally, we demonstrate that proteins in the inner solution affect GUV formation by increasing the viscosity and altering lipid adsorption kinetics. These results will not only contribute to a better understanding of GUV formation processes in cDICE, but ultimately also aid the development of more reliable and efficient methods for GUV production.

Currently under review at ACS Omega: L. Van de Cauter, Y. K. Jawale, D. Tam, L. Baldauf, L. van Buren, G. H. Koenderink, M. Dogterom, and K. A. Ganzinger, "High-speed imaging of giant unilamellar vesicle formation in cDICE", preprint, *bioRxiv*, 2023.

4.1 Introduction

The quest to understand and manipulate the building blocks of life, including the countless interacting molecules and biochemical reactions making up cellular life, is a major aim of biophysics and synthetic biology.[66] One key tool in these fields are giant unilamellar vesicles (GUVs) as cell-sized, lipid bilayer-enclosed reaction compartments.[73,74] Since their first description[77] in 1969, GUVs have proven to be a powerful and versatile tool as they can be directly observed using real-time microscopy and easily manipulated using biophysical tools, making them ideal *in vitro* model membrane systems.[74–76] More recently, GUVs have also been proposed as containers for a future synthetic cell[67,107,151,152] and as reaction containers for chemistry and more complex cargo carriers in drug delivery[153,154].

Despite the widespread research use of GUVs, there is still no one-size-fits-all method for their production.[152] Over the years, numerous methods have been developed to meet the demanding requirements of reproducibility, reliability, and high yield, while simultaneously achieving robust encapsulation. Historically, swelling-based methods (natural swelling[77], electroformation[78–81], and gel-assisted swelling[82–85]) have been used extensively for studying the biophysical properties of membranes. However, these easy-to-implement, high-yield methods offer poor control over encapsulation efficiency and the stoichiometry of encapsulated molecules. Thus, they only offer limited compatibility with establishing complex reconstituted systems. Emulsion-based techniques (water-in-oil droplets crossing an oil-water interface using gravity, centrifugation, microfluidic devices, or microfluidic jetting[86–92]) on the other hand, offer more control over GUV content and for complex encapsulation experiments. Despite the potential cost of residual membrane impurities[152,155,156], emulsion-based methods have therefore gained popularity in recent years.

One method that particularly gained a lot of traction is called continuous droplet interface crossing encapsulate (cDICE).[93–98,157] In cDICE, aqueous droplets that are produced at a capillary orifice are continuously forced through an oil-water interface by centrifugal force in a rotating chamber, thereby forming a lipid bilayer and thus GUVs.[93] Recent optimization has made the method compatible with a wide range of biological systems, thereby offering control over encapsulated content, a high GUV yield, and straightforward implementation.[157] However, our understanding to which degree the encapsulated contents' complexity in cDICE can be extended, with respect to both physical properties (e.g. viscosity of the encapsulated fluid) and physicochemical properties (e.g. which proteins and protein systems), remains limited. While many successes have been celebrated using cDICE, we still do not understand the underlying GUV formation process and how this affects the inherent variability in content encapsulation and yield seen in cDICE.[152]

To gain a deeper understanding of GUV formation in cDICE, we have developed a high-speed microscopy setup that allows us to visualize the GUV formation process inside the rotating chamber in real-time. We focused on the capillary orifice, where initial droplet formation occurs, and on the oil-water interface, where droplets are converted into GUVs. Our experiments reveal a complex droplet formation process occurring at the capillary

orifice, governing both the formation of larger droplets and, likely, satellite droplets of the size of typical cDICE GUVs (12 µm - average diameter of GUVs formed with cDICE [157]). The transfer of these droplets through the oil-water interface appears to exhibit selectivity toward GUV-sized droplets. We support these experimental observations with scaling arguments from fluid dynamics. Finally, we demonstrate that the addition of protein to the inner solution increases the viscosity and alters the kinetics of lipid adsorption, thereby significantly influencing the process of GUV formation.

4.2 Results and discussion

4.2.1 Design of an imaging setup to visualize droplet and GUV formation in cDICE

In the cDICE method, the initial step of GUV formation is the generation of droplets at a capillary orifice, which is inserted perpendicularly into the oil layer in the rotating chamber. In its original implementation, cDICE uses a capillary diameter of 2-25 µm to allow for tight control over GUV sizes.[93] However, we and others found such narrow capillaries to be very impractical when encapsulating protein solutions, as these capillaries are prone to rapid clogging, leading to highly irreproducible results. In our previous work, we showed that this issue can be circumvented by using wider capillaries with a diameter of 100 µm.[157] The flow regime is therefore significantly different from the original protocol[93], and one would not necessarily expect tight control over droplet sizes. Still, we found that these capillaries produced a surprisingly narrow size distribution of GUV sizes, roughly ten times smaller than the capillary orifice (~ 10 µm *vs* 100 µm).[157]

To better understand how a large capillary orifice can still lead to such relatively monodispersed GUV size distribution in cDICE, we developed a high-speed microscopy setup to, for the first time, visualize the processes of droplet and GUV formation in cDICE in real-time (Figure 4.1). We designed the setup so that the camera is suspended vertically above the cDICE apparatus, capturing the light of a light source located directly beneath the rotating chamber (see method section for a full description of the setup; Figure 4.1a). This way, we are able to capture the process along the horizontal axis of the rotational chamber: from the capillary orifice, where initial droplet formation occurs (Figure 4.1b i), to the oil-water interface, where droplets are converted into GUVs (Figure 4.1b ii). Due to the high rotation speeds that are used in cDICE (~ 1900 rpm), all processes happen on a very fast timescale, on the order of microseconds (10^{-6} - 10^{-5} s). To obtain a sufficiently high time resolution, we therefore used fast cameras in combination with brief exposure times up to 1 µs, reaching frame rates up to 30,000 fps.

4.2.2 Droplet formation at the capillary orifice is governed by shear forces

When we focused our imaging setup on the capillary orifice at our default conditions for GUV production (100 µm diameter capillary, a rotation speed of 1900 rpm, and a flow rate of 25 µL min^{-1}; see method section for further details), it immediately became clear that droplet formation under these conditions is a non-uniform, highly dynamic process with an irregular breakup pattern of a liquid filament into individual droplets (Figure 4.2a, Figure 4.6). Instead of the distinct droplet formation expected for low Reynolds numbers[93,158], we observed fluid exiting the capillary forming a liquid

filament, which often adhered to the capillary. Droplet breakup took place at the end of the liquid filament at a fast rate, with droplet sizes clearly larger than the average cDICE GUV ((68.6 ± 2.8) µm, approximately 2,500 droplets per second).

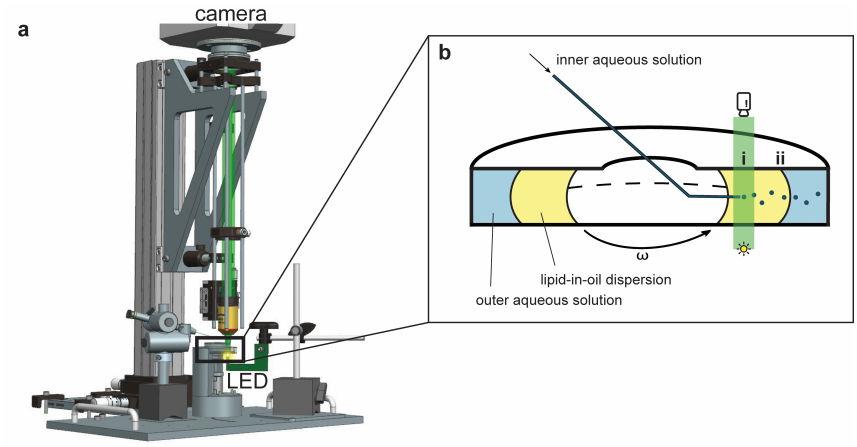

Figure 4.1 | Development of a high-speed imaging setup to visualize GUV formation in cDICE. (a) The imaging setup consists of a high-speed camera suspended above the rotating chamber and an intense light source located directly below the rotating chamber. For a full 360° view of the setup, see method section. (b) In cDICE, (i) aqueous droplets are generated at the capillary orifice; subsequently travel outward through the lipid-in-oil dispersion; and finally (ii) traverse the oil-water interface, where droplets are converted into GUVs.

Upon silanization of the capillary, we no longer observed the fluid adhering to the capillary, resulting in a more regular droplet breakup mechanism (Figure 4.7). This can likely be explained by an increased surface hydrophobicity upon silanization when compared to the default polyimide capillary coating surrounding the capillary and the uncoated cut tip cross-section with chipped coating edges, which results in less wetting of the capillary surfaces.

We observed a significant variability in the droplet breakup dynamics at the end of the liquid filament. Factors contributing to this variability include irregularities in the capillary orifices resulting from suboptimal cutting or capillary deterioration over sustained use, differences in capillary insertion angle, and the occasionally-observed presence of an air pocket at the base of the capillary (Figure 4.2c, Figure 4.8). Note that in all these cases, the experimental condition was indistinguishable by eye and the differences only became apparent when visualizing droplet formation with our dedicated imaging setup.

To better understand the observed droplet breakup mechanisms, we then turned to scaling arguments to rationalize our findings (Figure 4.2b). Our video recordings (Figure 4.6) suggest that droplet breakup at the tip of the capillary is not due to inertial jetting, but instead induced by viscous shear stresses. For droplets forming from a capillary of outer

diameter D, intertial jetting is expected for flow rates larger than a ciritcal flow rate scaling with ~ $\pi(D^3\gamma/2\rho_i)^{1/2}$, where ρ_i denotes the density of the inner solution and γ is the interfacial tension between the dispersed and the continuous phase.[158] In our experiments, the flow rate through the capillary is 25 µL min^{-1}, which is significantly lower than the critical flow rate. This is consistent with our observation that droplets are indeed sheared off the capillary. Here, we must therefore consider the balance between surface tension and viscous forces characterized by the criticial capillary number Ca, given by $Ca = \mu U/\gamma$. The flow velocity U at the point of insertion of the capillary is $U = \Omega R_i$, where R_i is the distance between the capillary orifice and the center of rotation of the chamber and Ω is the rotation speed. With $R_i \sim 1\ cm$, $\Omega \sim 1000 - 2700\ rpm$, $\mu \sim 4 - 5\ 10^{-3}\ kgm^{-1}s^{-1}$ and assuming an interfacial tension between the inner solution and the oil phase of $\gamma \sim 10^{-3} - 10^{-2} mNm^{-1}$ [157], tha capillary number ranges between 0.5 and 10. Monodispersed droplets form at the tip of the capillary through a dripping mechanism for low values of the capillary number.[158] Within the higher range of Ca reached in our experiments, droplets are therefore expected to deform and the breakup mechanism to be unstable, in agreement with our observations.

cDICE experiments require high angular velocities ω (> 1000 rpm), producing flow instabilities in the wake of the static capillary inserted into the rotation chamber. Indeed, the Reynolds number, characteristic of the flow around the capillary, $Re_D = \rho UD/\mu$, yields values in the range of $Re_D \sim 200–300$, with $\rho \sim 0.934\ gmL^{-1}$ being the density of the lipid-in-oil dispersion. For $Re_D \geq 47$, periodic vortex shedding in the wake of a cylinder is expected [159], and for $Re_D \geq 150$, further three-dimensional instabilities are predicted [159], suggesting that the wake around the capillary will also affect droplet breakup. Indeed, we observe oscillations in droplet breakup, caused by the non-linear effects in the wake, and the inner solution adhering to the outer capillary surface. Additionally, we observed that the droplets did not immediately travel outwards as expected, but rather initially exhibited an inward movement in the wake of the capillary and towards the center of the rotating chamber, before travelling outward. The larger diameter of the capillary leads to a larger capillary number Ca and to a wake instability, which both contribute to a less stable droplet breakup and larger variation in droplet size when compared to previous work[93].

4.2.3 Droplet size, in contrast to GUV size, is dependent on the rotation speed

To explore factors that influence droplet breakup in cDICE, we next altered the rotation speed of the rotating chamber. As the rotation speed of the chamber increases, the flow velocity at the capillary orifice also increases and the viscous forces become stronger. This leads to the droplets being more likely to break up, resulting in smaller droplets. In line with this expectation, an increase in rotation speed to 2700 rpm resulted in smaller droplets formed at a higher frequency ((28.5 ± 8.7) µm and ~ 34,500 droplets per second; Figure 4.3, Figure 4.9). Decreasing the rotation speed to 1000 rpm, the lowest speed at which oil and water layers maintain a vertical interface and GUVs can be produced, had the opposite effect, *i.e.* larger droplets formed at a lower frequency ((273 ± 41) µm and ~ 40 droplets per second; Figure 4.3, Figure 4.10). We can estimate the droplet size from a

force balance between the surface tension force ~ $\pi D\gamma$ and the viscous force ~ $6\pi\mu aU$, where D is the outer diameter of the capillary and a is the radius of the droplet.[158] The droplet size above which breakup is expected, scales with the inverse of the capillary number a/D ~ $(6Ca)^{-1}$ and we predict a droplet diameter of ~ 100 µm at 1900 rpm increasing to ~ 200 µm when the rotation speed is decreased to 1000 rpm, in agreement with out experimental results. Droplet formation is thus shear-induced in a broad range of rotation speeds, encompassing both lower and higher speeds than the default of 1900 rpm. Our observation that droplet size is dependent on chamber rotation speed contrasts with the size distributions for GUVs obtained using these conditions: these distributions are all indistinguishable from one another and centered around 12 µm[157], thus 3-30-fold smaller in diameter than the produced droplets. Hence, at least some of the droplets formed at the capillary orifice are not directly converted into GUVs.

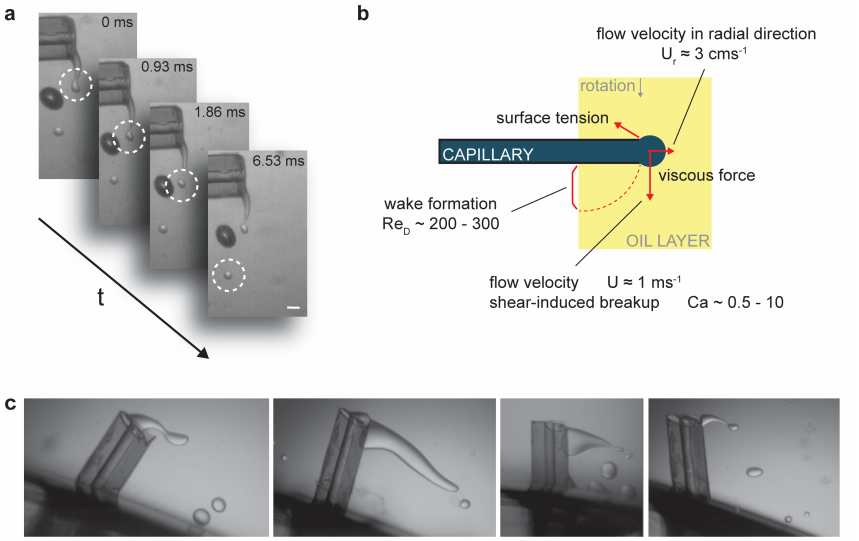

Figure 4.2 | Droplet formation at the capillary orifice is governed by shear forces. (a) Microscopic image sequence capturing a droplet of PBS buffer with 18.5 % v/v OptiPrep™ being sheared off from the liquid filament at the capillary orifice at a rotation speed of 1900 rpm. Scale bar indicates 100 µm. (b) Illustration depicting the different forces acting at the capillary orifice: the capillary number (Ca ~ 0.5 – 10) indicates a shear-induced breakup mechanism, while the Reynolds number (Re_D ~ 200 – 300) describes the wake formation behind the capillary. The shear velocity ($U \approx 1\ ms^{-1}$) is larger than the flow velocity in the radial direction ($U_r \approx 3\ cms^{-1}$), further indicating droplet formation is shear-induced. (c) Representative field-of-views highlighting the high inter-experiment variability. Noticeable differences can be seen, e.g. in liquid filament, capillary orifice, and insertion angle. The capillary opening is 100 µm in all cases.

While a rotation speed ω of 1900 rpm resulted in the narrowest droplet size distribution of all explored rotation speeds, interestingly, a rotation speed of 1000 rpm resulted in two distinct populations (Figure 4.3): one primary population of droplets with a mean diameter ϕ of (273 ± 41) µm and a secondary population consisting of smaller droplets

with a mean diameter ϕ of (15.9 ± 7.3) µm. Occasionally, this periodic droplet formation of large and small droplets was disrupted when e.g. a droplet merged with the liquid filament or collided with the capillary. Inspecting the video recordings more closely, we found that the observed population of small droplets are satellite droplets, produced when a bigger droplet breaks off from the main liquid thread at the tip of the capillary (Figure 4.10). Such satellite droplets have previously been observed in many breakup configurations, from T-junctions to the breakup of droplets in pure shear.[160] While we did not observe any satellite formation for rotation speeds > 1000 rpm, this may be due to our limited optical and temporal resolution: the satellite droplets observed for 1000 rpm (diameter ~ 15 µm) were at the limits of our image resolution, droplets of any smaller diameter were too small to be identified and measured with sufficient certainty (see method section for further details). It is therefore possible that satellite droplets of all sizes, within the size range of the final GUVs (1-20 µm), are also formed, but not detected by our imaging setup.

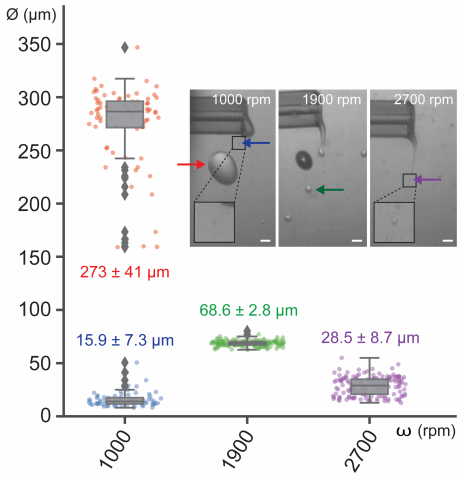

Figure 4.3 | Size distributions of droplets for different rotation speeds. Boxplots of droplet diameter ϕ at rotation speeds ω of 1000 rpm, 1900 rpm, and 2700 rpm (n = 148, 152, and 157, respectively, for N = 1). Individual data points indicate single droplets and boxplots indicate medians and quartiles, while outliers are marked with individual diamond shapes. A rotation speed of 1000 rpm resulted in two distinct droplet populations: large droplets of mean diameter ϕ (273 ± 41) µm (red) and satellite droplets of mean diameter ϕ (15.9 ± 7.3) µm (blue). A rotation speed of 1900 rpm resulted in the narrowest distribution, with a mean droplet diameter ϕ of (68.6 ± 2.8) µm (green). 2700 rpm resulted in the smallest droplet sizes, with a mean diameter ϕ of (28.5 ± 8.7) µm (purple). Inset: representative field-of-views for the different rotation speeds indicating the formed droplets with arrows. Scale bars indicate 100 µm.

In addition to the small satellite droplets we observed at 1000 rpm, smaller droplets could theoretically also be formed when larger droplets break up due to shear forces generated in the flow by the rapid relative motion of the bottom wall of the rotational chamber with respect to the capillary. Droplets formed at the tip of the capillary are

entrained by the flow in the rotation direction at a high velocity of $U \approx \Omega R_i \approx 1\ ms^{-1}$ when compared to the slow radial motion $U_r = (\rho_i - \rho_o)a_o^2\Omega^2 R_i/\mu \approx 3\ cms^{-1}$, determined by the balance between centrifugal and viscous forces. Here, ρ_i denotes the density of the inner solution, ρ_o the density of the outer solution and $(\rho_i - \rho_o) \sim 30\ kgm^{-3}$. These droplets therefore interact with the wake left behind the capillary for several rotations. In the wake, the characteristic shear rate $\dot{\varepsilon}$ scales with $\dot{\varepsilon} \sim \Omega R_i/l$, where the characteristic length scale l for shear around the capillary will range between the outer diameter of the capillary, $\approx 0.5\ mm$, and the distance between the capillary and the bottom of the rotation chamber, $\approx 5\ mm$. One can define another capillary number as $Ca_{\dot{\varepsilon}} = \mu\dot{\varepsilon}a/\gamma$, where a is the radius of the droplet.[161,162] This number characterizes the relative magnitude of the viscous shear forces due to the shear rate $\dot{\varepsilon}$ and the surface tension forces. $Ca_{\dot{\varepsilon}} = 1$ corresponds to a condition where the smallest droplets cannot be further broken up by the shear[161,162] and yields $a \sim \gamma/\mu\dot{\varepsilon}$. For $l \sim 5\ mm$, we find that the interfacial tension of the monolayer at the inner solution/oil interface needs to be approximately $\gamma \sim 10^{-6}\ Nm^{-1}$ to produce droplets of $a \sim 5\ \mu m$, equivalent to the final GUV size. This value for an interfacial tension at an aqueous/oil interface is extremely low and not expected, even in presence of surfactants or lipids. For reference, the interfacial surface tension between two miscible liquids is on the order of $10^{-6}\ Nm^{-1}$.[163] Hence, we conclude that it is unlikely GUV-sized droplets form by shear force-induced droplet breakup after droplet formation at the capillary orifice.

4.2.4 Protein in the inner solution affects viscosity and lipid adsorption

Next, we set out to study the effect of proteins on droplet formation at the capillary orifice. It is well known that encapsulation of more complex solute mixtures, such as proteins and their associated buffers, leads to a decreased yield and variable encapsulation efficiencies.[157,164] For cDICE specifically, it has been reported that the yield decreased at high protein concentration[101], yet it is still unknown why this is the case. We chose to investigate the effects of actin and tubulin, due to the widespread efforts for cytoskeletal reconstitution inside GUVs.

Upon addition of either protein, droplet breakup at the capillary orifice also occurred at the tip of the liquid filament exiting the capillary. However, the oscillations of the liquid filament in the wake of the capillary were significantly reduced (Figure 4.4a, Figure 4.11). Remarkably, in the case of tubulin, the liquid filament displayed a tendency to adhere to the air-oil interface. To explain these observations, we characterized the inner solution. We looked into both the physical properties, *i.e.* dynamic viscosity as determined by bulk shear rheology, and physicochemical properties, specifically lipid adsorption rate determined from pendant drop tensiometry.

In presence of actin and tubulin, the dynamic viscosity increased with respect to its accompanying buffer, G-buffer and MRB80 buffer, respectively (Figure 4.4a). For actin (1 µM in G-buffer, 6.5 % v/v OptiPrep™), an almost threefold increase from 1.58 cP to 4.61 cP was observed (Figure 4.4a, yellow bar), while for tubulin (33.33 µM in MRB80 buffer, 1.75 % w/v sucrose), the viscosity increased fourfold from 1.57 cP to 6.49 cP (Figure 4.4a, red bar). All solutions still exhibited Newtonian fluid behaviour. Important to note is that

the used concentrations of added proteins remained within the micromolar range and are widely used in the field. Interestingly, the viscosity of the inner solution containing protein was similar to the viscosity of the continuous phase, *i.e.* the surrounding lipid-in-oil dispersion (Figure 4.4a, middle 'LOD' bar). The fragmentation of the liquid filament into droplets at the end of the capillary is the consequence of complex instabilities beyond the scope of this study. These mechanisms are significantly affected by the viscosity of the inner solution and the increased viscosity due to the added protein will dampen the flow dynamics in the liquid filament. This dissipation in the liquid filament can explain the decrease in the fluctuations observed in the liquid filament exiting the capillary (Figure 4.4a, Figure 4.11). Moreover, previous studies on capillary breakup have reported the viscosity to affect the fragmentation pattern and the size distribution of satellite droplets significantly. In particular, the viscosity increase in a liquid filament has been associated with fewer and larger satellite droplets.[165,166] Therefore, proteins included in the inner solution can have a significant impact on the size distribution of droplets formed at the capillary orifice. Altogether, these results show a nuanced interplay between the physical properties of the encapsulation solution, varying with its composition even at low protein concentrations, and the fluid dynamic processes that govern droplet breakup.

To investigate how the addition of protein to the inner solution alters the physicochemical properties of the interface, we used pendant drop tensiometry[99] to study lipid monolayer formation in a controlled environment. We analyzed the lipid adsorption kinetics and interfacial tension dynamics of the water-oil interface for different encapsulation solutions, mimicking droplet formation at the capillary orifice. It has been shown that proteins spontaneously adsorb at the oil-water interface and their behaviour cannot unequivocally be attributed to a single protein property, with thermodynamic stability, structural properties, and concentration all being contributing factors.[167,168] Particularly, actin has been shown to exhibit surface activity in a charge-dependent manner, influenced by both lipid and buffer composition, with a more pronounced effect observed for the filamentous form compared to actin monomers.[169–171]

Upon adding 4 μM actin to the inner solution, a pronounced decline in interfacial tension was observed (Figure 4.4b, purple curve), with some droplets detaching before the end of the experiment (Figure 4.4b, dashed lines). This trend was consistent for tubulin (Figure 4.4b, green curve). To examine the roles of actin and tubulin as surface-active agents in the interfacial tension, we then compared the interfacial tension dynamics against a lipid-free oil dispersion. Both actin and tubulin had only a marginal impact on interfacial tension when compared to the protein-free condition (Figure 4.4b, black curve *vs* purple curve and grey curve *vs* green curve). Interestingly, while actin and lipids individually at the interface exhibited slow kinetics, their combined presence displayed an accelerated decrease (Figure 4.4b, yellow curve), suggesting a synergistic effect beyond mere additivity. We found this effect could not be countered via electrostatic or steric repulsion (*i.e.* presence of charged or PEGylated lipids, respectively, Figure 4.12). These results imply that actin could, for example, quickly cover the surface of the droplets traversing the lipid-in-oil dispersion, potentially impeding lipid monolayer formation

and/or monolayer zipping. However, the full extent of this synergistic effect is yet to be uncovered. Furthermore, these results underscore the importance of the compositions of both inner solution and lipid-in-oil dispersion, as both affect mono- and bilayer formation.

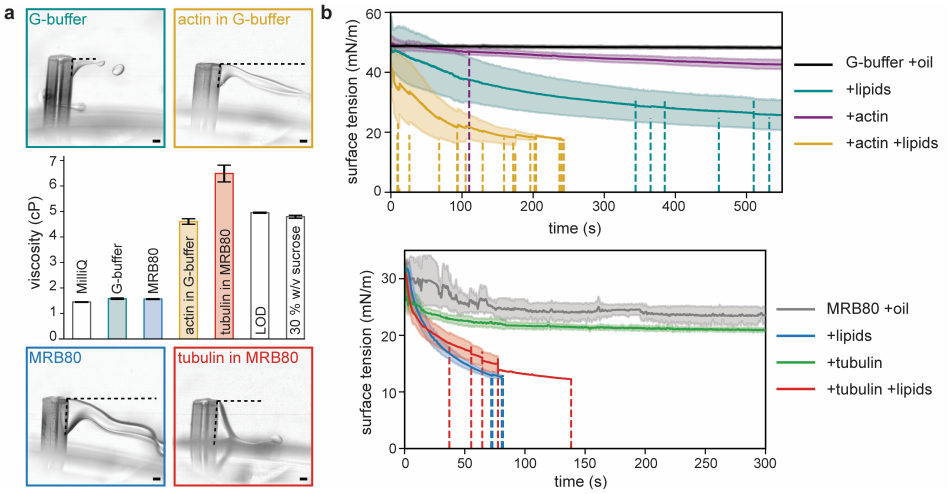

Figure 4.4 | Effect of protein on aqueous solution properties. (a) Representative field-of-views of droplet formation at the capillary orifice for different protein solutions. Horizontal dotted lines indicate the liquid filament length just before the drop breaks off, while vertical dotted lines along the capillary indicate the extent of external capillary surface wetted by the aqueous solution. Images are background subtracted for better contrast. Scale bars indicate 100 µm. Middle: Dynamic viscosity measured using a parallel plate rheometer for different buffers (G-buffer with 6.5 % v/v OptiPrep™, MRB80 with 1.75 % w/v sucrose) and protein solutions (actin and tubulin), along with water (MilliQ), lipid-in-oil dispersion (LOD) and 30 % w/v sucrose solution in MRB80 for reference. Error bars represent standard deviation. (b) Interfacial tension kinetics measured using pendant-drop tensiometry for different combinations of aqueous and oil solutions; G-buffer and actin (top), and MRB80 and tubulin (bottom). Solid lines represent the average values and the shaded region corresponds to standard deviation. The vertical dotted lines represent the event of falling of a drop and truncation of data.

4.2.5 GUV formation at the oil-water interface seems size selective

Droplet formation in cDICE occurs on extremely short timescales; for the default conditions (*i.e.* 1900 rpm, 25 µL min^{-1}) we observed droplets of approximately ~ 70 µm in diameter being sheared off at a frequency of ~ 2,500 Hz. Theoretically, given a total encapsulation volume of 100 µL, > 500,000 droplets are formed during a single experiment. Interestingly, this number does not correspond to the final number of GUVs produced using cDICE, as reported in other publications (~ 1000 GUVs[157]). Furthermore, the formed droplets larger than the finally observed GUVs (*i.e.* non-satellite droplets, 70 µm for the default conditions) do not subsequently shear to form smaller droplets, as discussed above. These two observations together indicate a sub-optimal GUV formation process downstream, whereby most droplets do not convert into GUVs at the oil-water interface and potentially additional hidden mechanisms generating smaller droplets.

To look more closely at droplet-to-GUV conversion in cDICE, we imaged the oil-water interface where the final step of GUV formation in cDICE occurs: droplets transfer through the oil-water interface where two monolayers fuse together to form a bilayer (Figure 4.5a). As postulated by Abkarian *et al.*[93], the two monolayers can also form a pore, thereby causing the droplet to burst, resulting in no GUV being formed. We note that when we collected GUVs in cDICE experiments, we observed that the outer solution after GUV generation also contained components of the inner solution, in agreement with the suggestion that a fraction of droplets bursts at the oil-water interface.

In our experiments, we unfortunately did not observe a clear transfer of droplets through the interface nor bursting of droplets, possibly because resolving GUV-sized droplets at the interface was not feasible with the limited imaging contrast of standard brightfield illumination. Instead, we made two other, striking observations. First, we observed droplets several orders of magnitude larger than the typical size of GUVs which were stationary on the oil-water interface (Figure 4.5b, Figure 4.13). These stationary droplets showed a decreased contrast on the side of the outer aqueous phase, suggesting partial transfer across the interface. Since the transfer time of a droplet to the oil-water interface is inversely proportional to the radius of the droplets squared[93], it is possible that the flight time of these larger droplets is too short for lipids to fully adsorb on the interface. Consequently, no zipping mechanism is possible, leading to these larger droplets crowding the interface, as we observed in our video recordings.

A second observation was the formation of comet tails (Figure 4.5c): droplets that did pass the interface dragged a tail of the oil solution into the outer aqueous solution, likely because the oil did not drain quickly enough and thus prevented monolayer fusion. Due to the difference in contrast with the outer aqueous phase, we infer that oil is still present between the part of the interface dragged into the outer phase and the droplet. The Bond number $Bo = \frac{\Delta\rho a r^2}{\gamma}$, where a is the acceleration and r the radius of droplet, represents the ratio of centrifugal force to surface tension force. For these large droplets, Bo is on the order of 1, meaning they will deform the interface, as observed in our video recordings, and drag the oil phase into the outer aqueous phase. This results in the observed comet tail formation and no GUV formation from the droplets undergoing this process.

As we find that the addition of protein to our inner solution significantly alters the characteristics of the solution and affects droplet formation at the capillary orifice, we asked how the increased viscosity and altered lipid adsorption kinetics might impact the transfer of droplets through the oil-water interface. The accelerated lipid adsorption due to the addition of protein does not lead to a decreased flight time of the droplets, thereby not adversely affecting droplet transfer or monolayer zipping. On the other hand, the increased viscosity of the inner solution could influence the timescale of the drainage of the lubrication film, *i.e.* the lipid-in-oil dispersion in between the droplet and the oil-water interface, required for successful monolayer zipping. Furthermore, the increased viscosity could reduce the flow caused by Marangoni stresses, which play a role in facilitating the zipping process.[93]

An approximate breakthrough condition for spherical objects of radius a to pass through an interface of interfacial tension γ is $(\rho_i - \rho_o)\Omega^2 R_o a^2 \geq 3/2$, where R_o is the distance between the axis of rotation and the location of the oil-outer solution interface.[172] For small droplets of radius $a \sim 5\ \mu m$ to cross the interface, a low surface tension on the order of $\gamma \sim 10^{-6}\ Nm^{-1}$ is required. Such low surface tension has been reported for lipid bilayers[173] and therefore if such small droplets are present in the oil phase, they can cross the interface to form GUVs. It should be emphasized that the breakthrough condition sets a criterion for the smallest droplet that can cross the interface. Any droplet larger than 10 µm in diameter would be expected to cross the interface as well and form larger GUVs. The fact that we do not observe GUVs of larger diameters than ~ 20 µm[157], but do observe large droplets at the oil-water interface, suggests that the upper size limit for GUV formation might be controlled by membrane zipping and/or lipid coverage of the droplet/interface. Insufficient lipid coverage could, for example, lead to droplet/GUV shrinkage during GUV forming until the lipid density to form a bilayer is reached, thereby resulting in smaller GUVs than originally produced droplets.

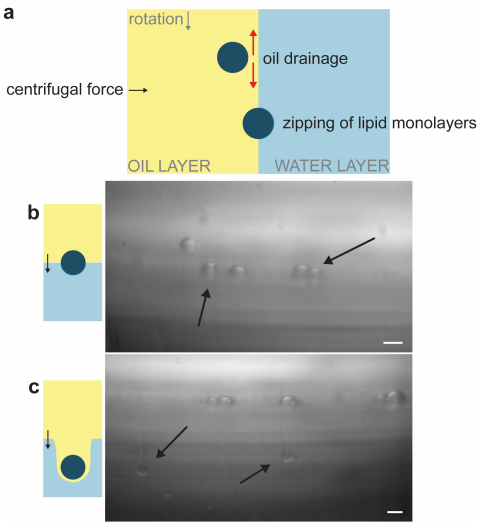

Figure 4.5 | Droplet transfer through the oil-water interface is suboptimal. (a) The lipid-in-oil dispersion in between the approaching lipid monolayer-covered droplets and the oil-water interface needs to be drained for the two monolayers to zip together and successful GUV formation to occur. (b) When droplets are not fully covered by a lipid monolayer when reaching the oil-water interface, successful transfer cannot occur and instead, stationary, semi-transferred droplets are observed. Scale bar indicates 100 µm. (c) When drainage of the oil layer between the approaching droplet and oil-water interface is insufficient, the formation of comet tails can be observed: a droplet distorts the oil-water interface and drags the lipid-in-oil dispersion into the outer aqueous solution, hindering successful GUV formation. The scale bar indicates 100 µm.

Comparing cDICE GUV size distributions to those obtained by eDICE, a recent adaptation of cDICE where the droplets are generated by vortexing, pipetting, or scraping instead of a capillary, but transferred through an oil-water interface in a rotational chamber,

identical to cDICE.[174] Interestingly, we noticed that the final GUV size distribution were similar for the two methods[174], despite vastly different droplet size distributions were used as a starting point (Figure 4.14). Furthermore, we found GUV sizes to be remarkably similar for different membrane compositions in eDICE (Figure 4.15). Taken together, these cDICE and eDICE results indicate a yet unknown mechanism for size-selectiveness at the oil-water interface that promotes the production of similarly-sized GUVs for a wide distribution of droplet sizes. For example, it is possible that GUVs form at the oil-water interface in cDICE and eDICE by pinching off from larger droplets sitting at the interface. While we did not observe any event like this, we would expect this process to happen on a length scale (and possibly time scale) beyond the resolution of our imaging setup.

4.3 Conclusion

In summary, by designing and building a custom imaging setup to visualize droplet formation and droplet interface transfer in cDICE in real-time, we were able to, for the first time, collect direct *in situ* imaging data to further understand the underlying mechanisms governing GUV formation in this technique. We found that droplet formation at the capillary orifice produced droplets that are much larger than the size of the final GUVs. For a capillary diameter of 100 μm, the formation of droplets in cDICE bears some similarities with the formation of droplets at T-junctions in microfluidics, a well-studied phenomenon.[175,176] In such microfluidic channels, the geometric confinement provided by the channels leads to flow restrictions on the continuous phase at the origin of a squeezing pressure. This pressure promotes droplet break up at much smaller values of Ca as compared to our experiments. However, there are similarities in the droplet formation regimes. For example, a decrease in droplet volume for increasing values of Ca has been widely reported.[175,176] These studies have also reported a transition from a breakup droplet formation mechanism for low values of Ca to a dripping mechanism at higher Ca, whereby a long thread of the dispersed phase forms and droplets pinch off at the end of the thread. This is in contrast to the use of smaller capillary openings in the original cDICE implementation, in the range of 2-25 μm[93], where the smaller inner diameter of the capillary leads to smaller droplet sizes by a combination of smaller total interfacial force resisting the breakup of the droplet and a smaller Reynolds number. Only as a side process, smaller satellite droplets are being formed. Even smaller droplets, including GUV-sized droplets, could not be resolved due to the limited resolution of our setup. Furthermore, we showed that the addition of protein to the inner solution increases its viscosity and changes interfacial tension dynamics, both directly impacting droplet formation and interface transfer. Imaging of the oil-water interface revealed that droplet transfer is frequently stalled, sub-optimal for large droplets, and exhibits a size-selectivity. This size-selectivity of droplet transfer to GUVs was further confirmed using eDICE, a variant of cDICE where no capillary is used, which yielded similar size distribution despite vastly different droplets as input. Further studies are needed to further elucidate the effect of lipid composition, including cholesterol or charged lipids, and different proteins or protein mixes. We believe the presented results can be of interest not only for cDICE but to other emulsion-based GUV formation methods as

well, ultimately contributing to the development of more reliable and efficient methods for GUV production. Our study furthermore emphasizes the need for inter-disciplinary collaboration to fully grasp the intricacies of the processes involved in emulsion-based GUV production methods. Altogether, this research is just a prologue to a larger narrative and we hope it will serve as a stepping stone for future research, enhancing emulsion-based GUV formation along the way.

4.4 Methods

4.4.1 Design and fabrication of the spinning device

The cDICE device was identical to Van de Cauter *et al.*[157]. An additional opening underneath the spinning chamber was created by removing part of the motor housing. This way, the light source could be placed directly below the spinning chamber to achieve transillumination. The design for the adjusted cDICE device is available on GitHub (https://github.com/GanzingerLab/cDICE_microscope).

4.4.2 Fabrication of spinning chambers

Transparent, cylindrical chambers, 35 mm in diameter and 10 mm in height, were made from two lids of Petri dishes (Falcon® REF 351008). To create a waterproof, closed chamber, the sides of the two lids were first sanded using sandpaper to create a rough surface after which they were glued together using a thin layer of optical glue (Norland Optical Adhesive 81). After curing of the glue using UV light, the side of the chamber was wrapped with a strip of Parafilm®. The chambers include a circular opening of 15 mm in diameter in the top to allow facile access to the solutions with the capillary.

4.4.3 General cDICE experimental workflow

While it is possible, and needed, to tweak various operational parameters to encapsulate a particular (non-)biological system in cDICE, we chose to use the parameters established in a recent optimization study by Van de Cauter *et al.*[157] as the default conditions for cDICE. Specifically, we used a 100 µm diameter capillary, a rotation speed of 1900 rpm, and a flow rate of 25 µL min^{-1}. For the lipid-in-oil dispersion, 18:1 1,2-dioleoyl-sn-glycero-3-phophocholine (DOPC) lipids were dispersed using chloroform in a mixture consisting of a 4:1 ratio silicon oil:mineral oil. A fused silica capillary tubing with polyimide coating (TSP-100375, Molex LLC) was used to inject inner aqueous solutions. The general cDICE experimental workflow and preparation of lipid-in-oil dispersion was based on Van de Cauter *et al.*[157]. The following parameters differed: The volume of the outer solution was increased to 1.07 mL to account for the difference in dimensions between the 3D printed spinning chambers, as used in Van de Cauter *et al.*[157], and the Petri dish spinning chambers that were used for imaging experiments, as mentioned above. Room humidity was not controlled during imaging experiments and the chambers were spun for the entirety of the imaging experiments instead of a predetermined time. G-buffer (5 mM tris(hydroxymethyl)aminomethane hydrochloride (Tris-HCl) pH 7.8 and 0.1 mM calcium chloride ($CaCl_2$), 0.02 mM adenosine triphosphate (ATP) and 4 mM dithiothreitol (DTT)) with 18.5 % v/v OptiPrep™ was encapsulated in every experiment (to achieve a density

difference between the inner and outer aqueous solution), unless specified otherwise. For experiments with a silanized capillary, the fused silica tubing was submerged for one minute in dichlorodimethylsilance (DMDCS) (40140, Sigma Aldrich), before removing excess with nitrogen gas.

4.4.4 Home-built imaging setup

The light of a single LED (Luxeon V2, 315lm@700mA; used without lens) or a Lumencor light engine (SOLA 6-LCR-SB) was collected by a 200 mm focal length achromatic lens (Thorlabs AC254-200-A-ML; lens mount: Thorlabs CXY1). The setup was equipped with a 4x or 10x objective (Nikon Plan Fluor 4x/0.13 PhL DL and Nikon Plan Fluor 10x/0.30 ∞/0.17 WD 16, respectively) that was mounted on a Z-stage (Thorlabs CT1; adapter: Thorlabs SM1A10). X/Y motion control was provided by two translational stages with a step size of 25 mm (Thorlabs PT1). Images were recorded using a high-speed camera (Kron Technologies Chronos 2.1-HD and Photron FASTCAM SA4) which was mounted on the setup using a custom-designed 3D printed construction. The full setup was mounted on a Thorlabs cage system that was mounted on a breadboard (Thorlabs MB1030/M) to easily move the full setup over the cDICE device. The full component list and design plans, including a 3D model of the setup, can be found on GitHub (https://github.com/GanzingerLab/cDICE_microscope).

4.4.5 Droplet size analysis

Droplet size analysis was performed manually using the Fiji software[177]. The image pixel size was derived from three independent measurements of the capillary opening, accounting for capillary size uncertainty. Triplicate measurements were performed for a subset of each dataset to quantify the measurement error. For each droplet, we then measured both area and diameter, yielding two independent measurements of the droplet diameter with associated error calculated through error propagation. The large pixel size ((2.431 ± 0.105) µm) in comparison to the droplet size characterized, in combination with a measurement error of 2 µm, calculated from measuring a subset of data in triplicate, posed a limit on our analysis. Additionally, the high speed of the process, resulting in motion blur and droplets quickly moving out of focus, as well as the limited contrast, caused by the small difference in refractive index between the droplets and the surrounding medium (1.333 for water *vs* 1.403 for silicone oil), makes it difficult to distinguish the droplets from the background in the video recordings. Data visualization was achieved through Python-generated plots. The frequency was estimated using the mean droplet size and the flow rate of the inner solution. Note that for the analysis of droplet size and frequency, we used video recordings in which the liquid filament did not adhere to the capillary surface (one experiment per condition).

4.4.6 Viscosity measurements

The dynamic viscosities of the solutions were measured on a Kinexus Malvern Pro rheometer. A stainless steel plate-plate geometry with 40 and 20 mm radius were used for buffer solutions and protein-containing solutions respectively. Viscosity was

measured every 5 seconds as a function of shear rate with a 2 min logarithmic viscometry ramp from 0.5 s^{-1} to 100 s^{-1}. As expected for simple viscous liquid, viscosities for higher shear rate were constant. The values at 100 s^{-1} were used to calculate the reported viscosity of each solution. MRB80 buffers consists of 80 mM piperazine-N,N'-bis(2-ethanesulfonic acid) (PIPES) pH 6.8, 4 mM magnesium chloride ($MgCl_2$), and 1 mM ethylene glycol-bis(beta-aminoethyl ether)-N,N,N',N'-tetraacetic acid (EGTA).

4.4.7 Tensiometry measurements

The pendant drop measurements were performed using a DSA 30S drop shape analyser (Kruss, Germany) and analysed with the Kruss Advanced software. Experimental conditions for G-buffer and actin-containing solutions were as described in Van de Cauter *et al.*[157], while changes for MRB80 buffer and tubulin-containing solutions are described below. Initially a 2 µL droplet of aqueous solution is drawn in a lipid-in-oil dispersion containing glass cuvette (Hellma Analytics) and then volume of the droplet is adjusted to 8 µL using an automated dosing system from a hanging glass syringe with needle diameter of 0.313 mm (Hamilton). As soon as the droplet reached its final volume, droplet was analysed (for 300 seconds at 25 fps for solutions containing tubulin and lipids and at 5 fps for rest of the solutions) by automatic contour detection and fitted with the Young-Laplace equation to yield the interfacial tension. The densities of lipid-in-oil dispersion (0.8685 g mL^{-1}), G-buffer with 18.5 %v/v OptiPrep™ (1.0574 g mL^{-1}), and MRB80 with 1.75 %w/v sucrose (1.0066 g mL^{-1}) were used in the interfacial tension calculations. These densities were measured by weighing 1 mL of solution. For G-buffer with OptiPrep™, the density was estimated using the volume-weighted-mean. The surface tension values were smoothened with a rolling-mean of 1 s. Room humidity was not controlled. In several experiments, interfacial tension decreased very rapidly (abnormally), causing the droplet to detach as soon as they are formed. These measurements were discarded from analysis.

4.5 Acknowledgements

We thank Roy Hoitink for his contributions during the initial exploration of the imaging setup, SaFyre Reese for experimental help during parameter screening, and Irene Istúriz Petitjean for help with rheology experiments. We would also like to thank Dr. Arjen Jakobi for generously lending us the Chronos 2.1-HD camera, and Iliya Cerjak and Bob Krijger for technical help with the design of the imaging setup and the light source, respectively. We acknowledge financial support by the "BaSyC – Building a Synthetic Cell" Gravitation grant (024.003.019) of The Netherlands Ministry of Education, Culture and Science (OCW) and The Netherlands Organization for Scientific Research (NWO) (M.D. and G.H.K.) and NWO-WISE funding (K.A.G.). Part of this research was funded by a Pieter Langerhausen Stipendium of the Koninklijke Hollandsche Maatschappij der Wetenschappen (K.A.G).

4.6 Appendix

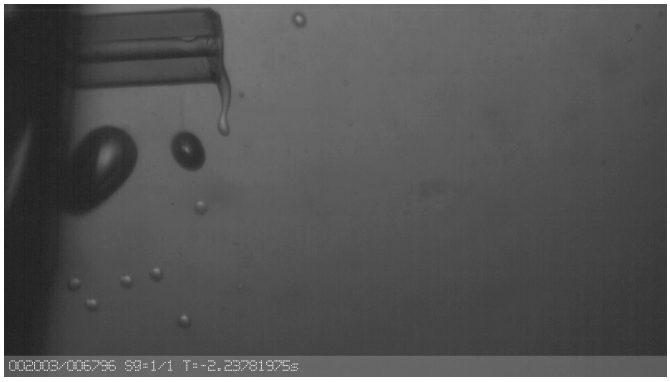

Figure 4.6 | Droplet formation at the capillary orifice at a rotation speed of 1900 rpm. Video recording of droplet formation at the capillary orifice at a rotation speed of 1900 rpm. The playback speed is 10 fps for a total of 250 frames. The capillary opening is 100 µm.

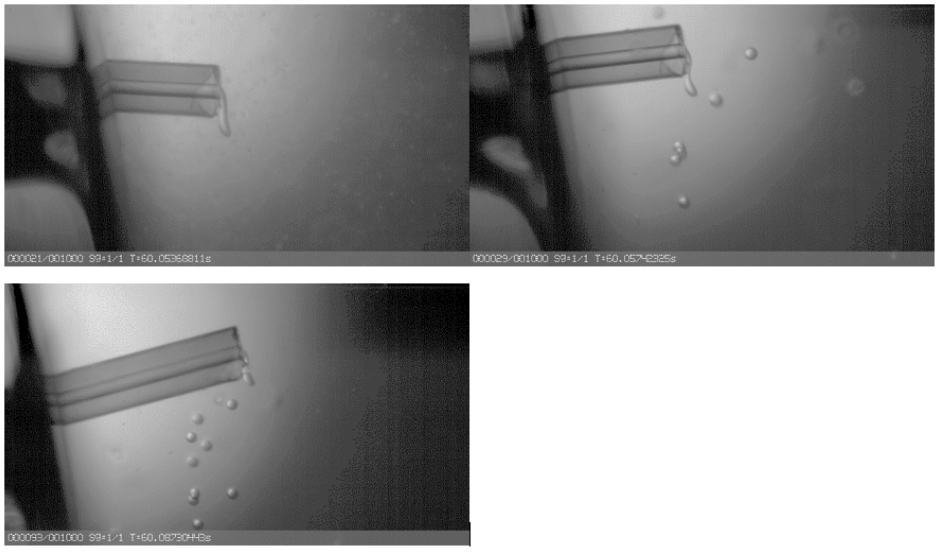

Figure 4.7 | Silanization of the capillary prevented attachment of the liquid thread to the capillary. Representative field-of-views, differences can be seen in insertion angle, insertion depth, and capillary orifice. In all three cases, the capillary was silanized, and the liquid filament did not adhere to the capillary. The capillary was silanized using dichlorodimethylsilane (40140, Sigma Aldrich) by submerging the tip of the capillary for one minute, before removing excess with nitrogen gas. The capillary opening is 100 µm.

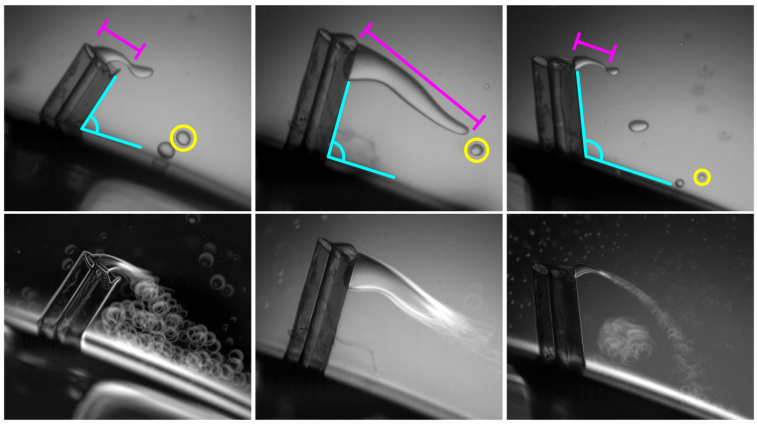

Figure 4.8 | Representative field-of-views highlighting the high inter-experiment variability in droplet formation at the capillary orifice at a rotation speed of 1900 rpm. Microscopy images capturing droplet formation at the capillary orifice at a rotation speed of 1900 rpm in independent, consecutive experiments using the same capillary. The inner solution consists of PBS buffer with 18.5 % v/v OptiPrep™. For identical experimental conditions, noticeable differences can be seen, e.g. in insertion angle (top row, cyan), liquid filament (top row, magenta), droplet size (top row, yellow) and motion (bottom row). Bottom row: standard deviation stack projection of 100 frames (every 50th frame of 5000 frames). White highlights indicate variations in movement, such as the occurrence of a droplet vortex in the wake of the capillary (left and right image) and the movements of the liquid filament end (left and middle). The capillary opening is 100 µm in all cases.

Figure 4.9 | Droplet formation at the capillary orifice at a rotation speed of 2700 rpm. Video recording of droplet formation at the capillary orifice at a rotation speed of 2700 rpm. The playback speed is 10 fps for a total of 250 frames. The capillary opening is 100 µm.

Figure 4.10 | Droplet formation at the capillary orifice at a rotation speed of 1000 rpm. Video recording of droplet formation at the capillary orifice at a rotation speed of 1000 rpm. The playback speed is 10 fps for a total of 250 frames. The capillary opening is 100 µm.

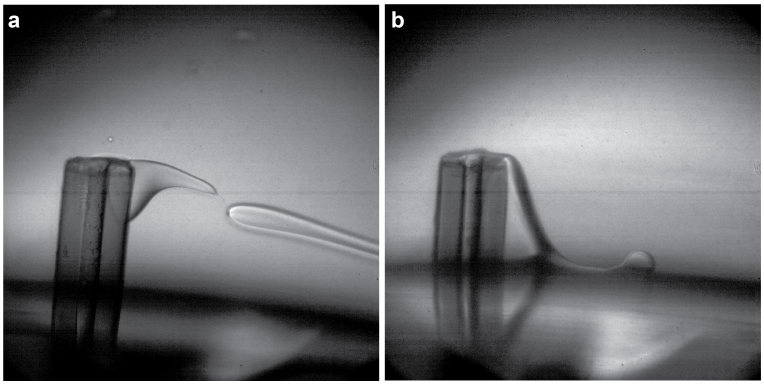

Figure 4.11 | Droplet formation of protein-containing solutions at the capillary orifice at a rotation speed of 1900 rpm. Video recordings of droplet formation at the capillary orifice at a rotation speed of 1900 rpm for an (a) actin-containing solution (1 µM in G-buffer, 6.5 % v/v OptiPrep™), and (b) tubulin-containing solution (33.33 µM in MRB80 buffer, 1.75 % w/v sucrose). The playback speed is 10 fps for a total of 250 frames. The capillary opening is 100 µm.

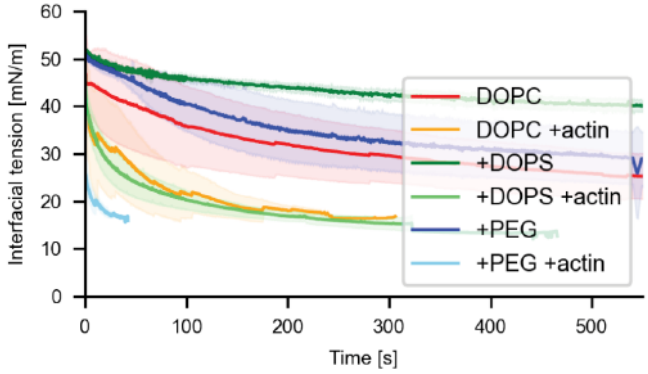

Figure 4.12 | Interfacial tension evolution with and without actin using different lipid compositions. Each curve represents the average over N measurements with the shaded region being the standard deviation. Only DOPC against inner aqueous solution (G-buffer with 18.5 % v/v OptiPrep™) without (red line, N=21) and with (orange line, N=19) 4.4 µM actin, DOPC with 20 % DOPS against inner aqueous solution without (dark green line, N=2) and with (light green line, N=3) 4.4 µM actin, and finally DOPC with 5 % PEG 2000 DOPE measured against inner aqueous solution without (dark blue line, N=3) and with 4.4 µM actin (light blue line, N=3). Total lipid concentration is 0.2 mg mL^{-1}.

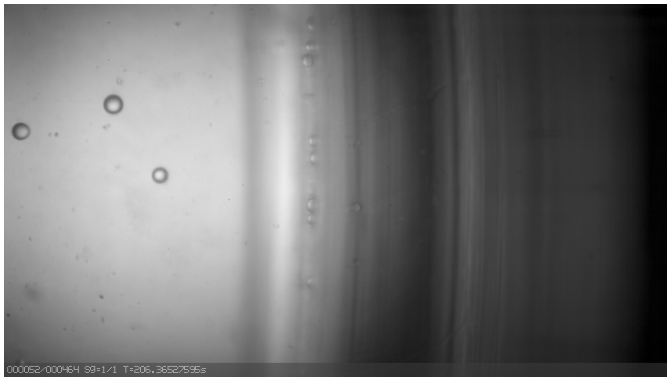

Figure 4.13 | Oil-water interface. Video recording of the oil-water interface. The playback speed is 2 fps for a total of 250 frames.

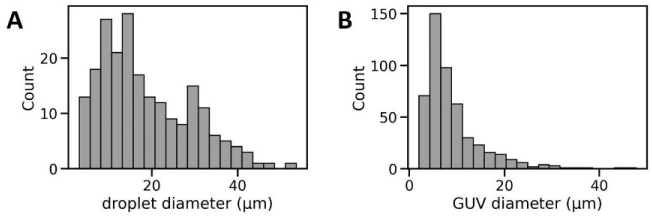

Figure 4.14 | Size distribution of droplets and GUVs in eDICE. (a) Histogram of the diameters of droplets generated in the first step of eDICE (N = 213 droplets from 2 separate experiments). Droplets contained 4.4 µM actin in F-buffer with 6.5 % v/v OptiPrep™ and were stabilized by surfactants in addition to lipids. (b) Histogram of GUV sizes generated by eDICE (N = 494 GUVs from 4 separate experiments).

eDICE GUVs were prepared as described in Baldauf *et al.*[174]. Emulsion droplets were produced in an identical fashion to those produced in the intermediate GUV preparation step in eDICE, where we emulsified disperse phase into 1 mL of oil phase by mechanical agitation. To allow us to image the aqueous droplets in oil, we additionally dissolved 2 % v/v Span80 (Sigma Aldrich) in the oil phase to stabilize the interface. This addition of surfactant was necessary to keep the droplets from coalescing before or during the ~ 30 min necessary for imaging, but it changes the interfacial properties and may thus have an impact on the droplet size distribution we generate. The addition of extra surfactant has been shown to decrease the average size of emulsion droplets generated in turbulent flow, so our measurements likely underestimate the true size of droplets generated during the eDICE GUV formation process. Epifluorescence images of water-in-oil droplets and GUVs were acquired on an inverted Nikon Ti Eclipse microscope equipped with a 60x water immersion objective (CFI Plan Apochromat VC), a digital CMOS camera (Orca Flash 4.0), and an LED light source (Lumencor Spectra Pad X). Phase contrast images were acquired on the same Nikon Ti microscope.

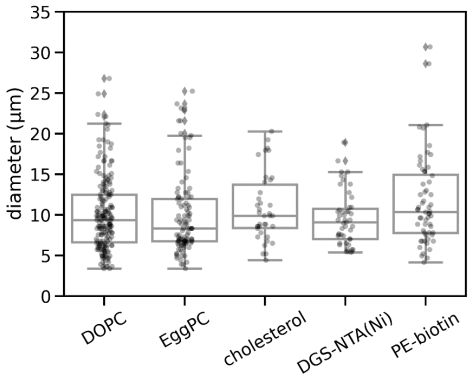

Figure 4.15 | Size distribution for GUVs produced using eDICE with various membrane composition. GUVs with different membrane composition produced by eDICE (see table above; GUVs were prepared as described in Baldauf *et al.*[174]). The membranes for widefield imaging also contained 0.05 % Cy5-labeled lipids. GUVs with 5 % Biotin-PE in the membrane also encapsulated 0.88 µM Atto 488-conjugated streptavidin (Sigma Aldrich), all others are without encapsulated proteins. Sizes were measured manually in Fiji, fitting circles to max projections of a Z-stack. Box plots comparing the GUV sizes are displayed on the graph, the distributions are not statistically different (p=0.070 by one-way ANOVA). Epifluorescence images of GUVs were acquired on an inverted Nikon Ti Eclipse microscope equipped with a 60x water immersion objective (CFI Plan Apochromat VC), a digital CMOS camera (Orca Flash 4.0), and an LED light source (Lumencor Spectra Pad X). Phase contrast images were acquired on the same Nikon Ti microscope.

Table 4.1 | Details of lipid compositions used and results obtained in Figure 4.15

Composition	Mean(d)	Std(d)	n	Imaged by
100 % DOPC	10.08	4.49	187	Phase contrast
100 % EggPC	9.844	4.89	108	Phase contrast
80:20 DOPC:cholesterol	10.88	4.20	38	Phase contrast
95:5 DOPC:DGS-NTA(Ni)	9.522	3.32	47	Widefield
95:5 DOPC:bioPE	11.68	5.43	60	Widefield

CHAPTER 5

Exploring giant unilamellar vesicle production for artificial cells - Current challenges and future directions

▸ Creating an artificial cell from the bottom up is a long-standing challenge and, while significant progress has been made, the full realization of this goal remains elusive. Arguably, one of the biggest hurdles that researchers are facing now, is the assembly of different modules of cell function inside a single container. Giant unilamellar vesicles (GUVs) have emerged as a suitable container with many methods available for their production. Well-studied swelling-based methods offer a wide range of lipid compositions but at the expense of limited encapsulation efficiency. Emulsion-based methods, on the other hand, excel at encapsulation but are only effective with a limited set of membrane compositions and may entrap residual additives in the lipid bilayer. Since the ultimate artificial cell will need to comply with both specific membrane and encapsulation requirements, there is still no one-method-fits-all solution for GUV formation available today. This review discusses the state-of-the-art in different GUV production methods and their compatibility with GUV requirements and operational requirements such as reproducibility and ease of use. It concluded by identifying the most pressing issues and proposes potential avenues for future research to bring us one step closer to turning artificial cells into a reality.

Published as: L. Van de Cauter, L. van Buren, G. H. Koenderink, and K. A. Ganzinger, "Exploring Giant Unilamellar Vesicle Production for Artificial Cells - Current Challenges and Future Directions", *Small Methods*, vol. 7, no. 12, 2300416, 2023.

5.1 Giant unilamellar vesicles in the artificial cell landscape

Cells are the smallest units considered to be alive and in turn the building blocks for other, more complex, living organisms. Despite being the smallest unit of life, they exhibit a bewildering complexity at the molecular level. The questions of how those non-living molecular assemblies can give rise to living cells and what life truly is [178], has sparked great interest for many decades. The concept of rebuilding life from its molecular components [179] has led to the development of synthetic cell research, a new interdisciplinary scientific field, synchronized with the establishment of various national and international research initiatives to further the goals of recreating life [180](such as BaSyC in the Netherlands [67], MaxSynBio in Germany [72], fabriCELL in the UK [181], Build-a-Cell community in the USA [71], and the European Synthetic Cell Initiative in Europe [70]). Despite significant research efforts and a widespread public interest, the recreation of life in the lab in the form of an artificial cell remains an immensely challenging task that is still in its early stages today.

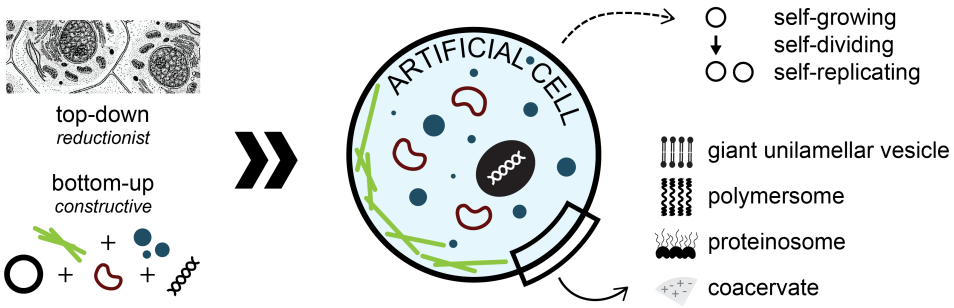

Figure 5.1 | Giant unilamellar vesicles in the artificial cell landscape. Schematic representation of the different strategies for constructing an artificial cell. A top-down approach involves modifying components in their biological context, while a bottom-up approach relies on the stepwise integration of different building blocks in a well-defined chemical environment. The aim is to construct an artificial cell, which we define as a self-growing, self-dividing, and self-replicating entity. Compartmentalization is a crucial step in the construction of such an artificial cell, and possible strategies involve the use of giant unilamellar vesicles with a lipid bilayer, polymersomes, proteinosomes, or coacervates as the container.

Generally, there are two possible strategies to constructing an artificial cell (Figure 5.1). The classic biological approach (also called a top-down or *in vivo* reductionist approach), which involves modifying components in their biological context, has provided valuable insights in vital genes [182,183], but has limitations in unravelling mechanistic working principles. The biological context is so overwhelmingly complex (human cells have 20,000 genes [184] and typical number density is 0.2 to 4 million protein molecules per cubic micron [185]), that it is generally challenging to unequivocally attribute a particular function to a single component. Even more difficult than understanding how single components function within the cell, is to understand how cooperation between molecules can give rise to complex emergent processes such as cell division and migration. [186] A top-down approach thus offers limited understanding of how life is assembled from its

non-living parts.[187] Instead, to obtain a mechanistic understanding of cellular parts and processes, it is often necessary to isolate the components of interest and study them in a well-defined chemical environment.[188] This bottom-up or constructive approach has gained significant traction over the past three decades and, in concert with technological advances, scientists have been aiming to reconstitute cellular processes of increasing complexity.[107,187] Typically, the aims of this bottom-up strategy are twofold: on the one hand the focus is on acquiring fundamental knowledge on the building blocks of life and how they interact, while on the other hand, efforts are directed toward engineering a fully artificial cell. The general strategy here involves enhancing complexity through the stepwise integration of different building blocks or modules in both time and space, eventually recreating complex dynamic processes like cell growth, replication, and division. At the same time, reconstituted systems of intermediate complexity hold potential in for example medical applications, e.g. as artificial blood cells or for drug-delivery.[189,190] In this review, we will think of an artificial cell as a self-growing, self-dividing, and self-replicating entity, constructed from the bottom up by integrating the various components needed inside a compartment (Figure 5.1).

An essential step for building artificial cells from the bottom up is hence the construction of a 'container' for its components. Compartmentalization is not only a fundamental feature of life but is often also considered to be essential for enabling life and its out-of-equilibrium chemistry in the first place.[132] The molecular content of an artificial cell thus needs to be contained within an aqueous compartment, in which all reconstituted cellular processes can take place. To allow for growth and division, this compartment should also have a deformable envelope. While proteins and metabolites stay confined, the container should allow for selective import of nutrients and export of waste products to grant survival. Structurally, a large array of design strategies for creating such compartments exists, all offering different benefits and drawbacks.[191] Possible strategies include membrane-less compartments (coacervates[192]), compartments confined by membranes composed of polymers (polymersomes[193,194]), proteins (proteinosomes[195]), or lipids (liposomes[73,196,197]), or hybrid approaches[198,199]. Given that all life as we know it is compartmentalized by lipid membranes across all kingdoms of life[200,201], liposomes are the closest mimic to biological cells and therefore ultimately the best choice as the compartment for an artificial cell made to closely mimic its biological inspiration. The use of liposomes also ensures compatibility with other biological building blocks, such as membrane-bound enzymes and transporters. Moreover, the size of giant liposomes, or giant unilamellar vesicles (GUVs), is similar to the size of eukaryotic cells (5 - 100 μm)[73]. These cell-like properties and their biological compatibility make GUVs the perfect chassis for building an artificial cell and, unsurprisingly, GUVs have already been used for a wide range of research applications in biophysics, biomedicine and synthetic biology.[73]

5.2 GUVs as the container for artificial cells - What are the requirements?

To achieve the properties and functions desired for an artificial cell, GUVs must satisfy a broad range of requirements (Table 5.1). A first important criterion to consider is size and the ability to tune the final size as desired. The GUV size sets the degree

of confinement and surface-to-volume ratio, which in turn influence growth (via lipid production), division (via establishment of cell polarity by reaction-diffusion and/or cytoskeletal systems), and replication (via energy metabolism).[202] Further requirements can be divided into two categories: the requirements for the container itself, *i.e.* the membrane surrounding the aqueous solution, and the requirements for the lumen, *i.e.* the encapsulation of different components.

Lipids are a highly diverse group of biomolecules with varying structures and properties.[203,204] While they all share the common property of having a hydrophilic head and two hydrophobic tails, which ensures their self-assembly into bilayers, they vary in head group size and charge (dependent on pH), length of hydrocarbon tails, and saturation of the tails. As such, lipid properties regulate interactions within the bilayer, thereby determining membrane elasticity and fluidity, as well as interactions with the external environment, like electrostatic interactions with proteins and ions. An important property arising from the lipid structure is its molecular shape, or intrinsic curvature, which determines the spontaneous curvature once assembled into mono- or bilayers.[205,206] Lipids with cylindrical molecular shapes lead to the formation of flat bilayers, while conical-shaped lipids lead to curved membranes. Certain lipids in cell membranes play important roles in the function of membrane proteins, anchoring of cytoskeletal proteins, or in signaling. Examples are phosphatidylserine, which interacts with many proteins via electrostatic interactions, and phosphoinositides, which play a prominent role in signaling processes.[207,208] In addition to lipids, biological membranes also contain other important molecules such as cholesterol in animal cells or hopanoids in bacteria[209]. Cholesterol, a hydrophobic organic molecule with a small hydrophilic head group, is a key component of animal cell membranes as it integrates into the bilayer where it modulates lipid packing, thereby controlling fluidity, permeability, and elasticity (reviewed in[210,211]). Being able to use a large range of lipids, including synthetic and natural lipids, and the option to include cholesterol is therefore crucial for producing a GUV-based artificial cell. Synthetic lipids can further be functionalized with a variety of synthetic polymers or interacting groups, e.g. poly(ethylene glycol) (PEG) linkers, fluorescent labels, nickel chelating groups, or azobenzene moieties. This functionalization can provide additional properties to the membrane, such as reducing nonspecific interactions[212], generating photoswitchable lipids[213], selective anchoring of molecules or proteins to the inner or outer leaflet, and more.

In biological membranes, the bilayer is compositionally asymmetric, with the inner leaflet being different in lipid and protein composition from the outer leaflet. This transmembrane asymmetry is vital for cell signaling, functioning, differentiation, and growth[214] and occurs because lipids cannot easily transfer from one leaflet to the other[215], a process known as flip-flop. In turn, compositional asymmetries give rise to spontaneous curvature effects, which in protein-free lipid membranes are known to lead to membrane deformations such as lipid nanotubes.[216] Besides compositional asymmetry, this spontaneous curvature can also be generated by an asymmetry of the presence of membrane-interacting solutes such as sugars[217], ions[218], and proteins[219]. Mimicking the asymmetrical bilayer composition of biological membranes in GUVs is

thus a way of enhancing complexity and transcending to more biologically relevant compositions, necessary for, for example, reconstituting cell-cell interactions.

Lipid bilayers are permeable to hydrophobic molecules and small uncharged polar molecules like water, but not to protons, ions, and large uncharged polar molecules like sugars and proteins.[220,221] This permeability can be modulated by altering the lipid composition, providing a means to fine-tune its properties.[222] As water can move across the membrane but solutes cannot, GUVs are subject to osmosis. *In vitro*, controlled osmosis allows for deformability and control of excess membrane area and membrane tension. *In vivo*, permeation of ions and large molecules is facilitated by membrane proteins such as transporters and channels.[223,224] For the construction of a GUV-based artificial cell, it would thus be desirable to have the ability to incorporate membrane proteins into GUVs.[225] To achieve this, a unilamellar membrane, and the absence of residual solvents or additives, is of particular importance.[225]

Table 5.1 | Overview of requirements for GUVs as the container of an artificial cell.

Category	Requirement	Considerations
general	size	5 - 100 µm range
		size control
membrane	composition	synthetic lipids
		natural lipids
		cholesterol
	functionalization	functionalized lipids
	compositional asymmetry	
	controlled permeability	to allow deformability for growth and division
	protein reconstitution	transmembrane proteins
	unilamellarity	for protein reconstitution
		mechanical properties
		for permeability control
	cleanliness	absence of residual oil and other inclusions
	mechanical stability	for manipulation, observation, and longevity
encapsulation	physiological buffers	physiological ionic strength (50 - 150 mM)
		absence of auxilary molecules
	efficiency	
	complex reconstitution	multiple components in right stoichiometry
	cross-compatibility	different biological systems within a single GUV

The unilamellar lipid bilayer furthermore affects the mechanical properties of GUVs, which determine the possible shape transformations and mechanical stability. The mechanical properties of GUVs are influenced by a range of physical parameters, including the membrane's bending rigidity, stretching modulus, and tension.[81] Membrane 'cleanliness', alluding to the membrane being composed of a controlled number of bilayers, with no entrapments, residual oil, or other inclusions altering the above-mentioned criteria, is an especially important criterion to consider with regard to mechanical properties. The mechanical properties of GUVs are crucial for the successful reconstitution of pro-

cesses that affect its size and shape (e.g. growth and division) as well as for the ease of experimental manipulation, observation, and longevity. However, GUV membranes are naturally unstable and lack robust mechanical properties as compared to their natural counterparts, cell membranes. As reviewed in Wubshet *et al.*[226], GUV stability can be enhanced by membrane modulation, e.g. by tuning the lipid composition, changing bilayer asymmetry, or altering the cholesterol concentration, or by luminal modulation, e.g. by encapsulating cytoskeletal components or other, structurally relevant molecules.

So far, we discussed the membrane requirements for GUVs, yet the membrane only comprises half of the challenge. Requirements concerning the lumen of the GUV, or encapsulation of molecules, are equally important. GUVs must be able to encapsulate physiological buffers (50 - 150mM) in absence of any type of chemical that can interfere with biological processes. Furthermore, it is important to have the ability to achieve complex, multi-component reconstitutions in which different types of proteins or protein machineries are efficiently encapsulated in the right stoichiometries. Moreover, emphasis should be placed on cross-compatibility, *i.e.* the ability to encapsulate diverse biological systems in a single GUV, which are often reconstituted under different buffer conditions. An ideal system should thus be able to accommodate multiple biological systems with ease, with a minimum of auxiliary molecules that may hinder their normal functioning.

In essence, producing GUVs for artificial cells thus requires meeting two main goals: having a complex and biologically analogous membrane while achieving a multi-component lumen. Careful consideration of these requirements is necessary to produce GUVs that can accurately mimic the physiological environment of a cell, and consequently serve as a suitable container for an artificial cell.

5.3 Overview of available methods for GUV production

Over the past 50 years[77], numerous methods for producing GUVs have been developed.[73,74] Currently, more than twenty different techniques exist, giving offspring to hundreds of different protocols, ranging from relatively straightforward bulk techniques to sophisticated microfluidic assembly lines.[88,107,226,227] GUV production methods are typically classified into two main categories: swelling-based approaches, which rely on rehydrating dried lipid bilayers, and emulsion-based approaches, where lipids are initially adsorbed to water-oil interfaces and a bilayer is only formed after subsequent transfer through an oil-water interface (Figure 5.2).

Originally proposed swelling methods involved hydration of a lipid film in aqueous environment, commonly referred to as natural or spontaneous swelling or gentle hydration.[77] Later, Angelova *et al.*[78] showed this natural swelling process could be accelerated by the application of an alternating electric field, leading to the development of electroformation. Historically, swelling-based approaches have been used widely in the biophysical community to study membrane biophysical properties outside of any cellular context, e.g. bilayer elasticity[228,229], lipid diffusion[230,231], membrane lateral organization[232], and membrane permeability[233]. While electroformation has been the gold standard for GUV formation since its invention, a major disadvantage has been the limited compatibility

of this method with charged lipids and physiological buffers. However, widespread research efforts have meanwhile led to the successful formation of GUVs in a wide range of buffer compositions while also incorporating a broad range of lipids, discussed in more detail in Rideau *et al.*[227] and Boban *et al.*[234,235]. Alternatively, porous hydrogels naturally promote GUV swelling in solutions of higher ionic strength.[82,83,115,142] However, gel-swollen GUV membranes can be contaminated with gel polymers, thereby leading to altered membrane properties.[236] To produce clean membranes, efforts have been concentrated on changing the physicochemical properties of the hydrogels[83], cross-linking the polymers[84], or using other (porous) substrates such as glass beads[148,237], and more recently, textile[238,239] and paper (PAPYRUS)[240,241]. Although these more recent techniques offer welcome simplicity and make GUV formation more accessible to a wider audience, they are still in their infancy. Altogether, a wide set of swelling-based GUV formation methods has been developed to produce GUVs with membranes of varying compositions, in buffers of different ionic strength. Notwithstanding these valuable results, swelling-based techniques generally only have limited compatibility with more complex biological reconstitution experiments as efficient encapsulation of large and charged water-soluble molecules remains hard to achieve using these methods.[73] This includes proteins, a synthetic genome, and other biomolecules that form the basis for the cell-mimicking content of artificial cells.

When complex encapsulation is required, researchers often resort to GUVs formed from emulsion droplets by emulsion-based techniques.[242] Here, water droplets are formed in an oil phase containing lipids, which adsorb to the droplet water-oil interface to create a lipid monolayer (*i.e.* water-in-oil emulsion). Next, after transfer of these droplets through another oil-water interface, likewise covered by a lipid monolayer, the droplets acquire a second lipid monolayer and transform into GUVs. As opposed to swelling-based methods, emulsion-based methods thus make use of solvent-displacement. This can lead to the undesirable entrapment of residual additives in the final lipid bilayer, thereby possibly altering the mechanical properties of the GUV[73], which is often regarded as the most significant drawback of emulsion-based methods. However, owing to this two-step solvent displacement process, emulsion-based methods do offer the ability to control the inner aqueous phase independently from the outer aqueous solution, and furthermore allow assembly of the lipid monolayers one by one, enabling the assembly of asymmetric bilayers.[86,102,243,244] Despite the introduction of inverted emulsion just fifteen years ago, and the even more recent emergence of various related methods, emulsion-based methods have already allowed numerous advancements in complex reconstitution experiments in this comparatively short period.[98,127,157,242] Furthermore, the working principle of inverted emulsion is suitable for automation and has given rise to a plethora of microfluidic assembly techniques (e.g. octanol-assisted liposome assembly (OLA)[92], other PDMS-based microfluidic methods[136,245–249], or hybrid methods[86,250]; reviewed in[88,251,252]) which allow additional control over GUV size and *in situ* observation of GUV formation. In addition, several other techniques that offer enhanced control of the inverted emulsion process have been developed. One example is continuous droplet interface crossing encapsulation (cDICE)[93,157], and its recent adaptation termed

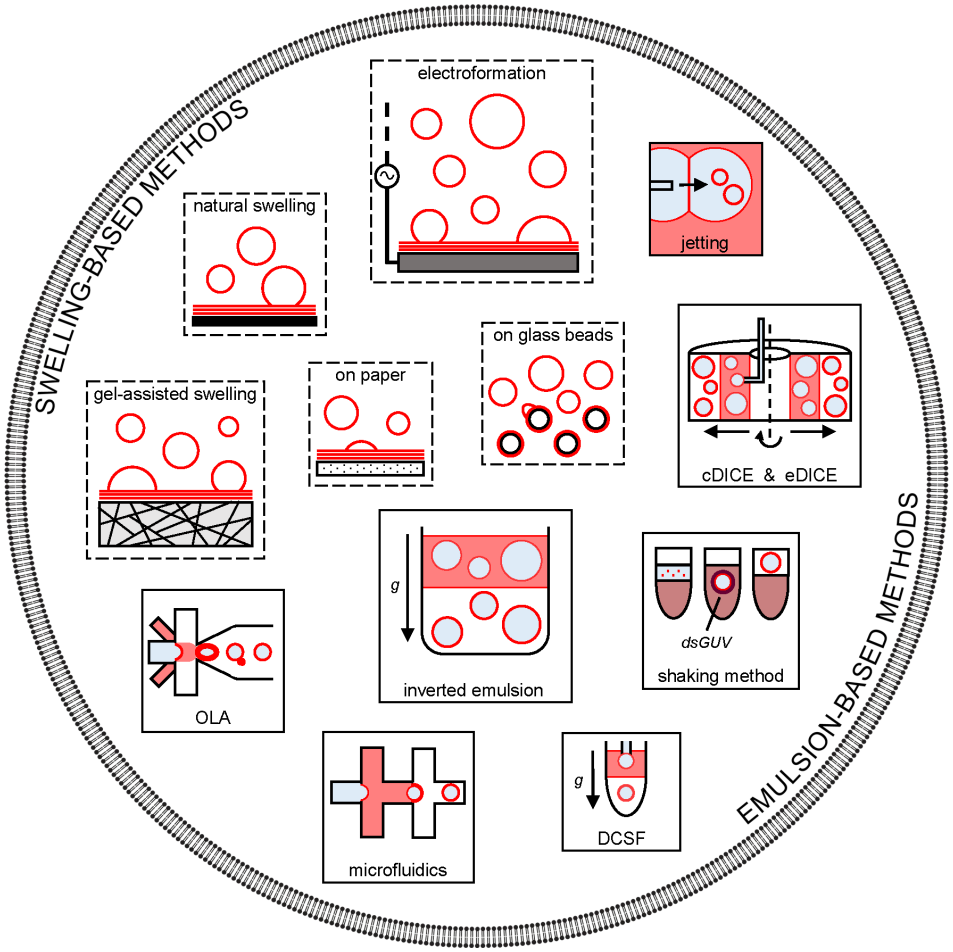

Figure 5.2 | Overview of GUV production methods. Generally, there are two different approaches to GUV formation. Swelling-based methods rely on natural hydration of a lipid film, while emulsion-based methods are based on the passage of a water-in-oil emulsion through an oil-water interface for bilayer formation. Swelling-based methods, indicated by the dashed lines, include natural/spontaneous swelling, gel-assisted swelling, swelling on various porous substrates such as glass beads or textile/paper, and electroformation. Emulsion-based methods, indicated by the solid lines, include inverted emulsion, microfluidic-based methods (e.g. octanol-assisted liposome assembly (OLA) and other PDMS-based microfluidic methods), jetting, continuous/emulsion droplet interface crossing encapsulation (cDICE/eDICE), the shaking method that forms GUVs via intermediate droplet-stabilized GUVs (dsGUVs), and droplet-shooting centrifugal formation (DSCF).

emulsion cDICE (or eDICE)[141,174,253], which have been successfully implemented for actin cytoskeleton reconstitution experiments by various labs.[93,95,141,157,174,254–256] Other successful examples are the shaking method, which uses droplet-stabilized GUVs as intermediates[257], and droplet-shooting centrifugal formation (DSCF), which makes use of a 3D-printed microcapillary[258]. While other techniques such as microfluidic jetting[89] have seen some success[90,259,260], they have not been widely adopted and further studies are needed to investigate the physicochemical properties of the resulting GUVs.

5.4 Strengths and limitations of current methods – a comparative, state-of-the-art overview

As discussed in the previous section, there are two main approaches to forming GUVs. Well-studied swelling-based methods offer a wide range of lipid compositions, but at the expense of a limited encapsulation efficiency. Emulsion-based methods, on the other hand, excel at encapsulation but have only been shown effective with a limited set of membrane compositions and may entrap residual additives in the lipid bilayer. Since the ultimate artificial cell will need to comply with both membrane and encapsulation requirements, there has been no one-method-fits-all solution so far. To compare the strengths and limitations of available GUV production methods, we review the state-of-the-art of different methods and their compatibility with the specific membrane and encapsulation requirements outlined in Table 5.1. Table 5.2 and 5.3 provide an overview of the compatibility of different methods with membrane and encapsulation requirements, respectively. Note that we did not include natural swelling, swelling on paper (PAPYRUS) or textile, and jetting due to their limited use, characterization, or applicability, respectively. Our discussion on microfluidic-based techniques specifically focuses on two key publications that have shown significant advances for the construction of artificial cells: OLA, as published by Deshpande *et al.*[92], and surfactant-free PDMS-based microfluidics, first published by Yandrapalli *et al.*[245]. For a comprehensive overview of other microfluidic-based techniques, we refer the interested reader to other reviews[88,251,252].

5.4.1 Size

All methods discussed can generate GUVs within the preferred size range of 5 - 100 µm in diameter. However, considerable differences arise when considering size control and size monodispersity. Microfluidic-based techniques, like OLA, provide tight control over GUV size through channel design of the microfluidic chip and dynamic control of the used flow rates.[92,245,261] Consequently, GUV monodispersity is the highest in these methods and they are the only ones offering high-throughput production of same-sized GUVs. Non-microfluidic emulsion-based methods generally produce less monodisperse GUV populations. DSCF, the newest method we found, does not report any GUV size distributions[258], but is thought to provide some selectiveness due to an inherent size filtration. For the inverted emulsion method and the shaking method using droplet-stabilized GUVs, no extensive size screenings and parameter studies have been reported to date, but recent studies gave first evidence that GUV sizes can be tuned to limited extent by changing the experimental conditions.[137,257] cDICE was originally presented as a promising method to allow for size tuning by controlling the capillary diameter used to

generate the emulsion droplets.[93] However, larger capillary openings have since become the default to overcome issues related to capillary clogging, resulting in a complete loss of size control.[157] The more recent adaptation of cDICE, eDICE, refrains from using a capillary and results in similar GUV size distributions as cDICE.[174] This indicates an inherent size selectivity in these methods beyond that induced by droplet formation at a capillary orifice, predominantly yielding GUVs with a diameter around 10 µm. By contrast, swelling-based methods typically result in an even more heterogeneous GUV size distribution.

While size control is useful for systematic screening, size polydispersity offers the advantage of screening size subpopulations within a single experiment, facilitating high throughput, provided that the GUV yield is sufficiently large.[148] Moreover, as experiments are often optically analyzed on a per-GUV basis, polydispersity in GUV size does not necessarily pose a disadvantage.

5.4.2 Compositional complexity of the lipid bilayer

Swelling-based methods allow for reconstitution of membranes with a wide set of lipid compositions. Both gel-assisted swelling and electroformation have considerable advantages over the original natural swelling method, which is why they have largely replaced the latter in the field.[227] Both methods have been shown to be compatible with a wide range of lipids, including synthetic lipids, charged (both anionic and cationic) lipids, and natural lipids, and to also allow for the incorporation of relatively high molar ratios of cholesterol, as reviewed in Rideau *et al.*[227]. Swelling-based methods, through swelling on heat-resistant surfaces, furthermore offer straightforward compatibility with elevated temperatures, making it possible to produce membranes with a wide set of phase transition temperatures, even including Archaeal lipid extracts with a melting temperature above 80 °C[262,263]. Incorporation of natural lipids or cholesterol into GUV membranes made by swelling on glass beads has not yet been shown experimentally.

While charged membranes can be reconstituted with electroformation, the charge affects the GUV formation process, requiring careful fine-tuning of the formation parameters. Steinkühler *et al.*[216] found charged lipids to distribute asymmetrically in electroformed GUVs, an effect which could be countered by careful tuning of the voltage and temperature during electroformation. At ratios of > 50% cholesterol, a demixing artefact occurred for electroformation, resulting in a lower final concentration of cholesterol when compared to the initial ratio. Boban *et al.*[235] showed this effect could be reduced by tuning the lipid deposition method.

All emulsion-based methods, except DSCF, have, likewise, been found to be compatible with anionic lipids. Two emulsion-based methods, the shaking method and inverted emulsion, have even successfully constructed GUVs using *Escherichia coli* polar extract, providing a close mimic to complex biological membranes.[257,264] Both methods have also been shown to work with cationic lipids.[257,265] In principle, cholesterol can be incorporated up to nominal ratios of 20 - 30% by the shaking method, inverted emulsion, and the OLA method, but the actual cholesterol content may differ from this input

concentration; in case of cDICE, it was for instance shown that cholesterol ended up in a lower stoichiometric ratio than expected[94]. This issue could be overcome by delivering cholesterol to already-formed GUVs using cholesterol-loaded methylated β cyclodextrin molecules.[94] Another adaptation of cDICE, called double layer cDICE[102], was introduced to overcome the cumbersome incorporation of cholesterol but has not led to any follow-up studies since. This sensitivity to cholesterol incorporation indicates a need for further clarification of the working principles of the emulsion-based GUV formation process.

While many methods have been shown to be compatible with different lipids, much less research has been conducted on the final stoichiometric ratios obtained in the lipid bilayer. As also illustrated by the examples above, a better understanding is needed of the extent to which different lipids and cholesterol are incorporated into the final membranes, so membrane functionality can be precisely tuned and controlled.

Obtaining an asymmetric bilayer composition requires sequential assembly of each lipid monolayer. Hence, asymmetry is inherently incompatible with swelling-based methods. Only inverted emulsion and eDICE offer the potential for obtaining a different lipid composition for inner and outer leaflet. Different groups have reported the assembly of asymmetric bilayers using inverted emulsion[243,244,266], but this has yet to be demonstrated using eDICE. We would like to note that jetting, which we did not include here due to its limited compatibility with artificial cell research, does offer a neat way of producing asymmetric GUVs, as first shown by Richmond *et al.*[91] and later by Kamiya *et al.*[259].

Reconstitution of transmembrane proteins in GUVs has been extensively reviewed by Jørgensen *et al.*[267]. In short, swelling-based methods generally allow for the direct incorporation of transmembrane proteins, yet protein dehydration is needed, which could potentially lead to denaturation in the process. Emulsion-based methods allow for transmembrane protein incorporation by solubilizing the protein in the oil phase, provided the protein is sufficiently soluble, but oil additives may be entrapped in the bilayer during incorporation. The shaking method is the only method providing a straightforward way of incorporating membrane proteins by making use of fusion of proteoliposomes during the GUV assembly process.[257] However, obtaining a controlled protein orientation is cumbersome, and generally, transmembrane protein reconstitution during GUV formation remains difficult. Several strategies exist for the incorporation of transmembrane proteins after GUV formation and encapsulation[225], which are not further discussed here.

It is useful to note that the total amount of lipids necessary for various methods varies significantly, typically being lower for swelling-based methods, with, for example, only ~ 10 µg of lipids required for gel-assisted swelling compared to ~ 1.5 mg for eDICE. The required quantity of lipids is particularly relevant when working with precious lipid samples, favoring swelling-based methods in those cases.

5.4.3 Mechanical properties of the GUVs

To mimic drastic shape changes during growth or division, it is important to consider the mechanical properties of GUVs. One common concern with emulsion-based methods is the possibility of entrapment of residual amounts of additives into the lipid bilayer during solvent displacement, which could affect the chemical and mechanical properties of the formed lipid bilayers. Since swelling-based methods do not rely on solvent displacement, these methods are not affected by this issue. However, in contrast to emulsion-based methods, swelling-based methods, by relying on the hydration of lipid bilayers, can more easily give rise to unwanted multilamellar vesicles.[148,234] Furthermore, it has been shown that swelling on some polymer gels such as agarose or polyvinyl alcohol (PVA), can lead to membrane contamination from molecules released from the gel support, resulting in altered membrane properties (e.g. increased permeability, altered membrane interfacial tension, and lowered diffusion coefficients for lipids).[82,227,236,268]

For all emulsion-based methods except DSCF, several control experiments have confirmed the minimal effects of residual additives on membrane properties. All emulsion-based methods have been shown to result in unilamellar bilayers, confirmed by leakage assays incorporating alpha hemolysin.[92,93,137,157,245,257] Furthermore, for none of the resulting GUVs, there were optically detectable traces of any residues in the lipid bilayer.[92,93,137,157,245,257] Fluorescence recovery after photobleaching (FRAP) has been used to study lateral lipid diffusion coefficients, and it was shown that both the OLA method, surfactant-free microfluidics, and the shaking method result in GUVs with similar lipid diffusion coefficients to electroformed GUVs.[138,245,257] Fluctuation spectroscopy has also shown that cDICE-formed GUVs exhibit a comparable bending rigidity to electroformed GUVs, while for inverted emulsion, somewhat lower values were found albeit these changes were not statistically different.[93,137] GUVs produced using the shaking method have additionally been analyzed using cryotransmission electron microscopy (cryoTEM) and zeta-potential measurements, which confirmed no significant effects of any potential residual additives present in the lipid bilayer.[257]

Despite these extensive control experiments, a recent study by Faizi *et al.*[269] showed an altered shear surface viscosity for GUVs produced using gel-assisted swelling and inverted emulsion, attributable to gel remnants and residual oil, respectively. For experiments requiring perfectly clean membranes, it is therefore worth noting that solvent-free electroformation sets the benchmark for clean lipid bilayers.[75,81] Overall, many membrane studies and extensive characterization have been carried out for swelling-based methods, unlike emulsion-based methods, which have not been studied as thoroughly in this aspect.

Table 5.2 | Overview of compatibility of different GUV production methods with membrane requirements based on state-of-the-art results.

	Method	Size[1]	Compositional complexity						Mechanical properties		References
			Synthetic	*Charged*	*Cholesterol*	*Natural*	*Asymmetry*	*Protein*[4]	*Residual additives*	*Characterization*[5]	
swelling	Gel-assisted swelling	-	⊠	⊠	⊠	⊠	□	⊠	agarose/PVA	++	82,83,115,227,270
	Swelling glass beads	-	⊠	⊠	□	□	□	□	N/A	◦	148,237,271–275
	Electroformation	-	⊠	⊠	⊠	⊠	□	⊠	N/A	+++	227,234,276–282
emulsion	Inverted emulsion	+	⊠	⊠	⊠	⊠	⊠	⊠	not significant[2]	+	98,127,137,139,164,242,264,265,283–294
	cDICE & eDICE	+	⊠	⊠	⊠[2]	⊠	⊠[3]	□	not significant[2]	+	93–96,98,101,108,141,157,174,253,254,256,295–297
	Shaking method	+	⊠	⊠	⊠	⊠	□	⊠	not significant[2]	+	257,298–301
	DSCF	+	⊠	□	⊠	□	□	□	not reported	◦	258,302
	OLA	++	⊠	⊠	⊠	□	□	□	not significant[2]	+	92,138,261,303
	Surfactant-free microfluidics	++	⊠	⊠	□	⊠	□	□	not significant[2]	+	245,304

5.4.4 Encapsulation of complex solute mixtures in physiological buffers

Encapsulation of macromolecules and essential small solutes in complex physiological buffers is indispensable for the reconstitution of a complex artificial cell. All discussed swelling and emulsion methods for GUV formation have been used with physiological buffers, often using standard protein buffers such as tris(hydroxymethyl)aminomethane (Tris) buffer, phosphate-buffered saline (PBS), or 4-(2-hydroxyethyl)-1-piperazineethanesulfonic acid (HEPES) buffer.

In emulsion-based methods, the outer aqueous solution is different from the inner aqueous solution but their osmolality needs to be matched, which is typically achieved by producing the GUVs in an outer aqueous solution supplemented with glucose. It is important to keep in mind that high concentrations of glucose can lower the pH of the outer solution, which in turn can have adverse effects on membrane properties. The lower pH is attributed to glucose's weak acidity resulting from the ability of its hydroxy groups to donate protons to water, in combination with the interconversion between the energetically favorable closed (α-D-glucopyranose), and open/linear (D-glucose) forms.[305,306] Additionally, emulsion-based methods such as inverted emulsion, cDICE, eDICE, and DSCF, require a density difference between the GUV interior and the outer solution for successful GUV formation. This can be achieved by adding equimolar concentrations of sucrose and glucose in the inner and outer solution, respectively. While concentrations up to 900 mM of sucrose/glucose have been used[283], the effect of these high concentrations of sugar on protein and membrane properties have barely been studied.[307] As an alternative to using sugars, density gradient medium OptiPrep™ has been successfully used in cDICE and eDICE.[98,141,157,174,253,256,296,297] In the case of OLA, glycerol is required in both the inner and outer solution, along with the nonionic triblock copolymer surfactant Poloxamer 188 (P188) in the outer solution. It is important to note that these additional additives, especially at the high concentrations typically used, will affect protein and membrane properties during the experiments.

Inverted emulsion has been used for, among other systems, reconstitution of actin cortices[127], encapsulation of tubulin[284], *in vitro* transcription-translation (IVTT) systems[139,264,285,287,290,292,293], RNA organelles[283], and FtsZ filaments[164,288], up to full *in vitro* reconstitution of the *E. coli* divisome machinery (including MinCDE, FtsZ and FtsA)[289]. Likewise, cDICE has been used to encapsulate a wide variety of systems. These include microtubules with kinesin motor clusters[96], an actomyosin network coupled to

[1] Size tuning and size monodispersity of GUVs for the different methods is categorized as follows: - (no size control whatsoever and/or large polydispersity), + (limited size control and/or relatively monodisperse GUV population), ++ (full size control and/or GUVs highly monodisperse).
[2] See in-text description for further details.
[3] Formation of asymmetric GUVs has not been demonstrated using this technique, however, the method in principle allows for the sequential assembly of lipid monolayers.
[4] Membrane protein reconstitution shown during the GUV formation process.
[5] Extent of characterization of resulting GUVs produced by a certain method is expressed as follows: ◦ (no characterization), + (limited amount of characterization studies; ≤ 2 publications), ++ (extensive characterization in literature; > 3 publications), +++ (used as benchmark for clean membranes, extensive characterization in literature).

the membrane[101] and contractile actomyosin rings[254]. Also the bacterial Min protein system[98], fascin-actin bundles[295] and keratin networks[95] have been encapsulated using cDICE. Successful encapsulation of IVTT systems has also been demonstrated.[157] Furthermore, cDICE has successfully been used to encapsulate colloids, red blood cells[93], small unilamellar vesicles (SUVs), DNA origami and even live bacteria[157]. Recently, there has been a clear shift from cDICE toward eDICE, implementing the proposed optimizations for cDICE presented in Van de Cauter *et al.*[157]. eDICE has since been used to reconstitute actin cortices nucleated by the Arp2/3 complex[256] and VCA[174] and reconstitution of actomyosin networks[141,295]. Similar results have been obtained using the shaking method: from encapsulation of F-actin with SUVs[298], a DNA cytoskeleton mimicking actin rings[301], and a DNA segregation module[299], to cells[257]. DSCF has, so far, only been used to encapsulate IVTT systems.[258,302] Surfactant-free microfluidics showed encapsulation of a wide range of (biological) systems, from polystyrene beads to SUVs, IVTT systems[304] and even fibroblast cells.[245] Direct encapsulation of protein systems using this microfluidic method has yet to be reported. The OLA method has shown encapsulation of bacterial divisome proteins FtsZ and sZipA, including the colocalization of FtsZ filaments and ZipA at the membrane.[92]

Swelling-based methods, unlike emulsion-based methods, do not require any additives. An overview of encapsulation studies with electroformation and gel-assisted swelling can be found in Rideau *et al.*[227]. Highlights are the successful reconstitution of actomyosin networks using gel-assisted swelling[115,142,308] and the reconstitution of an advanced protocell using electroformation, allowing light-controlled generation of ATP, in turn inducing the polymerization of actin[130]. Swelling on glass beads has proven particularly effective in encapsulating IVTT systems. Recent notable results include the *de novo* synthesis of MinD and MinE proteins[273], the formation of FtsA-FtsZ ring-like structures yielding constricting GUVs[271,272], the assembly of microtubules inside GUVs[274], and DNA-programmed membrane synthesis[275] from IVTT systems. Despite these promising results with encapsulating IVTT systems, the method has not been used for encapsulation of other biological systems.

Generally, swelling-based methods are used more for membrane-oriented studies, while emulsion-based studies focus on studying the encapsulated content. This is in line with the favorable membrane properties of GUVs formed via swelling and the inherently superior encapsulation abilities of emulsion-based methods. For a more extensive recent overview of protein reconstitution in GUVs, we refer to Lopes dos Santos *et al.*[309] and Litschel *et al.*[225].

5.4.5 Encapsulation efficiency

To ensure a controlled protein concentration in the lumen of the GUVs and to achieve the correct protein stoichiometries, encapsulation efficiency is an essential factor to consider. Unfortunately, there is no generally accepted, standardized way of quantifying encapsulation efficiency, making it challenging to directly compare between different methods. Often, encapsulation efficiency is expressed qualitatively, by showing successful reconstitution of functional biological systems inside GUVs, instead of determining

absolute luminal protein concentrations. First steps toward measuring absolute protein concentrations in GUVs have been taken by Supramaniam *et al.*[310], who developed a microfluidics-based single-molecule approach, further emphasizing the need for quantitatively determining encapsulation efficiency.

Swelling-based methods are known to offer low encapsulation efficiency due to the incompatibility of the GUV formation mechanism with the encapsulation of large and charged molecules.[311] Tsai *et al.*[115] reported an encapsulation efficiency of about 50% for cytoskeletal actin-myosin networks, quantified by fluorescence intensity, using gel-assisted swelling. For swelling on glass beads, the encapsulation efficiency of IVTT systems was shown to increase upon freeze-thaw cycles (also needed to break up multivesicular and multilamellar vesicles into GUVs).[148] The effect of content exchange between GUVs by repeated freeze-thaw cycles was also reported by Litschel *et al.*[97]. A benefit of swelling on glass beads is that it is compatible with sample volumes as low as a few microliters[237], which is convenient when working with precious samples.

Microfluidics-based methods offer the highest encapsulation efficiency as the injected solution gets directly encapsulated into GUVs. This has been shown for OLA and surfactant-free microfluidics. Yandrapalli *et al.*[245] reported a very high effective encapsulation efficiency of 95% for dispersible components (measured by fluorescence intensity), but a more variable encapsulation efficiency for large, solid objects like beads. No quantification has been reported for the shaking method while for DSCF an encapsulation efficiency of ~ 50% for IVTT systems was reported by comparing fluorescence intensity to a bulk solution.[258] Encapsulation efficiency in cDICE was shown to be tunable by changing the composition of the lipid-in-oil dispersion, which alters the lipid adsorption rate.[157] The inclusion of a small fraction of PEG-ylated lipids likewise increased the encapsulation efficiency, which was shown by an increased protein expression by IVTT systems.[157] Loiseau *et al.*[101] noted that higher protein concentrations reduced the GUV yield for cDICE and the same effect was observed by Ganzinger *et al.*[164], using inverted emulsion for GUV formation. Recently, Baldauf *et al.*[174], using eDICE, observed a supersaturation effect (up to 1.7x the nominal concentration) for encapsulation of higher actin concentrations, demonstrating that even emulsion-based methods give a polydispersity in encapsulation efficiency. It is important to note that for many emulsion-based methods, the detailed GUV formation mechanisms are still unknown. It is, therefore, also unknown how, and to what extent, different inner solutions and protein concentrations influence the GUV formation process.

5.4.6 Cross-compatibility of GUV production methods and different biological systems

Encapsulating the different modules needed for an artificial cell within a single GUV, arguably poses the biggest hurdle to date. Different GUV production methods show varying degrees of success in encapsulating different biological systems (*i.e.* peripheral membrane-localized protein, polymerizing protein, IVTT systems, and other). The above review clearly demonstrates strengths and limitations in terms of the different methods regarding the types of biological systems that can be encapsulated effectively. Highly specialized methods like swelling on glass beads have been found to be reliable for

encapsulating IVTT systems, but may not be as effective for encapsulating other biological systems. In contrast, cDICE and its improved variant eDICE have shown compatibility with encapsulating a wide variety of biological systems. [141,157,174]

Achieving successful GUV formation under the conditions needed for a given biological system of interest requires a thorough understanding of the chemical and physical properties of each system, as well as their impact on GUV formation and the encapsulation process. However, few studies have been conducted on the effects of different protein and protein systems on GUV formation mechanisms. Further research is needed to fully elucidate the underlying mechanisms and develop more effective strategies for making GUV production work seamlessly with different biological systems.

Table 5.3 | Overview of compatibility of different GUV production methods with encapsulation requirements based on state-of-the-art results.

	Method	Physiological buffers[1]	Biological systems[2]	Encapsulation efficiency[3]	Cross-compatibility[4]	References
swelling	Gel-assisted swelling	⊠	membrane-localized protein	-	low	82,83,115,227,270
			filamentous protein			
	Swelling glass beads	⊠	IVTT	-	low	148,237,271–275
	Electroformation	⊠	membrane-localized protein	-	low	227,234,276–282
			filamentous protein			
emulsion	Inverted emulsion	⊠[5]	membrane-localized protein	+	high	98,127,137,139,164,242,264,265,283–294
			filamentous protein			
			IVTT			
			other			
	cDICE & eDICE	⊠[5]	membrane-localized protein	+	high	93–96,98,101,108,141,157,174,253,254,256,295–297
			filamentous protein			
			IVTT			
			other			
	Shaking method	⊠[5]	membrane-localized protein	+	high	257,298–301
			filamentous protein			
			other			
	DSCF	⊠[5]	IVTT	+	low	258,302
	OLA	⊠[5]	membrane-localized protein	++	low	92,138,261,303
			filamentous protein			
	Surfactant-free microfluidics	⊠[5]	IVTT	++	low	245,304
			other			

5.4.7 Operational requirements

Thus far, we have exclusively discussed the requirements for the produced GUVs themselves. However, an additional and often undervalued factor to consider is the "workability" of the production method. Considerations include the accessibility of the method to potential new users, the adaptability of the method to new experimental conditions, or the vastness of the parameter space, all of which have not yet been extensively covered in the literature for any of the methods discussed.[227,234] We introduce these criteria here under the umbrella term 'operational requirements'. It may be argued that such operational requirements carry little significance if the primary objective is to show that a well-defined final goal (*i.e.* the formation of a complex artificial cell) can be achieved. Nonetheless, we would like to stress the importance of operational requirements for methods to become established within the field, be adopted by new research groups, and enhance collaboration between research groups. The current abundance of diverging protocols for each GUV formation method poses obstacles for reproducibility and suggests a lack of robustness for most methods as constant adaptations are required to apply a method to a new experimental system. Hence a balance needs to be struck between working toward scientific advancements with a certain method and ensuring the method works reproducibly and robustly.

As a general rule, swelling-based methods are simple to set up, require minimal equipment and do not require extensive training of the experimentalist. As outlined above, both gel-assisted swelling and swelling on glass beads have not proven their applicability in an equally wide range of experimental conditions when compared to electroformation. Electroformation excels under a wide variety of conditions, both regarding membrane composition and buffer conditions. While electroformation is, therefore, sometimes claimed to be applicable in virtually any condition, it needs to be acknowledged that these results were achieved with an equally wide range of protocols, often despite similar conditions[227], potentially related to the lack of understanding of the process of GUV formation. It is unclear to what extent this disparity in protocols results in GUVs with different physicochemical properties. The parameters affecting GUV formation in electroformation include the electroformation chamber (a.o. electrode materials, electrode cleaning protocol, dimensions), the lipid deposition method, electrical field parameters, temperature, and total duration of GUV formation. As many groups use homemade electroformation chambers, there is considerable variation in protocols. This makes it difficult to standardize protocols, even for similar conditions, resulting in a lack in translational reproducibility. To address this issue, there are commercially available

[1] Standard protein buffers such as Tris buffer, PBS, or HEPES buffer, or other buffers with physiological ionic strength (50 – 150mM).

[2] Biological systems are divided into the following categories: peripheral membrane-localized protein, filamentous protein, IVTT systems, and other.

[3] Encapsulation efficiency for the different methods is categorized as follows: - (low encapsulation efficiency), + (strategies described to increase encapsulation efficiency), ++ (encapsulation efficiency of ~ 100%)

[4] Cross-compatibility of different methods with different biological systems is categorized as low (number of different biological systems encapsulated ≤ 2) or high (number of different biological encapsulated systems > 3).

[5] See in-text description for further details.

devices such as the Vesicle Prep Pro, which has already been used for a small number of recent studies [278–280,312]. Exploring the parameter space of electroformation experiments given by the method itself thus remains a time-intensive endeavor, yet important, as lipid oxidation (which occurs at different voltages for different lipid species) [313], duration, and temperature are all important factors to consider upfront.

Compared to swelling-based methods, relatively little information is available for the operational requirements of emulsion-based methods. Emulsion-based methods like inverted emulsion, the shaking method, or cDICE/eDICE only require simple laboratory setups and are therefore relatively accessible to new users. Microfluidic-based techniques, on the other hand, often have a high entry point due to their reliance on advanced fabrication techniques like soft lithography and the need for specialized devices. The adoption of these techniques typically requires additional resources, expertise, and investments compared to other emulsion-based and swelling-based methods, further illustrated by the limited number of follow-up studies for many microfluidic-based methods proposed. Recent studies have focused on mapping the input parameters of emulsion-based methods and highlighted its day-to-day variability [157], with the role of factors such as humidity and lipid-in-oil solution preparation yet to be fully investigated.

In summary, the operational requirements for both swelling- and emulsion-based methods remain an area of active research, with significant efforts underway to address the associated challenges. While for swelling-based methods, particularly electroformation, the focus is on countering the divergence of protocols, the primary aim for emulsion-based methods is on elucidating the vast parameter space. There are ongoing efforts in the scientific community that aim to address the reproducibility gaps in these methods by an open-science approach.

5.5 Moving forward: a blueprint for advancing GUV formation for artificial cell research

The creation of an artificial cell has been a hotly tackled challenge over the past decade and, while significant progress has been made, the artificial cell is still far from being a reality. In this review, we explored the potential of GUVs as a suitable artificial cell container, needed for building an artificial cell from the bottom-up. To assemble different modules of cell function inside a single GUV, the GUVs and GUV production methods should comply with a list of requirements including obtaining biologically relevant membrane properties and controlled encapsulation, and further ideally meet operational requirements such as reproducibility and ease of use. Here, we provided an overview of the current state-of-the-art in GUV production methods. Despite the availability of more than 10 commonly used methods, none of them fully meets all the necessary requirements for the artificial cell at this moment. Most promising results (*i.e.* challenging multicomponent reconstitution experiments) have been achieved using emulsion-based methods, yet exactly for these methods characterization studies remain limited.

On the road ahead, we propose efforts should be intensified to elucidate physical principles behind the different GUV formation methods to provide a basis for knowledge-based

optimization and adaptation. Swelling-based methods are relatively well-characterized, but emulsion-based methods, despite their widespread use in the field, still lag behind, likely mainly due to their relatively short history. For these methods, it is important to further evaluate the effects of residual additives in the lipid bilayer and the effect of density-increasing chemicals to ensure optimal mechanical properties. Since lipid composition is crucial for controlling mechanical and biological functionality of the membrane, it is important to know its exact composition. Some initial work has been done on comparing the ratio of input lipids to the final ratio obtained in the GUV bilayer, yet a detailed understanding of what determines the final lipid composition of the GUV produced, is still missing. Comparative qualitative and quantitative analysis of the GUVs produced by different methods is likewise important. While there are competing priorities and these studies are often time-consuming, they can provide a solid foundation for future progress by establishing standardized protocols and by providing appropriate metrics for assessing and comparing GUVs and the method used to provide them.

In addition, our focus should be on convergence rather than expansion. The ultimate goal of creating an artificial cell should serve as the driving force, with resources directed toward encouraging challenging integration experiments. Promoting open science, for example by including comprehensive methods sections and full protocols in published papers, will encourage exchange and collaboration between different labs, and help move toward a more systematic and collaborative approach to GUV formation and ultimately the creation of an artificial cell. Collaboration between different research groups, sharing of data and resources, and open access to publications and protocols can accelerate progress and avoid duplication of effort. This way, we can continuously push the limits in our efforts to mimic the essence of life and move one step closer to turning the artificial cell into a reality, ultimately recreating life in the lab.

5.6 Acknowledgements

The authors acknowledge financial support by the “BaSyC - Building a Synthetic Cell” Gravitation grant (024.003.019) of The Netherlands Ministry of Education, Culture and Science (OCW) and The Netherlands Organization for Scientific Research (NWO) (G.H.K.) and NWO-WISE funding (K.A.G.).

Part III

Toward a 'minimal phagocyte'

CHAPTER 6

A toolbox for bottom-up reconstitution of phagocytosis in giant unilamellar vesicles

▸ Phagocytosis, the cellular process of engulfing large particles, plays a crucial role not only in our immune response to pathogens but also in processes such as tissue homeostasis and as a feeding mechanism in single-cell organisms. Given the vast diversity of cells performing phagocytosis and of the objects targeted for phagocytosis, a highly diverse set of mechanisms, signalling pathways, and receptors are involved. Despite this diversity, all pathways lead to the common outcome of particle engulfment, suggesting overlap in membrane reshaping processes. The inherent complexity and underlying redundancy make studying these mechanisms in living cells, as discussed in Part I of this thesis, particularly challenging. Here, we aim to explore the basic physical principles underlying phagocytosis by *in vitro* reconstitution of a minimal functional system – the 'minimal phagocyte'. To this end, we introduce a specialized toolbox containing all elements needed to strip this complex phagocytotic process to its minimal set of components. This toolbox serves as a framework for development of an experimental platform facilitating the study of membrane remodelling and cytoskeletal rearrangements during phagocytosis. Ultimately, this approach will shed light on the fundamental biophysical principles of phagocytosis.

6.1 Introduction

Phagocytosis is the cellular process through which cells recognise, engulf, and eliminate particles larger than 0.5 µm, including pathogens and cells. As such, phagocytosis plays a pivotal role in our immune response to pathogens and contributes to tissue homeostasis by removing apoptotic cells.[314] This process is highly conserved and not only occurs in multicellular organisms, but it also serves as an essential feeding mechanism for protists or single-cell organisms.[12] Given the vast diversity of cells performing phagocytosis and the objects targeted for phagocytosis, a highly diverse set of mechanisms, signalling pathways, and receptors are involved, all leading to the same outcome of particle engulfment. This complexity reflects, in part, the underlying redundancy in biology. While phagocytic processes are phenotypically related, they exhibit mechanistic differences. Typically, the process involves the recognition of the particle, leading to activation of the engulfment process by forming a phagocytic cup, which in turn is followed by formation of the phagosome, and finally maturation of the phagosome.[5,7,12,15,315] A common denominator in all phagocytic processes is the restructuring of the actin cytoskeleton and plasma membrane. However, our current understanding of these processes remains limited, despite considerable research interest.[41,316]

To unravel some of the fundamental aspects of phagocytosis, specifically focusing on membrane remodelling and cytoskeletal rearrangements, we aim to construct an *in vitro*, bio-inspired system that simplifies the complex phagocytotic process by stripping it to its minimal components. By combining such a synthetic biology approach with tools from biophysics and microfabrication, we can study the physical principles of phagocytosis in isolation from the complex cellular environment, generally challenging to achieve *in vivo*. This minimal functional system – the 'minimal phagocyte' – will include all essential components necessary for spatially directed actin polymerization, thereby promoting membrane wrapping around a particle (Figure 6.1).

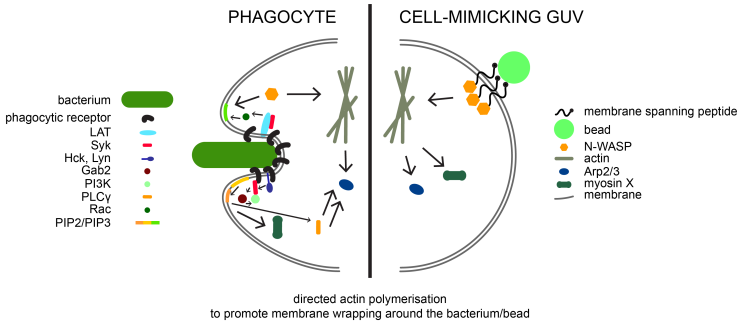

Figure 6.1 | Overview of the 'minimal phagocyte'. Schematic representation of a phagocyte *in vivo* and its cell-mimicking GUV counterpart containing only the minimally required components for directed actin polymerisation to promote membrane wrapping around an external particle.

Figure 6.2 provides an overview of the components we envision for the 'minimal phagocyte'. We aim to reconstitute it within giant unilamellar vesicles (GUVs), serving as an

ideal container for the artificial, cell-mimicking system.[152] Within the GUV membrane, a membrane spanning linker will enable the transduction of particle binding on the external GUV membrane to actin filament nucleation on the intracellular side of the GUV, effectively connecting 'out' to 'in'. Upon binding of an extracellular particle, a local upconcentration of the actin nucleator VCA via the membrane spanning linker will induce local actin polymerisation. To not only exert spatial but also temporal control over actin polymerization and to avoid depleting the actin and ATP pools, we further aim to reconstitute alpha-hemolysin pores in the GUV. Observing the full process and studying potential membrane rearrangements will be achieved using microfluidic GUV traps.

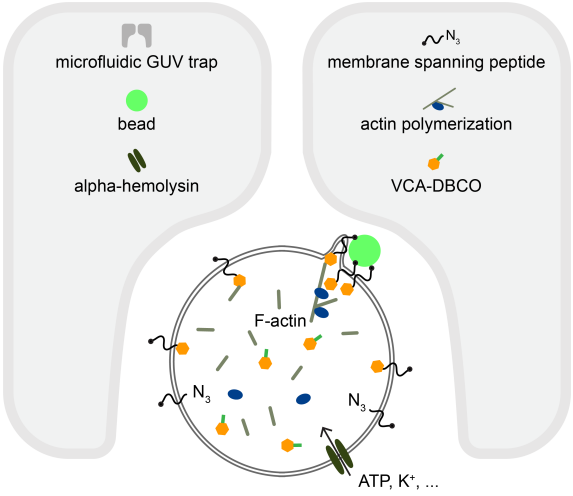

Figure 6.2 | Overview of components needed for the 'minimal phagocyte'. The set of components needed for the 'minimal phagocyte' include: GUV formation that enables efficient actin encapsulation. Alpha-hemolysin pore formation in the GUV membrane for temporal control over actin polymerization. The incorporation of a membrane-spanning linker into the GUV membrane to spatially direct actin polymerization to the site of external particle binding. This is achieved by anchoring the peptide to VCA on the luminal side of the membrane, thereby effectively localizing actin polymerisation to the sites of the membrane-spanning peptide. Finally, using microfluidic GUV traps allows for extended imaging and efficient buffer exchange.

Two of these components have already been extensively covered in the literature. Firstly, the reconstitution of a minimal actin cortex inside GUVs, nucleated at the membrane by Arp2/3, VCA, and profilin, was demonstrated in Chapter 3, Figure 3.4. More recent publications have further explored reconstituting cortical actin networks using emulsion-based methods. For example, Bashirzadeh *et al.*[253] provided a detailed protocol for minimal cortex reconstitution using eDICE, studying actin patterns and membrane deformation in GUVs[297]. Baldauf *et al.*[174] further optimized this eDICE protocol and explored curvature sensing of actin cortices nucleated by VCA and Arp2/3 and studied membrane deformations[256]. Secondly, alpha-hemolysin pore formation has been routinely used

as an assay to assess unilamellarity of GUVs, as demonstrated in Chapter 3, Figure 3.2. Alpha-hemolysin spontaneously inserts into the vesicular membrane as heptameric pores, enabling the passage of small molecules through the lipid bilayer. Given the availability of extensive protocols and wide array of successful results for both components, we anticipate a straightforward adoption into our workflow. Hence, they will hereafter not be our primary focus.

In this chapter, we have dissected the 'minimal phagocyte' into its individual components, allowing us to focus our efforts on a select few. Through systematic exploration, we successfully incorporated two membrane-spanning peptides into the GUV membrane, designed to enable the localization of actin polymerization. To induce this localized actin polymerization, we explored binding of streptavidin-coated beads and DBCO-labelled VCA to this membrane spanning peptide from the outside and the luminal side, respectively. Furthermore, we replicated a microfluidic GUV trapping protocol[317], enabling time-resolved and parallel studies of single GUVs. Finally, we present an initial experiment towards the integration of different components, marking a crucial step toward spatially triggering actin polymerization and highlighting the future potential of our approach.

6.2 Results and discussion

6.2.1 From cDICE to eDICE for GUV fabrication

Instead of using cDICE, extensively discussed in Chapters 4, 5, and 6, we here use eDICE – emulsion-based cDICE.[174,253] As the name implies, the capillary is omitted in eDICE and droplet formation is achieved through emulsification instead. As this approach avoids the use of a capillary, clogging and alteration of GUV formation through capillary effects is circumvented. This at no loss over GUV size control, as the used capillaries have been shown to provide no additional control over final GUV size compared to eDICE.[318] eDICE also allows for faster encapsulation, crucial for polymerising proteins, and allows encapsulation of volumes as low as 25 µL, while resulting in GUVs comparable in size to those previously obtained using cDICE.[174] Several other, small modifications were implemented in the protocol, essential for protein reconstitution. Notably, a lower OptiPrep™ concentration (*i.e.*, 6.5 % v/v *vs* 18.5 % v/v in case of cDICE) was used, as higher concentrations were found to alter actin polymerization kinetics.[174] The changes outlined above are particularly significant for actin encapsulation and, by extension, for our 'minimal phagocyte'. Consequently, we concluded that eDICE is the preferred method moving forward. Due to the extensive overlap of both protocols, we were able to seamlessly adapt the new approach. Furthermore, we found the workflow to be significantly easier.

6.2.2 A membrane-spanning peptide to connect in and out

Arguably, the quintessential component in the 'minimal phagocyte' is the membrane-spanning peptide. It serves as the linchpin for replicating receptor-mediated actin polymerisation in a minimal way, facilitating spatial localisation of actin polymerisation to the membrane. This effectively simplifies the complex *in vivo* interactions to a one-step

interaction *in vitro*. We opted to explore synthetic transmembrane peptides, frequently used for studying transmembrane proteins, which are renowned for their challenging reconstitution in lipid bilayers. Given their widespread use, we had multiple options at our disposal and we decided to screen two peptides, the WALP peptide and the SNARE peptide.

The WALP peptide is a single-pass transmembrane alpha-helical peptide composed of leucine and alanine repeats ('LA') of variable length, flanked on both sides by two tryptophans ('WW').[319,320] Originally designed as a synthetic analogue of widely studied alpha-helical peptides, its sequence represents a standard sequence for a transmembrane alpha-helical segment of intrinsic membrane proteins: a long stretch of hydrophobic residues flanked on either side by aromatic amino acids. Previous studies confirmed its expected incorporation as an alpha-helix into lipid bilayers and showed a spatially homogenous distribution.[321,322] For our experiments, we opted for WALP23, which contains 8 repeats of the 'LA' sequence and has a total length of 34.5 Å, sufficiently long to span the lipid bilayer.[323] WALP23 was previously successfully reconstituted in GUVs by Podolsky *et al.*[324], who also confirmed its correct incorporation as an alpha-helical fold. For our purposes, we modified the peptide by introducing a functionalized lysine at each end, featuring a biotin and an azide group. To ensure proper exposure of these tags outside the membrane, we included an additional three-glycine linker at each end (Figure 6.3a).

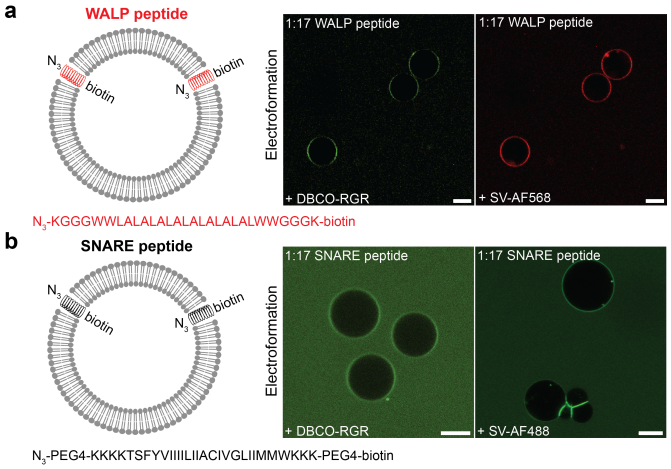

Figure 6.3 | Incorporation of the membrane-spanning peptides into electroformed GUVs. (a) Illustration of the DBCO- and biotin-functionalized WALP peptide in GUVs. The peptide randomly insert into the GUV membrane, resulting in both functionalisations being present on either side of the membrane. Assessment of WALP peptide incorporation through binding of DBCO-PEG4-5/6-Carboxyrhodamine 110 and streptavidin-Alexa Fluor 488 to the external surface of electroformed GUVs with a 1:17 peptide:lipid ratio. Membrane-localized fluorescence of the DBCO group indicates successful incorporation of the WALP peptide into the GUV membrane. All scale bars indicate 10 µm. (b) Same as in (a), but for the SNARE peptide. All scale bars indicate 10 µm.

As an alternative and parallel approach, we explored a SNARE-based peptide. SNAREs, soluble N ethylmaleimide-sensitive factor attachment protein receptors, constitute a family of proteins that are key components in driving membrane fusion processes.[325] Characterized by a simple domain structure, SNAREs exhibit a distinctive feature known as the SNARE motif - a highly conserved stretch of 60 - 70 amino acids arranged in heptad repeats. Typically, most SNAREs possess a single transmembrane domain at their C-terminal ends, linked to the SNARE motif by a short linker. At the N-terminal region, many SNAREs showcase independently folded domains that vary among subgroups.[325] Synaptobrevin is an example of such a SNARE, containing an alpha-helical transmembrane sequence.[326] Synthetic reconstitution of SNAREs has proven to be a valuable tool to simplify the intricacies of SNARE assembly into a functional complex, helping elucidate the structure-function relationship in membrane fusion.[326–328] Starting from the native protein sequence of synaptobrevin, we introduced the required biotin and azide functionalisations on either end and additionally included a PEG4 spacer to ensure the tags protrude from the lipid bilayer and are available for binding (Figure 6.3b).

To incorporate the membrane-spanning peptide into the GUV membrane, we added the peptide to the lipid fraction. For electroformation, this is the dried lipid film, while for eDICE, this is the lipid-in-oil dispersion. Due to its hydrophobic nature, the peptide is expected to spontaneously integrate into the lipid bilayer during GUV formation. However, this has not yet been demonstrated using eDICE. First, we validated the correct integration of the peptides into electroformed GUVs by assessing the two functionalizations. Since the peptide inserts randomly oriented as the bilayer is molecularly flat, both functionalizations should be present on either side of the membrane, both in- and outside the GUV. We confirmed this for both the WALP and SNARE peptide by binding a fluorescently labelled DBCO and streptavidin group, respectively, to the azide and biotin group of the peptide, from the outside. Clear membrane localization was observed for electroformed GUVs for both peptides (Figure 6.3).

Next, we sought to confirm peptide integration into the GUV membrane using eDICE. Simultaneously, this allowed us to confirm binding from the inside of the GUV, which is challenging with electroformation since the inner and outer solutions of the GUVs are identical, in turn making discerning inside from outside binding impossible. This is not applicable to eDICE. It is important to note that we had to reduce the peptide amount, as eDICE requires a large volume of lipid-in-oil dispersion, as it is needed to fill the rotating chamber. Despite only using a relatively low lipid concentration (*i.e.*, 0.2 mg mL^{-1}), the large volume still meant significant amounts of peptide were needed. Therefore, we opted to lower the peptide concentration by tenfold. Upon addition of labelled DBCO in the outside solution, we still observed clear membrane localization (Figure 6.4a, b). When we then also encapsulated fluorescently labelled streptavidin, we could likewise observe membrane localization inside the GUV (Figure 6.4a). In a control experiment without added peptide, no membrane localization could be seen (Figure 6.4c).

These results, combined with earlier successful reconstitution of such peptides into the lipid bilayer[324,326], made us confident that the peptides were incorporated as anticipated,

with both functionalizations available for binding their respective soluble binding partners. The caveat of using eDICE is the necessity of reducing the peptide amount; however, one could think to explore the possibility of spontaneous insertion of the peptide post GUV formation; a phenomenon which has been demonstrated previously when lipids added in solution integrated into preformed GUVs. [329]

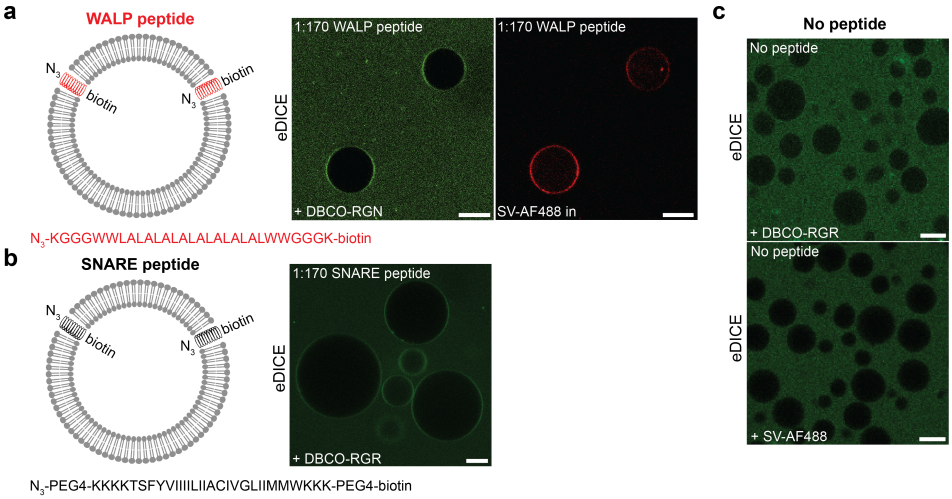

Figure 6.4 | Incorporation of the membrane-spanning peptides into eDICE GUVs. (a) Illustration of the DBCO- and biotin-functionalized WALP peptide in GUVs. The peptide randomly insert into the GUV membrane, resulting in both functionalizations being present on either side of the membrane. Assessment of WALP peptide incorporation through binding of DBCO-PEG4-5/6-Carboxyrhodamine 110 to the external surface and encapsulation of streptavidin-Alexa Fluor 488 in the lumen of eDICE GUVs with a 1:170 peptide:lipid ratio. Membrane-localized fluorescence of the DBCO group and streptavidin confirms successful incorporation of the membrane-spanning peptide into the GUV membrane. All scale bars indicate 10 µm. (b) Illustration of the DBCO- and biotin-functionalized SNARE peptide in GUVs. Assessment of SNARE peptide incorporation through binding of DBCO-PEG4-5/6-Carboxyrhodamine 110 to the external surface of eDICE GUVs with a 1:170 peptide:lipid ratio. Membrane-localized fluorescence of the DBCO group indicates successful incorporation of the membrane-spanning peptide into the GUV membrane. Scale bar indicates 10 µm. (c) Control without the addition of membrane-spanning peptide: upon addition of DBCO-PEG4-5/6-Carboxyrhodamine 110 and streptavidin-Alexa Fluor 488 to the external surface of the eDICE GUVs, no membrane localization is observed. All scale bars indicate 10 µm.

6.2.3 DBCO-labelled VCA allows targeting actin polymerisation to the membrane-spanning peptide

To anchor VCA to the peptide in order to enable nucleation of actin polymerization on the membrane, we employed copper-free click chemistry. In previous studies [174], VCA was usually attached to the membrane through binding to nickelated lipids via its His-tag. For our work, however, we aim to attach VCA specifically to the azide of the membrane-spanning peptide to allow precise spatial control by confinement to the peptide only. Copper-free click chemistry, known for its compatibility with biological

systems, facilitates the formation of covalent bonds without the need for a copper catalyst.[330] In this context, a dibenzocyclooctyne (DBCO) moiety reacts with an azide group through strain-promoted alkyne azide cycloaddition (SPAAC), resulting in a stable triazole and covalent bond. This approach is not only biorthogonal and highly specific, but also efficient under various aqueous buffer conditions, demonstrating a rapid reaction rate. Its versatility and potential applications in synthetic biology make it a valuable tool. To achieve this specific localization at the membrane-spanning peptide, we devised DBCO-labeled VCA, ensuring a covalent bond at the desired site.

Two distinct labelling strategies were explored. First, maleimide labelling, targeting unspecific cysteine residues, provided controlled labelling due to VCA's singular cysteine residue. This approach allows site-specific labelling through a thiol-Michael reaction.[331] We were able to label VCA with DBCO-PEG4-maleimide, confirmed by reacting an azide-PEG2000 and an azide-TAMRA (Figure 6.5a). The binding of azide-PEG2000 increased the molecular weight of VCA with approximately 2 kDa, resulting in a total molecular weight of around 19 kDa. On a Coomassie Blue stained gel, this is visible as an upward shift of the original protein bands (Figure 6.5a). Azide-TAMRA, on the other hand, fluorescently labeled VCA, which was confirmed by the appearance of a fluorescent protein band as viewed on the corresponding brightfield and fluorescent image (Figure 6.5a). Increasing the incubation time to 12 h made no discernable difference, which we attribute to the fast click-chemistry reaction. It is thus possible to label the VCA with a single DBCO using maleimide chemistry; however, previous work has shown that this labeling renders the protein inactive[123]. Therefore, while a useful control experiment, maleimide-labelled VCA is of no use for our final 'minimal phagocyte' assay.

As an alternative, we pursued sortase-mediated labelling, enabling covalent attachment of a functionalisation at an N-terminal polyglycine sequence. By cleaving the His-tag of VCA, we exposed this N-terminal polyglycine sequence. Sortase catalyses transpeptidation, recognizing a short peptide tag (LPETGG), to which a DBCO can be conjugated. This process forms an acyl intermediate with the threonine, resolving into a covalent bond between the functionalized peptide and VCA.[332] We were able to show a successful labeling reaction with VCA using an ATTO 488-labeled peptide, visible as a molecular weight shift of approximately 2 kDa and fluorescent labeling of the protein band on an SDS PAGE gel (Figure 6.5b). Different incubation temperatures (37 °C, room temperature, and 4 °C) and times (2 h, 4 h, and 18 h, respectively) led to no apparent improvement of sortase-labeling efficiency. Labeling of VCA with a DBCO-group was initially not achieved due to inactivity of the custom-synthesised DBCO-LPETGG, as was confirmed by Peptide Specialty Laboratories GmbH[1]. However, preliminary results of sortase-mediated labeling of VCA with a resynthetised DBCO-LPETGG peptide indicate succesfull labeling of VCA, resulting in DBCO-labelled VCA (Figure 6.9).

[1] Personal communication with Peptide Specialty Laboratories GmbH.

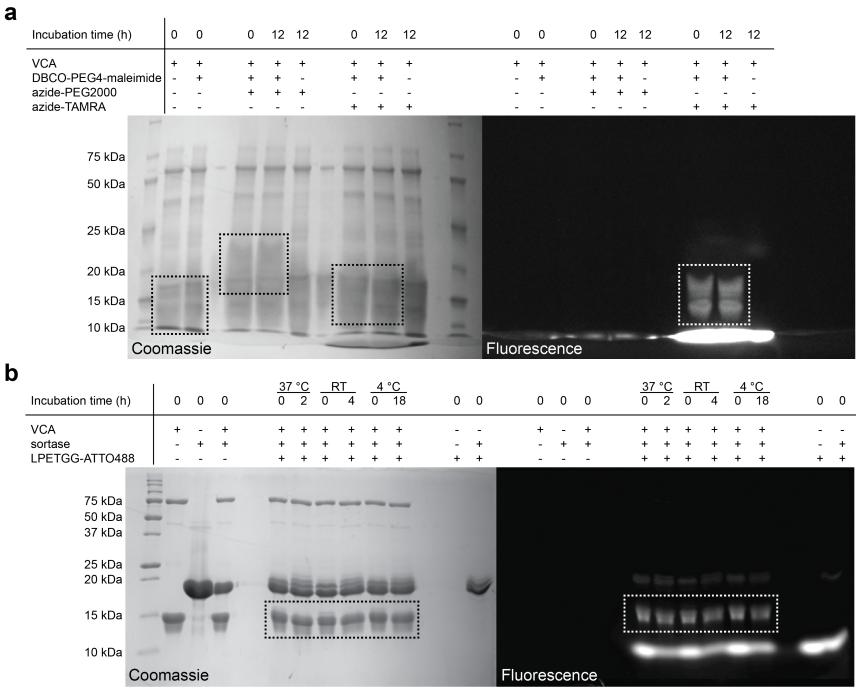

Figure 6.5 | SDS PAGE gel analysis of VCA labelling with maleimide and sortase. (a) SDS-PAGE gel showing the labeling reaction of VCA with DBCO-PEG4-maleimide, assessed through click chemistry reactions with azide-PEG2000 and azide-TAMRA. Both reactions were incubated for 12 h before being run on a SDS PAGE gel, alongside a protein ladder and control samples. Coomassie Blue staining (left) shows a small molecular weight shift of 2 kDa in VCA, indicating successful conjugation of azide-PEG2000 to the DBCO-labelled VCA (black dotted box). The corresponding brightfield and fluorescence image (right) shows fluorescently labeled VCA (white dotted box), confirming successful conjugation of azide-TAMRA to the DBCO-labeled VCA. Excess, unreacted azide-TAMRA is visible in the right image at approximately 10 kDa. (b) SDS PAGE gel showing the labelling reaction of VCA with ATTO 488-LPETGG via sortase-mediated labelling. Multiple labelling reactions were incubated at different temperatures (37 °C, room temperature, and 4 °C) and stopped at various timepoints (2 h, 4 h, and 18 h, respectively) before being run on an SDS PAGE gel, alongside a protein ladder and control samples. Coomassie Blue staining (left) shows a small molecular weight shift of 2 kDa in VCA (black dotted box), attributed to the successful conjugation of the ATTO 488-peptide to VCA. The corresponding brightfield and fluorescence gel imager image (right) confirms the presence of fluorescently labelled VCA (white dotted box), further indicating successful labelling. Excess, unreacted ATTO 488-peptide is visible in the right image at approximately 10 kDa.

6.2.4 Microfluidic GUV traps allow prolonged imaging and efficient buffer exchange

To allow for prolonged fluorescence imaging, studying multiple GUVs in parallel, and to facilitate efficient buffer exchange, we utilized microfluidic GUV traps introduced by Wang *et al.*[317]. Microfluidic systems provide effective control over micrometer-scale objects such as cells or GUVs while offering precise control over environmental conditions due to laminar flow inside the chip.[66,333] Consequently, they are considered a reliable experimental tool often employed in biology.[164,334]

The PDMS microfluidic chip as designed by Wang *et al.*[317] enables spatial confinement of single GUVs by trapping them in between two PDMS posts and is designed to trap as many GUVs in parallel as possible. The design consists of two distinct channels, each housing an array of 352 individual traps capable of capturing a single GUV (Figure 6.6a). Furthermore, the chip features progressively narrowing trap posts along the horizontal axis. In the first quadrant, trap posts have an 8 µm spacing, which transitions to openings of 6, 4.5, and 3 µm in subsequent quadrants (Figure 6.6b). This arrangement allows for the capture of smaller vesicles downstream that might escape the wider traps initially, thereby increasing the overall trapping efficiency. An angular separation of 12° between the individual traps further ensures efficient trapping of multiple GUVs in parallel (Figure 6.6b).

Using these traps, we efficiently captured both single GUVs (Figure 6.6c) and multiple GUVs simultaneously (Figure 6.6d). We observed instances where multiple GUVs were trapped in a single trap (Figure 6.6d) or the traps were covered in lipid debris. We found these issues could be mitigated by finely tuning the density of GUVs. Moreover, the large number (704) of traps, allows us to select single, clean GUVs of preferred sizes, thereby essentially circumventing the issues stated above.

One of the main advantages of using such microfluidic chips is the option to quickly and efficiently exchange the surrounding buffer. This feature is particularly valuable when working with electroformed GUVs, where the composition of the inner and outer solution is identical. We were able to successfully exchange the surrounding buffer efficiently, without losing the trapped GUVs in the process (Figure 6.6d). This procedure proved to be quick and straightforward.

Given the high cost high cost and labor-intensive nature of producing silicon wafers and to alleviate stress on the wafer by repeated use, we opted to replicate the wafer using replica molding. This technique is known for preserving the design of the original wafer at the length scale we employed, at no significant loss of quality.[335] We recreated the original silicon wafer by casting a PDSM master in clear epoxy. The resulting PDMS microfluidic chips exhibited no discernible differences from those made directly from the silicon wafer.

6.2.5 Polystyrene beads can serve as a synthetic external object to be engulfed

To replicate the external object in phagocytosis, we devised a minimal system where the object is mimicked by binding of an external bead, thus essentially recreating the *in vivo* receptor-mediated binding through a biotin-streptavidin interaction. The membrane-

spanning peptide is functionalized with biotin at one end, facilitating its binding to a streptavidin-coated bead. Although the binding of beads to giant unilamellar vesicles (GUVs) has been previously explored, it has been in vastly different contexts. A common biophysical assay involves pulling membrane tubes from GUVs stabilized with a micropipette, focusing on membrane curvature and protein studies.[75,336]

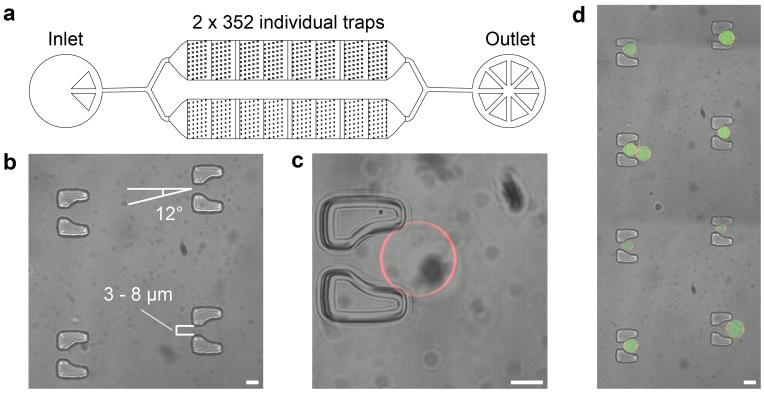

Figure 6.6 | Microfluidic GUV traps enable studying GUVs in parallel. (a) Schematic illustration of the microfluidic chip design for trapping single GUVs. Buffer solutions can be introduced through the inlet and withdrawn via the outlet under a continuous flow. The chip consists of two distinct channels, each housing an array of 352 individual traps. (b) Brightfield image of an array of GUV traps inside the microfluidic chip. GUV trap openings vary along the horizontal axis of the chip, transitioning gradually to narrower sizes (8 µm - 6 µm - 4.5 µm - 3 µm), thus optimizing trapping efficiency as smaller vesicles pass by initial traps but get captured further downstream. The traps are angularly separated by 12°, enhancing overall trapping efficiency. Scale bar indicates 10 µm. (c) Brightfield image of a single GUV (red, 0.1 mol% ATTO 655-DOPE membrane stain) spatially confined within a GUV trap by maintaining a constant flow, the GUV is securely positioned within the trap, allowing extended imaging and buffer exchange. Scale bar indicates 10 µm. (d) Brightfield image of multiple GUVs (red, 0.1 mol% ATTO 655-DOPE membrane stain) encapsulating G-actin (green, Alexa Fluor 488-labeled actin) can be simultaneously trapped, demonstrating the system's efficiency. The surrounding buffer was exchanged with a plain buffer, effectively washing away any inner solution present in the surrounding medium. Scale bar indicates 10 µm.

In our experiments, when streptavidin-coated beads were incubated with biotinylated GUVs (1 mol% DSPE-PEG2000-biotin), clear binding of the bead to the GUV membrane was observed (Figure 6.7a). By titrating the bead concentration, we were able to bind single beads to single GUVs. The success of binding was assessed through visual monitoring over extended periods. A mobile bead on the GUV surface indicated successful binding, whereas a drifting bead due to Brownian motion indicated a lack of binding.

Next, we attempted the same approach using GUVs with a 1:170 peptide:lipid ratio in the membrane (Figure 6.7b). Surprisingly, binding was not observed (Figure 6.7c). One straightforward explanation could be the lower relative concentration of the membrane-spanning peptide compared to biotinylated lipids. With only 50 % of the peptide oriented correctly, there was a threefold lower amount of reactive peptide when compared to the amount of available biotinylated lipids. However, in previous studies on pulling mem-

brane tubes, concentrations of biotinylated lipids lower than 1 mol%[337–339], some as low as 0.01 mol% were used[340]. This indicates the used concentration range should be sufficient to allow robust binding. Interestingly, all biotinylated lipids used in those studies contained a PEG2000 spacer, which has a length of 12.5 nm.[341] This spacer likely reduces steric hindrance, making the group more available to binding partners and thereby also reducing any electrostatic interactions of the membrane with the streptavidin-coated beads, leading to an improved binding efficiency. Since the membrane-spanning peptide only has a three glycine linker, this is likely to negatively impact the efficiency of the biotin-streptavidin interaction.

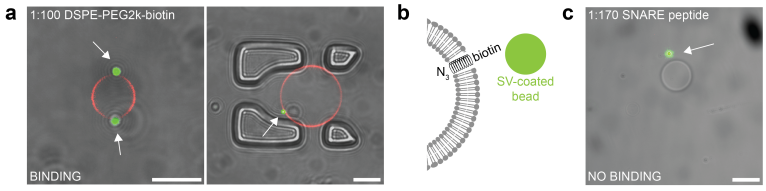

Figure 6.7 | Binding of streptavidin-coated beads to GUVs. (a) Brightfield image of a single GUV (red, 0.1 mol% ATTO 655-DOPE membrane stain) containing 1 mol% DSPE-PEG2000-biotin binding to 1 µm fluorescent streptavidin-coated beads. The beads were diluted 1:4000 upon incubation with GUVs, resulting in approximately one bead binding per GUV. Binding of streptavidin-coated beads to GUVs containing biotinylated lipids was assessed by visual monitoring of the membrane and bead for extended times. Scale bars indicate 10 µm. (b) Illustration of the binding of streptavidin-coated beads to GUVs containing the membrane-spanning peptide. Binding will only occur to the peptides with the biotin group pointing outward. (c) No apparent binding of fluorescent streptavidin-coated beads to GUVs could be observed when the peptide was added at a 1:170 peptide:lipid ratio. Scale bar indicates 10 µm.

Notably, one study mentioned that the addition of PBS to the buffer was necessary for robust binding of the bead to the GUVs.[342] Unsurprisingly, all mentioned research used such buffered solutions. Therefore, using a higher ratio of beads to GUVs, an increased concentration of peptide, adding a PEG spacer, and carefully tuning buffer conditions will likely enhance the efficiency of bead binding to GUVs. It is worth noting that current actin encapsulation protocols with eDICE routinely incorporate a small percentage of PEGylated lipids, as it has been shown to improve encapsulation efficiency.[157] It is important to consider this when designing further experiments, as a PEG brush could potentially hinder successful binding.

6.2.6 GUV-GUV contact assay shows upconcentration of membrane-spanning peptide

As a first experiment toward the integration of different building blocks, we aimed to conduct a GUV contact assay in which two GUVs containing the labelled SNARE peptide are brought into close proximity in the presence of streptavidin (Figure 6.8a). Since streptavidin binds to the biotinylated side of the SNARE peptide, it can attach to the outside of the GUVs. However, upon contact between two different GUVs, it is expected that the presence of streptavidin will lead to a local upconcentration of the SNARE peptide and to colocalization of both at the contact site. This experiment serves

as a simple proof-of-principle, demonstrating that an external trigger, such as the local binding of streptavidin, can result in an internal effect - specifically, local clustering of the SNARE peptide at the binding site of streptavidin. This represents a simplified version of the final working mechanism we have envisioned for the 'minimal phagocyte'. Upon adding streptavidin to electroformed GUVs containing the labelled SNARE peptide, we indeed observed colocalization and local upconcentration at the contact site between two GUVs (Figure 6.8b).

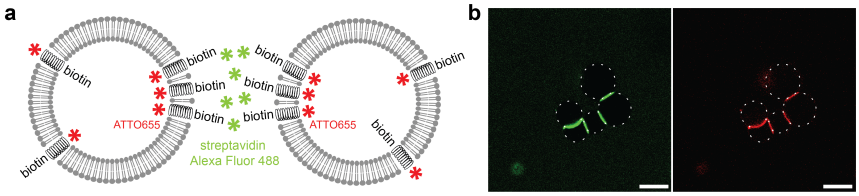

Figure 6.8 | Colocalisation of the membrane-spanning peptide with streptavidin at the binding site between GUVs. (a) Illustration depicting the binding of streptavidin to GUVs containing the fluorescently labeled membrane-spanning peptide. Colocalisation and local upconcentration of both streptavidin and the membrane-spanning peptide are expected at the contact site between two GUVs. (b) Streptavidin Alexa Fluor 488 (green; 0.5 µM) was added to GUVs containing ATTO655-labelled peptide (red; 1:170 peptide:lipid ratio), showing colocalisation at contact sites between GUVs, indicating a localisation and local upconcentration of the membrane-spanning peptide to the external binding site of streptavidin. GUVs are delineated by dotted circles for improved visibility. Scale bars indicate 10 µm.

6.3 Outlook

In this chapter, we have laid the groundwork for the development of the 'minimal phagocyte', a reconstituted system designed to facilitate the study of membrane rearrangements through cytoskeletal remodelling, specifically in phagocytosis. We introduced the essential components necessary for such a system, including a membrane-spanning linker, DBCO-labelled VCA, microfluidic GUV traps, and external beads. As a step toward integrating these various building blocks into a single unit, we conducted a proof-of-principle assay, showing peptide clustering.

The observed peptide clustering in the GUV-GUV contact assay could have implications beyond the field of synthetic biology and the 'minimal phagocyte', as it demonstrates a synthetic system replicating receptor clustering, resembling for example the immune synapse. To further confirm the obtained results, it would be beneficial to titrate the concentration of the labelled SNARE peptide. Additionally, real-time observation of clustering dynamics would provide valuable insights. This could be achieved, for example, with optical tweezers and a micropipette for fine spatial control over GUVs and real-time monitoring. Alternatively, GUV traps could be designed to be larger, able to trap multiple GUVs. By first trapping GUVs and only then adding streptavidin-coated GUVs, it would be possible to study the contact in real-time via fluorescence readout. These results form a solid starting point for further integration of the aforementioned building blocks comprising the 'minimal phagocyte'.

Future work will involve extending this proof-of-principle in a stepwise fashion toward the 'minimal phagocyte'. For instance, preliminary experiments could assess if a membrane-bound particle can serve as a scaffold for actin-driven membrane invagination. This could be achieved by binding an external bead to the GUVs via biotin-mediated interactions while nucleating the actin cortex to the membrane using nickelated lipids. Previous studies have shown that in cells with an impaired cytoskeleton, no uptake is observed [343], whereas in GUVs containing a minimal cytoskeleton, membrane deformations do occur [256]. GUVs have been shown to wrap around particles when tuning adhesion strength to be sufficiently high, showing a delicate interplay between membrane tension and adhesion strength. [344,345] Since in phagocytosis, tension is at first high and adhesion only relatively low, combining both approaches would provide valuable insights in the role of the cytoskeleton in engulfment. From there, the membrane-spanning linker could be employed to spatially localize actin polymerization to the site of binding, addressing the question of whether directed actin polymerization alone is sufficient to drive particle engulfment. Subsequent experiments could then for example explore the role of myosin II, known for its involvement in the closure of the phagocytic cup. [346]

The experimental platform could find use in a myriad of application, offering numerous possibilities to further our understanding. For example, recent studies have tried to uncover effects of surface morphology, dependent on protein coverage, on phagocytosis. [347] Additionally, exploring the influence of shape, size, and adhesion strength was addressed in some earlier studies. [344,345,348,349] Other studies have focused on forces, using deformable microparticles (DAAM-particles) as cellular stress sensors, providing a simple and versatile method for force sensing. [316] This approach enables the study of subcellular mechanical behaviour during cell–target interactions. [350] Furthermore, recent work has explored the localization of actin polymerization to the membrane through phase separation [351] and synthetic protein-based anchoring [352]. These ideas present interesting avenues to explore within our minimal system.

If the final 'minimal phagocyte' is successfully realized, it would then also function as a synthetic transmembrane receptor; especially relevant given the challenges associated with reconstituting membrane proteins. Recently endeavours established transmembrane signalling through a synthetic receptor, achieving enzyme activation [353] and intracellular transcription [354]. Other efforts have explored membrane-spanning DNA origami signaling units as synthetic receptors. [355] Involving the actin cytoskeleton in a synthetic transmembrane receptor, however, has not been demonstrated to date.

In conclusion, our gained expertise, combined with expertise available in the literature, yields a specialized toolbox containing all elements needed to strip the complex phagocytotic process to its minimal set of components. This 'minimal phagocyt' toolbox serves as a framework for development of a valuable experimental platform offering legion opportunities to further elucidate the hitherto unknown roles of the cytoskeleton in phagocytosis. Ultimately, this approach will shed light on unresolved biophysical questions, providing fundamental insights into the mechanics of phagocytosis and answering basic questions, such as if a minimal actin cytoskeleton is sufficient to drive engulfment.

6.4 Methods

6.4.1 Membrane-spanning peptide

WALP peptide

The WALP peptide was ordered from Peptide Specialty Laboratories GmbH and had the following sequence: K(azide)-GGGWWLALALALALALALALWWGGG-K(biotin). The sequence consists of WALP23, which contains 8 'L' repeats and is flanked by two tryptophan (W) residues on either side. An additional three-glycine linker was added on both sides, ensuring protrusion of both functionalisations, which were added though labelling to a lysine (K) residue.

SNARE peptide

The SNARE peptide was designed by Kristina A. Ganzinger based on a previous sequence by Lygina *et al.*[326]. and was synthesised by the core facility at the Max Planck Institute for Biochemistry in Martinsried, Germany. It had the following sequence: azide-PEG4-KKKKTSFYVIIIILIIACIVGLIIMMWKKK-PEG4-biotin. Additionally, a fluorescently labelled peptide was used with the following sequence: ATTO 655-PEG4-KKKKTSFYVIIIILIIACIVGLIIMMWKKK-PEG4-biotin.

6.4.2 GUV formation

Electroformation

Electroformation was performed in custom-made polytetrafluoroethylene (PTFE) chambers with two platinum electrodes spaced 4 mm apart.[356] The chambers and electrodes were cleaned via sonication before use. First, they were sonicated in chloroform (Uvasol, Sigma-Aldrich) for 20 min, followed by sonication in ethanol (Uvasol, Sigma-Aldrich) for 20 min, and finally they were dried under nitrogen flow. Lipids and membrane-spanning peptide were mixed at the desired ratio to a final concentration of 1 mg mL^{-1} in chloroform and were stored at -20 °C until use. To form a lipid film, 3 µL of the lipid mixture was spread evenly onto each electrode and subsequently dried for 30 min in a vacuum desiccator. The electroformation chamber was then filled with 350 µL of a 300 mM sucrose solution and closed by screwing on the cap with the electrodes. Next, the chamber was connected to a function generator (Rigol DG1032Z) using custom-made connectors. For GUV formation, a sinus wave at a voltage of 2 V (RMS) and a frequency of 10 Hz was applied for 1.5 h, followed by a GUV detachment step at a lowered frequency of 2 Hz for 45 min. The formed GUVs were transferred to a glass observation chamber that was passivated using 1 mg mL^{-1} beta-casein (C6905, Sigma-Aldrich) in Milli-Q water for imaging. GUVs were diluted in an iso-osmolar solution of phosphate-buffered saline buffer (PBS buffer) of which the osmolarity was adjusted using glucose as needed.

eDICE

The protocol of eDICE was similar to the cDICE protocol previously described in Van de Cauter *et al.*[157] (see Chapter 3). When using the membrane-spanning peptide, it was added to the lipids at the desired ratio. The lipid-in-oil dispersion was then made as described before, using 50 µL of chloroform and 400 µL of decane (99+ %, pure, Acros Organics) as organic solvents to rehydrate the dried lipid film inside a glovebox. The inner

solution contained 6.5 % v/v OptiPrep™ as compared to the higher concentration of 18.5 % v/v OptiPrep™ described in Chapter 3.[174] Omitting the capillary led to the following changes in the workflow: first, the rotation chamber was filled with 700 µL of the outer solution, followed by 5 mL of the lipid-in-oil dispersion. Next, 1 mL of the remaining lipid-in-oil dispersion was transferred to a 2 mL Eppendorf tube. Emulsification of 40 µL of inner solution in this 1 mL of lipid-in-oil dispersion was then achieved by scraping the Eppendorf tube vigorously across a tube rack for a total of 13 times. Finally, the resulting emulsion was carefully pipetted into the spinning rotation chamber and left to spin for a total of 3 minutes.

Image acquisition
50 µL of the GUV solution was deposited on a custom-made glass coverslip and covered. Confocal images were acquired using a Nikon A1R-MP confocal microscope, using a Plan APO IR 60x water immersion objective. The 561 nm (laser power 10.0) and 488 nm (laser power ranging from 1.0 to 5.0) laser lines were used in combination with the appropriate emission filters to image the ATTO 655-labeled SNARE peptide and streptavidin-Alexa Fluor 488 and DBCO-PEG4-5/6-Carboxyrhodamine 110, respectively.

6.4.3 Assessment of incorporation of membrane-spanning peptide in GUVs
Streptavidin Alexa Fluor 568 conjugate (S11226, Fisher Scientific), streptavidin Alexa Fluor 488 conjugate (S11223, Fisher Scientific), or dibenzocyclooctyne-poly(ethylene)glycol4-5/6-Carboxyrhodamine 110 (DBCO-PEG4-5/6-Carboxyrhodamine 110; CLK-A127-1, Jena Bioscience) was added at final concentrations ranging from 0.1 µM to 10 µM in the outer solution of the GUVs to assess incorporation of the membrane-spanning peptide in GUVs. For electroformation GUVs, the outer solution consisted of osmolarity-adjusted PBS buffer, while for eDICE the outer solution consisted of a glucose-solution.

6.4.4 Expression and purification of N-WASP VCA
The 10x His-tagged VCA domain (Verprolin-rich, Central and Acidic regions) of murine N-WASP (amino acids 400-501) was expressed in a 1 L culture of BL21 (DE3) competent *E. coli* cells and induced with 1 mM isopropyl beta-D-1-thiogalactopyranoside (IPTG). Cells were grown overnight at 20 °C before lysing via sonication. The cell lysate was purified using His-tag purification using a His Trap FF Crude (5 mL) column (GE Healthcare) using the ÄKTA pure protein purification system. All protein containing fractions were then combined for anion exchange chromatography using a MonoQ 5/50 GL (1mL) column (GE Healthcare). Next, the 10x His-tag was cleaved using presission protease to make the protein available for sortase-mediated labelling. After subsequent His-tag purification, the protein was unconcentrated and buffer exchanged to storage buffer (20 mM tris(hydroxymethyl)aminomethane (TRIS) pH 8.0, 0.5 mM ethylenediaminetetraacetic acid (EDTA) pH 9.0, 5 % v/v glycerol, 1 mM tris(2-carboxyethyl)phosphine (TCEP)).

6.4.5 Labeling of N-WASP VCA

Random cysteine labelling

VCA was functionalised with DBCO-PEG4-maleimide (760676, Sigma-Aldrich). The label was used in tenfold excess and the mixture was incubated for 12 h at 4 °C. Azide-PEG2000 (689807, Sigma-Aldrich) and azide-TAMRA (760757, Sigma-Aldrich) were added in fortyfold excess before all samples were analysed on an SDS PAGE gel.

Sortase-mediated labelling

N-terminally DBCO- and ATTO 488-conjugated peptides with sequence LPETGG were synthetised by Peptide Speciality Laboratories GmbH. Sortase was expressed and purified as described in Freiburger *et al.*[357], while sortase-mediated labelling was performed as described in Theile *et al.*[332]. A single test reaction contained 50 μM VCA, 100 μM sortase, and 500 mM of peptide and was performed in buffer containing 10 mM calcium chloride ($CaCl_2$) and 100 mM sodium hydrogencarbonate ($NaHCO_3$). The mixture and was left to incubate for various amount of time before quenching the reaction using 20 mM EDTA and analysing all samples on an SDS PAGE gel.

6.4.6 Microfluidic chip fabrication

The silicon wafer with GUV trap design was made previously using soft lithography by Wang *et al.*[317]. To make the microfluidic chips, polydimethylsiloxane (PDMS) base and curing agent (SYLGARD™ 184 Silicone Elastomer Kit, Dow) were mixed at a 10:1 weight ratio using a Thinky ARE-250 mixer (2 x 2 min at 2000 rpm) and poured onto the wafer in a glass petri dish to a thickness of 4 mm. Next, the mixture was degassed for 45 min in a vacuum dessicator after which the PDMS was cured at 80 °C for 2 h. The cured PDMS was peeled off the wafer, cut into individual chips and a fluid inlet and outlet were punched with a 4 mm and 0.75 mm diameter biopsy hole puncher (World Precision Instruments Germany), respectively. Individual microfluidic chips were sealed by plasma bonding to glass coverslips (24 x 60 mm # 1.5 spezial, Menzel-Gläser) using a plasma cleaner (45 s at 0.3 Torr; PDC-002-HPCE, Harrick Plasma) and bonding was completed by baking the chips at 80 °C for 30 min. Before use, each chip was coated with 1 % w/v Pluronic F-127 (Sigma-Aldrich) in PBS buffer using centrifugation (10 min at 900 G). To operate the chip and exchange buffers, the outlet of the chip was connected to a syringe pump (Nemesys S, CETONI) via a stainless steel 90° bent PDMS coupler (PN-BEN-20G-20, Darwin Microfluidics), tubing (Adtech PTFE Tubing BIOBLOCK/05 (PTFE Tubing 0.3mm ID x 0.76mm OD), Fisher Scientific), and syringe (250 μL precision glass syringe Nemesys S, CETONI). The syringe pump was operated at negative flow rates of 1 – 10 μL h^{-1}. Initial tests of the microfluidic chips were done using GUVs made using cDICE, see Chapter 3.

6.4.7 Replica moulding using epoxy

Epoxy moulds were made through replica moulding. Epoxy resin and hardener (EasyCast clear casting epoxy) were mixed in a 1:1 volume ratio using a Thinky ARE-250 mixer (2 x 2 min at 2000 rpm) and poured onto the PDMS master in a silicon mould (Silicone moulds SF029, Silkomart). Next, the mixture was degassed for 45 min in a vacuum desiccator

after which the epoxy was cured at room temperature for 24 h. The PDMS master was then peeled from the mould and discarded. The epoxy mould was placed in a petri dish and silanised using chlorotrimethylsilane (TMCS; 92361, Sigma-Aldrich) by adding 4 – 5 drops on to the mould before sealing the petri dish. After incubating for 15 min, the remaining TMCS was left to evaporate for 10 min. Microfluidic chips from the epoxy mould were prepared as described above, with the exception that the PDMS was cured for 1 h at 65 °C instead of 80 °C.

6.4.8 Streptavidin-coated beads

Fluorescent streptavidin-coated polymer microspheres (1 µm diameter; CFDG004, Sanbio) were tenfold diluted in PBS buffer and washed three times for 10 min at 10.000 rpm. The beads were then further diluted to a final concentration of 1:4000 when used with GUVs. Electroformed GUVs contained 99 mol% 18:1 1,2-dioleoyl-sn-glycero-3-phophocholine (DOPC, Avanti Polar Lipids), 0.05 mol% ATTO 655 labeled 1,2-dioleoyl-sn-glycero-3-phosphoethanolamine (DOPE, ATTO-TEC), and 1 mol% 1,2-distearoyl-sn-glycero-3-phosphoethanolamine-N-[biotinyl(polyethylene glycol)-2000] (DSPE-PEG(2000)-biotin, Avanti Polar Lipids). Binding of streptavidin-coated beads to GUVs containing either biotinylated lipids or biotin-functionalised membrane-spanning peptide was assessed by visual monitoring of the membrane and bead for extended times.

6.4.9 GUV-GUV contact assay

GUVs were formed via electroformation using a lipid mixture consisting of 100 mol% DOPC and ATTO 655-labeled SNARE peptide in a 1:170 peptide:lipid ratio. Following GUV formation, 0.5 µM streptavidin Alexa Fluor 488 was added and the mixture was left to incubate for a period of 15 min in which spontaneous formation of contact sites between different GUVs occurred.

6.5 Acknowledgements

We thank Jeffrey den Haan and Vanda Sunderlikova for help with expression and purification of VCA, Claudia Concu for work on the microfluidic GUV traps, and Christian Niederauer and Marcel Winter for their contribution to the labelling of VCA.

6.6 Appendix

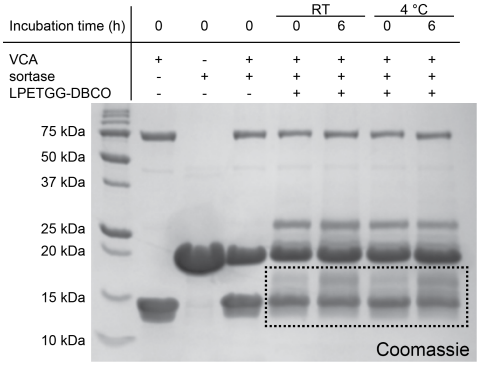

Figure 6.9 | SDS PAGE gel analysis of VCA labelling with sortase. SDS PAGE gel showing the labelling reaction of VCA with DBCO-LPETGG via sortase-mediated labelling. Before use, the peptide was incubated with azide-PEG2000 in a 1:1 ratio for 12 h at room temperature. Multiple labelling reactions were incubated at different temperatures (room temperature and 4 °C) and stopped after a 6 h incubation period before being run on an SDS PAGE gel, alongside a protein ladder and control samples. Coomassie Blue staining shows a molecular weight shift of ~ 2 kDa for VCA (black dotted box), attributed to the successful conjugation of the LPETGG-DBCO-azide-PEG2000 to VCA.

Part IV

Epilogue

CHAPTER 7

A perspective on the future

Throughout this thesis, our focus has been twofold. In Part II, we expanded on existing GUV research by optimizing the GUV production method called cDICE, while also revealing the complex processes underlying GUV formation in cDICE through the use of a custom-built high-speed microscope. The insights gained enabled us to review the wide range of GUV formation methods within the field, pinpointing cDICE's unique position in the GUV methods landscape. In Part III, armed with this knowledge, we introduced a novel bottom-up synthetic biology approach to studying phagocytosis and presented all components needed to reconstitute the process in a minimal system, the 'minimal phagocyte'.

GUVs play a central role in synthetic biology, serving not only as model membrane systems for biophysical characterization but also as a 'container' for synthetic-like cells. Our exploration of the various factors relevant for high-quality GUV formation and encapsulation efficiency in cDICE resulted in a more reproducible workflow. This we demonstrated by showcasing its workability across different labs, achieved through reciprocal sharing of expertise. By embracing and actively pursuing such an open science approach, cDICE, and its more recent successor eDICE, have since found their use within the field, proving our efforts toward a standardized protocol have not gone unnoticed. The follow-up study, in which we aimed to further our understanding of the physical principles of GUV formation in cDICE, led to somewhat surprising, yet significant results. High-speed imaging allowed us to reveal the different steps of GUV formation and the influence of protein of these processes, lifting the veil on what was essentially a black box. This is a first step toward more knowledge-based optimization of cDICE and other emulsion-based methods in the future, a prerequisite for the standardization of GUV production protocols.

A key aspect of our work was the multidisciplinary approach we pursued. By seeking perspectives beyond the experimentalist's one, specifically by including fluid dynamics, omnipresent in the biological world[358], we tried bridging the existing gap between experiment and theory. Advocating for such multidisciplinary work, and fostering an environment where such collaboration finds fertile grounds, will prove crucial for future advancements.[359–361]

Our detailed review of the different GUV fabrication methods available today highlighted that, while a diverse array of methods may prove beneficial for certain research endeavors, it presents challenges for others. This is especially exemplified for synthetic cell research, such as the BaSyC consortium, which tries to build a synthetic cell[67]. This ambitious endeavor has generated complex questions and puzzles, and while significant progress has been made in our understanding of the different building blocks, the realization of an actual synthetic cell remains elusive. It is clear the next steps lies in converging the existing research and expertise within a single unit, and as the 'container' of such a future synthetic cell arguably forms a quintessential component, decisions regarding a favorable GUV fabrication method become crucial. Establishing coherence across methods and encouraging standardized protocols is not only a step in the right direction for this research but also beneficial for the entire scientific community.

While GUVs form a big chunk of this thesis, they merely serve as a starting point for our 'minimal phagocyte', introduced in Part III. We outlined the first steps toward studying phagocytosis in a bottom-up synthetic biology way, thereby circumventing the inherent complexity of phagocytosis encountered when studying living cells. Since we here only introduced the necessary parts to reconstitute this process *in vitro*, it leaves much room for future research opportunities. Nevertheless, purposely adopting fresh perspective will undoubtedly yield new insights, a sentiment stretching beyond the realm of science.

While all presented results are merely pieces of a larger puzzle, I aim for them to find their place within the multidimensional network that is science. I hope they can be a stepping stone for others to continue their pursuit of knowledge, gain new insights, and find inspiration. In the words of Elie Metchnikoff: For me, it is time to go to the seashore in order to collect my thoughts.

Bibliography

[1] O. Metchnikoff, *Life of Elie Metchnikoff, 1845-1916.* Houghton Mifflin Company, 1921. Cited on page 3.

[2] A. I. Tauber, "Metchnikoff and the phagocytosis theory," *Nature Reviews Molecular Cell Biology*, vol. 4, no. 11, pp. 897–901, 2003.

[3] S. H. E. Kaufmann, "Immunology's foundation: the 100-year anniversary of the Nobel Prize to Paul Ehrlich and Elie Metchnikoff," *Nature Immunology*, vol. 9, no. 7, pp. 705–712, 2008. Cited on page 3.

[4] Published for the Nobel foundation by Elsevier, *Nobel Lectures, Physiology or Medicine 1901–1921.* Amsterdam: Elsevier Publishing Company, 1967. Cited on page 3.

[5] R. S. Flannagan, V. Jaumouillé, and S. Grinstein, "The cell biology of phagocytosis," *Annual Review of Pathology: Mechanisms of Disease*, vol. 7, no. 1, pp. 61–98, 2012. Cited on pages 4, 5, 7, 10, and 92.

[6] V. Jaumouillé and S. Grinstein, "Molecular Mechanisms of Phagosome Formation," in *Myeloid Cells in Health and Disease* (S. Gordon, ed.), pp. 507–526, Washington, DC, USA: ASM Press, 2017. Cited on pages 4, 7, 8, and 9.

[7] E. Uribe-Querol and C. Rosales, "Phagocytosis: Our current understanding of a universal biological process," *Frontiers in Immunology*, vol. 11, 2020. Cited on pages 4 and 92.

[8] S. A. Freeman and S. Grinstein, "Phagocytosis: Mechanosensing, traction forces, and a molecular clutch," *Current Biology*, vol. 30, no. 1, pp. R24–R26, 2020. Cited on pages 4, 7, and 8.

[9] C. Z. Han, I. J. Juncadella, J. M. Kinchen, M. W. Buckley, A. L. Klibanov, K. Dryden, S. Onengut-Gumuscu, U. Erdbrügger, S. D. Turner, Y. M. Shim, K. S. Tung, and K. S. Ravichandran, "Macrophages redirect phagocytosis by non-professional phagocytes and influence inflammation," *Nature*, vol. 539, no. 7630, pp. 570–574, 2016. Cited on page 4.

[10] L. M. Stuart and R. A. Ezekowitz, "Phagocytosis and comparative innate immunity: learning on the fly," *Nature Reviews Immunology*, vol. 8, no. 2, pp. 131–141, 2008. Cited on page 4.

[11] V. Jaumouillé and C. M. Waterman, "Physical constraints and forces involved in phagocytosis," *Frontiers in Immunology*, vol. 11, p. 1097, 2020. Cited on pages 4 and 10.

[12] S. A. Freeman and S. Grinstein, "Phagocytosis: receptors, signal integration, and the cytoskeleton," *Immunological Reviews*, vol. 262, no. 1, pp. 193–215, 2014. Cited on pages 4, 5, 7, 8, 10, and 92.

[13] V. Jaumouillé and S. Grinstein, "Receptor mobility, the cytoskeleton, and particle binding during phagocytosis," *Current Opinion in Cell Biology*, vol. 23, no. 1, pp. 22–29, 2011. Cited on page 4.

[14] R. R. Kay, "Macropinocytosis: Biology and mechanisms," *Cells & Development*, p. 203713, 2021. Cited on page 4.

[15] J. A. Swanson, "Shaping cups into phagosomes and macropinosomes," *Nature Reviews Molecular Cell Biology*, vol. 9, no. 8, pp. 639–649, 2008. Cited on pages 4 and 92.

[16] J. M. Kinchen and K. S. Ravichandran, "Phagosome maturation: going through the acid test," *Nature Reviews Molecular Cell Biology*, vol. 9, no. 10, pp. 781–795, 2008. Cited on page 5.

[17] H.-J. Lee, Y. Woo, T.-W. Hahn, Y. M. Jung, and Y.-J. Jung, "Formation and maturation of the phagosome: A key mechanism in innate immunity against intracellular bacterial infection," *Microorganisms*, vol. 8, no. 9, p. 1298, 2020. Cited on page 5.

[18] P. Chugh and E. K. Paluch, "The actin cortex at a glance," *Journal of Cell Science*, vol. 131, no. 14, p. jcs186254, 2018. Cited on page 5.

[19] T. M. Svitkina, "Actin cell cortex: Structure and molecular organization," *Trends in Cell Biology*, vol. 30, no. 7, pp. 556–565, 2020. Cited on page 5.

[20] P. Lappalainen, T. Kotila, A. Jégou, and G. Romet-Lemonne, "Biochemical and mechanical regulation of actin dynamics," *Nature Reviews Molecular Cell Biology*, vol. 23, pp. 836–852, 2022. Cited on page 5.

[21] D. Sept and J. A. McCammon, "Thermodynamics and kinetics of actin filament nucleation.," *Biophysical Journal*, vol. 81, no. 2, pp. 667–674, 2001. Cited on page 5.

[22] T. D. Pollard, "Actin and actin-binding proteins," *Cold Spring Harbor Perspectives in Biology*, vol. 8, no. 8, p. a018226, 2016. Cited on page 5.

[23] A. Colin, T. Kotila, C. Guérin, M. Orhant-Prioux, B. Vianay, A. Mogilner, P. Lappalainen, M. Théry, and L. Blanchoin, "Recycling of the actin monomer pool limits the lifetime of network turnover," *The EMBO Journal*, vol. 42, no. 9, p. e112717, 2023. Cited on page 5.

[24] A. Yonis, M. Bovellan, Y. Romeo, P. Chugh, E. K. Paluch, R. Thorogate, P. P. Roux, G. Charras, A. Boden, M. Vaghela, A. Jégou, D. Moulding, M. Fritzsche, A. J. Thrasher, G. Romet-Lemonne, and M. Biro, "Cellular control of cortical actin nucleation," *Current Biology*, vol. 24, no. 14, pp. 1628–1635, 2014. Cited on page 5.

[25] H. N. Higgs, L. Blanchoin, and T. D. Pollard, "Influence of the C terminus of Wiskott-Aldrich syndrome protein (WASp) and the Arp2/3 complex on actin polymerization," *Biochemistry*, vol. 38, no. 46, pp. 15212–15222, 1999. Cited on page 5.

[26] R. C. Robinson, K. Turbedsky, D. A. Kaiser, J.-B. Marchand, H. N. Higgs, S. Choe, and T. D. Pollard, "Crystal Structure of Arp2/3 Complex," *Science*, vol. 294, no. 5547, pp. 1679–1684, 2001. Cited on page 5.

[27] D. M. Veltman and R. H. Insall, "WASP Family Proteins: Their Evolution and Its Physiological Implications," *Molecular Biology of the Cell*, vol. 21, no. 16, pp. 2880–2893, 2010. Cited on page 5.

[28] S. H. Zigmond, "How WASP Regulates Actin Polymerization," *Journal of Cell Biology*, vol. 150, no. 6, pp. F117–F120, 2000. Cited on page 5.

[29] K. Hüfner, H. N. Higgs, T. D. Pollard, C. Jacobi, M. Aepfelbacher, and S. Linder, "The Verprolin-like Central (VC) Region of Wiskott-Aldrich Syndrome Protein Induces Arp2/3 Complex-dependent Actin Nucleation," *Journal of Biological Chemistry*, vol. 276, no. 38, pp. 35761–35767, 2001. Cited on page 5.

[30] A. M. Gautreau, F. E. Fregoso, G. Simanov, and R. Dominguez, "Nucleation, stabilization, and disassembly of branched actin networks," *Trends in Cell Biology*, vol. 32, no. 5, pp. 421–432, 2021. Cited on page 5.

[31] S. Romero, C. Le Clainche, D. Didry, C. Egile, D. Pantaloni, and M.-F. Carlier, "Formin is a processive motor that requires profilin to accelerate actin assembly and associated atp hydrolysis," *Cell*, vol. 119, no. 3, pp. 419–429, 2004. Cited on page 5.

[32] M. Fritzsche, C. Erlenkämper, E. Moeendarbary, G. Charras, and K. Kruse, "Actin kinetics shapes cortical network structure and mechanics," *Science Advances*, vol. 2, no. 4, p. e1501337, 2016. Cited on page 5.

[33] L. Blanchoin, R. Boujemaa-Paterski, C. Sykes, and J. Plastino, "Actin dynamics, architecture, and mechanics in cell motility," *Physiological Reviews*, vol. 94, no. 1, pp. 235–263, 2014. Cited on page 5.

[34] F. S. Southwick, "Gelsolin and adf/cofilin enhance the actin dynamics of motile cells," *Proceedings of the National Academy of Sciences of the United States of America*, vol. 97, no. 13, pp. 6936–6938, 2000. Cited on page 6.

[35] K. Krishnan and P. D. J. Moens, "Structure and functions of profilins," *Biophysical Reviews*, vol. 1, no. 2, pp. 71–81, 2009. Cited on page 6.

[36] J. Pieters, P. Müller, and R. Jayachandran, "On guard: coronin proteins in innate

and adaptive immunity," *Nature Reviews Immunology*, vol. 13, no. 7, pp. 510–518, 2013. Cited on page 6.

[37] H. Ennomani, G. Letort, C. Guérin, J.-L. Martiel, W. Cao, F. Nédélec, E. M. De La Cruz, M. Théry, and L. Blanchoin, "Architecture and connectivity govern actin network contractility," *Current Biology*, vol. 26, no. 5, pp. 616–626, 2016. Cited on page 6.

[38] G. H. Koenderink and E. K. Paluch, "Architecture shapes contractility in actomyosin networks," *Current Opinion in Cell Biology*, vol. 50, pp. 79–85, 2018. Cited on page 6.

[39] Y. Cai, O. Rossier, N. C. Gauthier, N. Biais, M.-A. Fardin, X. Zhang, L. W. Miller, B. Ladoux, V. W. Cornish, and M. P. Sheetz, "Cytoskeletal coherence requires myosin-IIA contractility," *Journal of Cell Science*, vol. 123, no. 3, pp. 413–423, 2010. Cited on page 6.

[40] C. W. Pak, K. C. Flynn, and J. R. Bamburg, "Actin-binding proteins take the reins in growth cones," *Nature Reviews Neuroscience*, vol. 9, no. 2, pp. 136–147, 2008. Cited on page 6.

[41] S. Mylvaganam, S. A. Freeman, and S. Grinstein, "The cytoskeleton in phagocytosis and macropinocytosis," *Current Biology*, vol. 31, no. 10, pp. R619–R632, 2021. Cited on pages 6, 8, 9, 10, and 92.

[42] S. R. Barger, D. Vorselen, N. C. Gauthier, J. A. Theriot, and M. Krendel, "F-actin organization and target constriction during primary macrophage phagocytosis is balanced by competing activity of myosin-I and myosin-II," *Molecular Biology of the Cell*, vol. 33, no. 14, 2022. Cited on pages 6 and 8.

[43] H. L. Poulsen, "Interstitial fluid concentrations of albumin and immunoglobulin g in normal men," *Scandinavian Journal of Clinical and Laboratory Investigation*, vol. 34, no. 2, pp. 119–122, 1974. Cited on page 7.

[44] A. Kusumi, T. K. Fujiwara, R. Chadda, M. Xie, T. A. Tsunoyama, Z. Kalay, R. S. Kasai, and K. G. Suzuki, "Dynamic Organizing Principles of the Plasma Membrane that Regulate Signal Transduction: Commemorating the Fortieth Anniversary of Singer and Nicolson's Fluid-Mosaic Model," *Annual Review of Cell and Developmental Biology*, vol. 28, no. 1, pp. 215–250, 2012. Cited on pages 7 and 8.

[45] G. D. Brown, "Dectin-1: a signalling non-TLR pattern-recognition receptor," *Nature Reviews Immunology*, vol. 6, no. 1, pp. 33–43, 2006. Cited on page 7.

[46] F. Nimmerjahn and J. V. Ravetch, "Fcγ receptors as regulators of immune responses," *Nature Reviews Immunology*, vol. 8, no. 1, pp. 34–47, 2008. Cited on page 7.

[47] S. A. Freeman, J. Goyette, W. Furuya, E. C. Woods, C. R. Bertozzi, W. Bergmeier, B. Hinz, P. A. van der Merwe, R. Das, and S. Grinstein, "Integrins form an expanding diffusional barrier that coordinates phagocytosis," *Cell*, vol. 164, no. 1-2, pp. 128–140, 2016. Cited on page 7.

[48] V. Jaumouillé, A. X. Cartagena-Rivera, and C. M. Waterman, "Coupling of $\beta 2$ integrins to actin by a mechanosensitive molecular clutch drives complement receptor-mediated phagocytosis," *Nature cell biology*, vol. 21, no. 11, pp. 1357–1369, 2019. Cited on page 7.

[49] T. G. Kuznetsova, M. N. Starodubtseva, N. I. Yegorenkov, S. A. Chizhik, and R. I. Zhdanov, "Atomic force microscopy probing of cell elasticity," *Micron*, vol. 38, no. 8, pp. 824–833, 2007. Cited on page 7.

[50] A. Amir, F. Babaeipour, D. B. McIntosh, D. R. Nelson, and S. Jun, "Bending forces plastically deform growing bacterial cell walls," *Proceedings of the National Academy of Sciences of the United States of America*, vol. 111, no. 16, pp. 5778–5783, 2014.

[51] Y. Deng, M. Sun, and J. W. Shaevitz, "Direct measurement of cell wall stress stiffening and turgor pressure in live bacterial cells," *Physical Review Letters*, vol. 107, no. 15, p. 158101, 2011.

[52] N. I. Nikolaev, T. Müller, D. J. Williams, and Y. Liu, "Changes in the stiffness of human mesenchymal stem cells with the progress of cell death as measured by atomic force microscopy," *Journal of Biomechanics*, vol. 47, no. 3, pp. 625–630, 2014. Cited on page 7.

[53] S. Arandjelovic and K. S. Ravichandran, "Phagocytosis of apoptotic cells in homeostasis," *Nature Immunology*, vol. 16, no. 9, pp. 907–917, 2015. Cited on page 7.

[54] S. M. Kelley and K. S. Ravichandran, "Putting the brakes on phagocytosis: "don't-eat-me" signaling in physiology and disease," *EMBO reports*, vol. 22, p. e52564, 2021. Cited on page 7.

[55] F. B. Chekeni and K. S. Ravichandran, "The role of nucleotides in apoptotic cell clearance: implications for disease pathogenesis," *Journal of molecular medicine*, vol. 89, no. 1, pp. 13–22, 2011. Cited on page 7.

[56] V. A. Fadok, D. R. Voelker, P. A. Campbell, J. J. Cohen, D. L. Bratton, and P. M. Henson, "Exposure of phosphatidylserine on the surface of apoptotic lymphocytes triggers specific recognition and removal by macrophages," *Journal of Immunology*, vol. 148, no. 7, pp. 2207–2216, 1992. Cited on page 7.

[57] S. M. Mylvaganam, S. Grinstein, and S. A. Freeman, "Picket-fences in the plasma membrane: functions in immune cells and phagocytosis," *Seminars in Immunopathology*, vol. 40, no. 6, pp. 605–615, 2018. Cited on pages 8 and 9.

[58] F. Niedergang and S. Grinstein, "How to build a phagosome: new concepts for an old process," *Current Opinion in Cell Biology*, vol. 50, pp. 57–63, 2018. Cited on pages 8 and 9.

[59] D. Vorselen, R. L. D. Labitigan, and J. A. Theriot, "A mechanical perspective on phagocytic cup formation," *Current Opinion in Cell Biology*, vol. 66, pp. 112–122, 2020. Cited on pages 8, 9, and 10.

[60] D. Cox, J. S. Berg, M. Cammer, J. O. Chinegwundoh, B. M. Dale, R. E. Cheney, and S. Greenberg, "Myosin x is a downstream effector of pi(3)k during phagocytosis," *Nature Cell Biology*, vol. 4, no. 7, pp. 469–477, 2002. Cited on page 9.

[61] P. P. Ostrowski, S. Grinstein, and S. A. Freeman, "Diffusion barriers, mechanical forces, and the biophysics of phagocytosis," *Developmental Cell*, vol. 38, no. 2, pp. 135–146, 2016. Cited on page 9.

[62] N. Touret, P. Paroutis, and S. Grinstein, "The nature of the phagosomal membrane: endoplasmic reticulum versus plasmalemma," *Journal of Leukocyte Biology*, vol. 77, no. 6, pp. 878–885, 2005. Cited on page 9.

[63] S. R. Barger, N. C. Gauthier, and M. Krendel, "Squeezing in a meal: myosin functions in phagocytosis," *Trends in cell biology*, vol. 30, no. 2, pp. 157–167, 2020. Cited on page 10.

[64] Y. Seta, K. Kawakatsu, S. Degawa, T. Goto, and T. Nishikata, "Morphological evidence for novel roles of microtubules in macrophage phagocytosis," *International Journal of Molecular Sciences*, vol. 24, no. 2, p. 1373, 2023. Cited on page 10.

[65] M. Dogterom and G. H. Koenderink, "Actin–microtubule crosstalk in cell biology," *Nature Reviews Molecular Cell Biology*, vol. 20, no. 1, pp. 38–54, 2019. Cited on page 10.

[66] K. A. Ganzinger and P. Schwille, "More from less – bottom-up reconstitution of cell biology," *Journal of Cell Science*, vol. 132, no. 4, p. 11, 2019. Cited on pages 10, 18, 46, and 100.

[67] "BaSyC - Building a Synthetic Cell." (Online: https://www.basyc.nl/; accessed 2020-11-23). Cited on pages 10, 18, 46, 68, and 114.

[68] K. Göpfrich, I. Platzman, and J. P. Spatz, "Mastering Complexity: Towards Bottom-up Construction of Multifunctional Eukaryotic Synthetic Cells," *Trends in Biotechnology*, vol. 36, no. 9, pp. 938–951, 2018. Cited on page 18.

[69] T. J. Lagny and P. Bassereau, "Bioinspired membrane-based systems for a physical approach of cell organization and dynamics: usefulness and limitations," *Interface Focus*, vol. 5, p. 20150038, 2015. Cited on page 18.

[70] "Synthetic Cell initiative." (Online: https://www.syntheticcell.eu/; accessed 2020-11-23). Cited on pages 18 and 68.

[71] "Build-a-Cell." (Online: https://www.buildacell.org; accessed 2020-11-23). Cited on page 68.

[72] P. Schwille, J. Spatz, K. Landfester, E. Bodenschatz, S. Herminghaus, V. Sourjik, T. J. Erb, P. Bastiaens, R. Lipowsky, A. Hyman, P. Dabrock, J.-C. Baret, T. Vidakovic-Koch, P. Bieling, R. Dimova, H. Mutschler, T. Robinson, T.-Y. D. Tang, S. Wegner, and K. Sundmacher, "MaxSynBio: Avenues Towards Creating Cells from the Bottom Up," *Angewandte Chemie International Edition*, vol. 57, no. 41, pp. 13382–13392, 2018. Cited on pages 18 and 68.

[73] P. Walde, K. Cosentino, H. Engel, and P. Stano, "Giant Vesicles: Preparations and Applications," *ChemBioChem*, vol. 11, no. 7, pp. 848–865, 2010. Cited on pages 18, 46, 69, 72, and 73.

[74] R. Dimova and C. M. Marques, *The Giant Vesicle Book*. CRC Press, 1 ed., 2019. Cited on pages 26, 46, and 72.

[75] R. Dimova, "Giant Vesicles and Their Use in Assays for Assessing Membrane Phase State, Curvature, Mechanics, and Electrical Properties," *Annual Review of Biophysics*, vol. 48, no. 1, pp. 93–119, 2019. Cited on pages 78 and 101.

[76] D. Papahadjopoulos and H. K. Kimelberg, "Phospholipid vesicles (liposomes) as models for biological membranes: Their properties and interactions with cholesterol and proteins," *Progress in Surface Science*, vol. 4, pp. 141–144, 1974. Cited on pages 18 and 46.

[77] J. P. Reeves and R. M. Dowben, "Formation and properties of thin-walled phospholipid vesicles," *Journal of Cellular Physiology*, vol. 73, no. 1, pp. 49–60, 1969. Cited on pages 18, 46, and 72.

[78] M. I. Angelova and D. S. Dimitrov, "Liposome Electroformation," *Faraday Discussions of the Chemical Society*, vol. 81, pp. 303–311, 1986. Cited on pages 18, 46, and 72.

[79] L.-R. Montes, A. Alonso, F. M. Goñi, and L. A. Bagatolli, "Giant Unilamellar Vesicles Electroformed from Native Membranes and Organic Lipid Mixtures under Physiological Conditions," *Biophysical Journal*, vol. 93, no. 10, pp. 3548–3554, 2007.

[80] M. Breton, M. Amirkavei, and L. M. Mir, "Optimization of the Electroformation of Giant Unilamellar Vesicles (GUVs) with Unsaturated Phospholipids," *The Journal of Membrane Biology*, vol. 248, no. 5, pp. 827–835, 2015.

[81] R. Dimova, S. Aranda, N. Bezlyepkina, V. Nikolov, K. A. Riske, and R. Lipowsky, "A practical guide to giant vesicles. Probing the membrane nanoregime via optical microscopy," *Journal of Physics Condensed Matter*, vol. 18, no. 28, pp. S1151–S1176, 2006. Cited on pages 18, 46, 71, and 78.

[82] K. S. Horger, D. J. Estes, R. Capone, and M. Mayer, "Films of Agarose Enable Rapid Formation of Giant Liposomes in Solutions of Physiologic Ionic Strength," *Journal of the American Chemical Society*, vol. 131, no. 5, pp. 1810–1819, 2009. Cited on pages 18, 25, 46, 73, 78, 79, and 84.

[83] A. Weinberger, F.-C. Tsai, G. H. Koenderink, T. F. Schmidt, R. Itri, W. Meier, T. Schmatko, A. Schröder, and C. Marques, "Gel-Assisted Formation of Giant Unilamellar Vesicles," *Biophysical Journal*, vol. 105, no. 1, pp. 154–164, 2012. Cited on pages 73, 79, and 84.

[84] N. López Mora, J. S. Hansen, Y. Gao, A. A. Ronald, R. Kieltyka, N. Malmstadt, and A. Kros, "Preparation of size tunable giant vesicles from cross-linked

dextran(ethylene glycol) hydrogels," *Chemical Communications*, vol. 50, no. 16, pp. 1953–1955, 2014. Cited on page 73.

[85] J. Schultze, A. Vagias, L. Ye, E. Prantl, V. Breising, A. Best, K. Koynov, C. M. Marques, and H.-J. Butt, "Preparation of Monodisperse Giant Unilamellar Anchored Vesicles Using Micropatterned Hydrogel Substrates," *ACS Omega*, vol. 4, no. 5, pp. 9393–9399, 2019. Cited on pages 18 and 46.

[86] P. C. Hu, S. Li, and N. Malmstadt, "Microfluidic Fabrication of Asymmetric Giant Lipid Vesicles," *ACS Applied Materials and Interfaces*, vol. 3, no. 5, pp. 1434–1440, 2011. Cited on pages 18, 46, and 73.

[87] H. Ito, T. Yamanaka, S. Kato, T. Hamada, M. Takagi, M. Ichikawa, and K. Yoshikawa, "Dynamical formation of lipid bilayer vesicles from lipid-coated droplets across a planar monolayer at an oil/water interface," *Soft Matter*, vol. 9, no. 40, pp. 9539–9547, 2013.

[88] D. van Swaay and A. deMello, "Microfluidic methods for forming liposomes," *Lab on a Chip*, vol. 13, no. 5, p. 752, 2020. Cited on pages 72, 73, and 75.

[89] K. Funakoshi, H. Suzuki, and S. Takeuchi, "Formation of Giant Lipid Vesiclelike Compartments from a Planar Lipid Membrane by a Pulsed Jet Flow," *Journal of the American Chemical Society*, vol. 129, no. 42, pp. 12608–12609, 2007. Cited on page 75.

[90] J. C. Stachowiak, D. L. Richmond, T. H. Li, A. P. Liu, S. H. Parekh, and D. A. Fletcher, "Unilamellar vesicle formation and encapsulation by microfluidic jetting," *Proceedings of the National Academy of Sciences*, vol. 105, no. 12, pp. 4697–4702, 2008. Cited on page 75.

[91] D. L. Richmond, E. M. Schmid, S. Martens, J. C. Stachowiak, N. Liska, and D. A. Fletcher, "Forming giant vesicles with controlled membrane composition, asymmetry, and contents," *Proceedings of the National Academy of Sciences*, vol. 108, no. 23, pp. 9431–9436, 2011. Cited on page 77.

[92] S. Deshpande, Y. Caspi, A. E. C. Meijering, and C. Dekker, "Octanol-assisted liposome assembly on chip," *Nature Communications*, vol. 7, no. 1, p. 10447, 2016. Cited on pages 18, 46, 73, 75, 78, 79, 81, and 84.

[93] M. Abkarian, E. Loiseau, and G. Massiera, "Continuous droplet interface crossing encapsulation (cDICE) for high throughput monodisperse vesicle design," *Soft Matter*, vol. 7, no. 10, pp. 4610–4614, 2011. Cited on pages 18, 19, 21, 27, 28, 46, 47, 49, 55, 57, 73, 75, 76, 78, 79, 81, and 84.

[94] M. C. Blosser, B. G. Horst, and S. L. Keller, "cDICE method produces giant lipid vesicles under physiological conditions of charged lipids and ionic solutions," *Soft Matter*, vol. 12, no. 35, pp. 7364–7371, 2016. Cited on pages 18, 21, 27, and 77.

[95] J. Deek, R. Maan, E. Loiseau, and A. R. Bausch, "Reconstitution of composite actin

and keratin networks in vesicles," *Soft Matter*, vol. 14, no. 10, pp. 1897–1902, 2018. Cited on pages 18, 21, 27, 75, and 81.

[96] F. C. Keber, E. Loiseau, T. Sanchez, S. J. DeCamp, L. Giomi, M. J. Bowick, M. C. Marchetti, Z. Dogic, and A. R. Bausch, "Topology and dynamics of active nematic vesicles," *Science*, vol. 345, no. 6201, pp. 1135–1139, 2020. Cited on pages 79, 80, and 84.

[97] T. Litschel, K. A. Ganzinger, T. Movinkel, M. Heymann, T. Robinson, H. Mutschler, and P. Schwille, "Freeze-thaw cycles induce content exchange between cell-sized lipid vesicles," *New Journal of Physics*, vol. 20, p. 055008, 2018. Cited on page 82.

[98] T. Litschel, B. Ramm, R. Maas, M. Heymann, and P. Schwille, "Beating Vesicles: Encapsulated Protein Oscillations Cause Dynamic Membrane Deformations," *Angewandte Chemie International Edition*, vol. 57, no. 50, pp. 16286–16290, 2018. Cited on pages 18, 19, 21, 27, 46, 73, 79, 80, 81, and 84.

[99] J. D. Berry, M. J. Neeson, R. R. Dagastine, D. Y. Chan, and R. F. Tabor, "Measurement of surface and interfacial tension using pendant drop tensiometry," *Journal of Colloid and Interface Science*, vol. 454, pp. 226–237, 2015. Cited on pages 19 and 53.

[100] "KNMI - Daggegevens van het weer in Nederland - Download." (Online: http://projects.knmi.nl/klimatologie/daggegevens/selectie.cgi; accessed 2020-12-04). Cited on page 20.

[101] E. Loiseau, J. A. M. Schneider, F. C. Keber, C. Pelzl, G. Massiera, G. Salbreux, and A. R. Bausch, "Shape remodeling and blebbing of active cytoskeletal vesicles," *Science Advances*, vol. 2, no. 4, p. e1500465, 2016. Cited on pages 21, 52, 79, 81, 82, and 84.

[102] K. Dürre and A. R. Bausch, "Formation of phase separated vesicles by double layer cDICE," *Soft Matter*, vol. 15, no. 47, pp. 9676–9681, 2019. Cited on pages 21, 73, and 77.

[103] L. Song, M. R. Hobaugh, C. Shustak, S. Cheley, H. Bayley, and J. E. Gouaux, "Structure of Staphylococcal a-Hemolysin, a Heptameric Transmembrane Pore," *Science*, vol. 274, no. 5294, pp. 1859–1866, 1998. Cited on page 21.

[104] H. Ostolaza, B. Bartolomé, I. Ortiz de Zárate, F. de la Cruz, and F. M. Goñi, "Release of lipid vesicle contents by the bacterial protein toxin a-haemolysin," *Biochimica et Biophysica Acta*, vol. 1147, no. 1, pp. 81–88, 1993. Cited on page 21.

[105] P. H. J. Kouwer, M. Koepf, V. A. A. Le Sage, M. Jaspers, A. M. van Buul, Z. H. Eksteen-Akeroyd, T. Woltinge, E. Schwartz, H. J. Kitto, R. Hoogenboom, S. J. Picken, R. J. M. Nolte, E. Mendes, and A. E. Rowan, "Responsive biomimetic networks from polyisocyanopeptide hydrogels," *Nature*, vol. 493, no. 7434, pp. 651–655, 2013. Cited on pages 21 and 31.

[106] R. B. Lira, J. Steinkühler, R. L. Knorr, R. Dimova, and K. A. Riske, "Posing for a picture: vesicle immobilization in agarose gel," *Scientific Reports*, vol. 6, no. 1, p. 25254, 2016. Cited on page 21.

[107] Y. Mulla, A. Aufderhorst-Roberts, and G. H. Koenderink, "Shaping up synthetic cells," *Physical Biology*, vol. 15, no. 4, p. 041001, 2018. Cited on pages 22, 46, 69, and 72.

[108] C. Claudet, M. In, and G. Massiera, "Method to disperse lipids as aggregates in oil for bilayers production," *The European Physical Journal E*, vol. 39, no. 1, p. 9, 2016. Cited on pages 23, 27, 79, and 84.

[109] A. Doerr, E. de Reus, P. van Nies, A. Wahl, and C. Danelon, "Modelling cell-free RNA and protein synthesis with minimal systems," *Phys. Biol.*, vol. 16, no. 2, p. 025001, 2019. Cited on page 24.

[110] H. Saito, Y. Kato, M. Le Berre, A. Yamada, T. Inoue, K. Yosikawa, and D. Baigl, "Time-Resolved Tracking of a Minimum Gene Expression System Reconstituted in Giant Liposomes," *ChemBioChem*, vol. 10, no. 10, pp. 1640–1643, 2009. Cited on page 24.

[111] T. Sunami, K. Sato, T. Matsuura, K. Tsukada, I. Urabe, and T. Yomo, "Femtoliter compartment in liposomes for in vitro selection of proteins," *Analytical Biochemistry*, vol. 357, no. 1, pp. 128–136, 2006.

[112] K. Hosoda, T. Sunami, Y. Kazuta, T. Matsuura, H. Suzuki, and T. Yomo, "Quantitative Study of the Structure of Multilamellar Giant Liposomes As a Container of Protein Synthesis Reaction," *Langmuir*, vol. 24, no. 23, pp. 13540–13548, 2008. Cited on page 24.

[113] S. Ota, S. Yoshizawa, and S. Takeuchi, "Microfluidic Formation of Monodisperse, Cell-Sized, and Unilamellar Vesicles," *Angewandte Chemie International Edition*, vol. 48, no. 35, pp. 6533–6537, 2009. Cited on page 24.

[114] Y. Shimizu, A. Inoue, Y. Tomari, T. Suzuki, T. Yokogawa, K. Nishikawa, and T. Ueda, "Cell-free translation reconstituted with purified components," *Nature Biotechnology*, vol. 19, no. 8, pp. 751–755, 2001. Cited on page 24.

[115] F.-C. Tsai, B. Stuhrmann, and G. H. Koenderink, "Encapsulation of Active Cytoskeletal Protein Networks in Cell-Sized Liposomes," *Langmuir*, vol. 27, no. 16, pp. 10061–10071, 2011. Cited on pages 25, 73, 79, 81, 82, and 84.

[116] J. D. Castile and K. M. Taylor, "Factors affecting the size distribution of liposomes produced by freeze–thaw extrusion," *International Journal of Pharmaceutics*, vol. 188, no. 1, pp. 87–95, 1999.

[117] Y. Yamashita, M. Oka, T. Tanaka, and M. Yamazaki, "A new method for the preparation of giant liposomes in high salt concentrations and growth of protein microcrystals in them," *Biochimica et Biophysica Acta (BBA) - Biomembranes*, vol. 1561, no. 2, pp. 129–134, 2002. Cited on page 25.

[118] T. H. Cheffings, N. J. Burroughs, and M. K. Balasubramanian, "Actomyosin Ring Formation and Tension Generation in Eukaryotic Cytokinesis," *Current Biology*, vol. 26, no. 15, pp. R719–R737, 2016. Cited on page 25.

[119] G. H. Koenderink and E. K. Paluch, "Architecture shapes contractility in actomyosin networks," *Current Opinion in Cell Biology*, vol. 50, pp. 79–85, 2018. Cited on page 25.

[120] L. M. Machesky and K. L. Gould, "The Arp2/3 complex: a multifunctional actin organizer," *Current Opinion in Cell Biology*, vol. 11, no. 1, pp. 117–121, 1999. Cited on page 25.

[121] D. Pantaloni, R. Boujemaa, D. Didry, P. Gounon, and M.-F. Carlier, "The Arp2/3 complex branches filament barbed ends: functional antagonism with capping proteins," *Nature Cell Biology*, vol. 2, no. 7, pp. 385–391, 2000. Cited on page 25.

[122] D. M. Veltman and R. H. Insall, "WASP Family Proteins: Their Evolution and Its Physiological Implications," *Molecular Biology of the Cell*, vol. 21, no. 16, pp. 2880–2893, 2010. Cited on page 25.

[123] Sonal, K. A. Ganzinger, S. K. Vogel, J. Mücksch, P. Blumhardt, and P. Schwille, "Myosin-II activity generates a dynamic steady state with continuous actin turnover in a minimal actin cortex," *Journal of Cell Science*, vol. 132, no. 4, p. jcs219899, 2019. Cited on pages 25 and 98.

[124] R. Wang and A. E. Carlsson, "How capping protein enhances actin filament growth and nucleation on biomimetic beads," *Physical Biology*, vol. 12, no. 6, p. 066008, 2015. Cited on page 25.

[125] O. Akin and R. D. Mullins, "Capping Protein Increases the Rate of Actin-Based Motility by Promoting Filament Nucleation by the Arp2/3 Complex," *Cell*, vol. 133, pp. 841–851, 2008. Cited on page 25.

[126] K. Guevorkian, J. Manzi, L.-L. Pontani, F. Brochard-Wyart, and C. Sykes, "Mechanics of Biomimetic Liposomes Encapsulating an Actin Shell," *Biophysical Journal*, vol. 109, no. 12, pp. 2471–2479, 2015. Cited on page 25.

[127] L.-L. Pontani, J. van der Gucht, G. Salbreux, J. Heuvingh, J.-F. Joanny, and C. Sykes, "Reconstitution of an Actin Cortex Inside a Liposome," *Biophysical Journal*, vol. 96, no. 1, pp. 192–198, 2009. Cited on pages 25, 73, 79, 80, and 84.

[128] B.-j. Jeon, D. T. Nguyen, G. R. Abraham, N. Conrad, D. K. Fygenson, and O. A. Saleh, "Salt-dependent properties of a coacervate-like, self-assembled DNA liquid," *Soft Matter*, vol. 14, no. 34, pp. 7009–7015, 2018. Cited on pages 26 and 34.

[129] P.-Y. Bolinger, D. Stamou, and H. Vogel, "An Integrated Self-Assembled Nanofluidic System for Controlled Biological Chemistries," *Angewandte Chemie International Edition*, vol. 47, no. 30, pp. 5544–5549, 2008. Cited on page 26.

[130] K. Y. Lee, S.-J. Park, K. A. Lee, S.-H. Kim, H. Kim, Y. Meroz, L. Mahadevan, K.-H. Jung, T. K. Ahn, K. K. Parker, and K. Shin, "Photosynthetic artificial organelles sustain and control ATP-dependent reactions in a protocellular system," *Nature Biotechnology*, vol. 36, no. 6, pp. 530–535, 2018. Cited on page 81.

[131] J. W. Hindley, Y. Elani, C. M. McGilvery, S. Ali, C. L. Bevan, R. V. Law, and O. Ces, "Light-triggered enzymatic reactions in nested vesicle reactors," *Nature Communications*, vol. 9, no. 1, p. 1093, 2018. Cited on page 26.

[132] R. Phillips, J. Kondev, and J. Theriot, *Physical Biology of the Cell*. New York: Garland Science, Taylor & Francis Group, 2008. Cited on pages 26 and 69.

[133] T. E. Miller, T. Beneyton, T. Schwander, C. Diehl, M. Girault, R. McLean, T. Chotel, P. Claus, N. S. Cortina, J.-C. Baret, and T. J. Erb, "Light-powered CO_2 fixation in a chloroplast mimic with natural and synthetic parts," *Science*, vol. 368, no. 6491, pp. 649–654, 2020. Cited on page 26.

[134] O.-P. Lehtinen, R. W. N. Nugroho, T. Lehtimaa, S. Vierros, P. Hiekkataipale, J. Ruokolainen, M. Sammalkorpi, and M. Österberg, "Effect of temperature, water content and free fatty acid on reverse micelle formation of phospholipids in vegetable oil," *Colloids and Surfaces B: Biointerfaces*, vol. 160, pp. 355–363, 2017. Cited on page 27.

[135] R. Koynova and B. Tenchov, "Phase Transitions and Phase Behavior of Lipids," in *Encyclopedia of Biophysics* (G. C. K. Roberts, ed.), pp. 1841–1854, Berlin, Heidelberg: Springer Berlin Heidelberg, 2013. Cited on page 27.

[136] K. Karamdad, R. V. Law, J. M. Seddon, N. J. Brooks, and O. Ces, "Preparation and mechanical characterisation of giant unilamellar vesicles by a microfluidic method," *Lab on a Chip*, vol. 15, no. 2, pp. 557–562, 2015. Cited on pages 27 and 73.

[137] A. Moga, N. Yandrapalli, R. Dimova, and T. Robinson, "Optimization of the Inverted Emulsion Method for High-Yield Production of Biomimetic Giant Unilamellar Vesicles," *ChemBioChem*, vol. 20, no. 20, pp. 2674–2682, 2019. Cited on pages 75, 78, 79, and 84.

[138] M. Schaich, D. Sobota, H. Sleath, J. Cama, and U. F. Keyser, "Characterization of lipid composition and diffusivity in OLA generated vesicles," *Biochimica et Biophysica Acta (BBA) - Biomembranes*, vol. 1862, no. 9, p. 183359, 2020. Cited on pages 27, 78, 79, and 84.

[139] D. Garenne, A. Libchaber, and V. Noireaux, "Membrane molecular crowding enhances MreB polymerization to shape synthetic cells from spheres to rods," *Proceedings of the National Academy of Sciences*, vol. 117, no. 4, pp. 1902–1909, 2020. Cited on pages 28, 79, 80, and 84.

[140] L. Raleigh, "VI. On the capillary phenomena of jets," *Proceedings of the Royal Society of London*, vol. 29, pp. 71–79, 1879. Cited on page 28.

[141] Y. Bashirzadeh, S. A. Redford, C. Lorpaiboon, A. Groaz, H. Moghimianavval, T. Litschel, P. Schwille, G. M. Hocky, A. R. Dinner, and A. P. Liu, "Actin crosslinker competition and sorting drive emergent GUV size-dependent actin network architecture," *Communications Biology*, vol. 4, no. 1, p. 1136, 2021. Cited on pages 28, 75, 79, 80, 81, 83, and 84.

[142] F.-C. Tsai and G. H. Koenderink, "Shape control of lipid bilayer membranes by confined actin bundles," *Soft Matter*, vol. 11, no. 45, pp. 8834–8847, 2015. Cited on pages 28, 73, and 81.

[143] P. B. Stranges, M. Palla, S. Kalachikov, J. Nivala, M. Dorwart, A. Trans, S. Kumar, M. Porel, M. Chien, C. Tao, I. Morozova, Z. Li, S. Shi, A. Aberra, C. Arnold, A. Yang, A. Aguirre, E. T. Harada, D. Korenblum, J. Pollard, A. Bhat, D. Gremyachinskiy, A. Bibillo, R. Chen, R. Davis, J. J. Russo, C. W. Fuller, S. Roever, J. Ju, and G. M. Church, "Design and characterization of a nanopore-coupled polymerase for single-molecule DNA sequencing by synthesis on an electrode array," *Proceedings of the National Academy of Sciences*, vol. 113, no. 44, pp. E6749–E6756, 2016. Cited on page 31.

[144] J. Canny, "A Computational Approach to Edge Detection," *IEEE Transactions on Pattern Analysis and Machine Intelligence*, vol. PAMI-8, no. 6, pp. 679–698, 1986. Cited on page 32.

[145] P. Virtanen, R. Gommers, T. E. Oliphant, M. Haberland, T. Reddy, D. Cournapeau, E. Burovski, P. Peterson, W. Weckesser, J. Bright, S. J. van der Walt, M. Brett, J. Wilson, K. J. Millman, N. Mayorov, A. R. J. Nelson, E. Jones, R. Kern, E. Larson, C. J. Carey, İ. Polat, Y. Feng, E. W. Moore, J. VanderPlas, D. Laxalde, J. Perktold, R. Cimrman, I. Henriksen, E. A. Quintero, C. R. Harris, A. M. Archibald, A. H. Ribeiro, F. Pedregosa, P. van Mulbregt, and S. . Contributors, "SciPy 1.0: fundamental algorithms for scientific computing in Python," *Nature Methods*, vol. 17, no. 3, pp. 261–272, 2020. Cited on page 32.

[146] S. van der Walt, J. L. Schönberger, J. Nunez-Iglesias, F. Boulogne, J. D. Warner, N. Yager, E. Gouillart, and T. Yu, "scikit-image: image processing in Python," *PeerJ*, vol. 2, p. e453, 2014. Cited on page 32.

[147] P. van Nies, A. S. Canton, Z. Nourian, and C. Danelon, "Monitoring mRNA and Protein Levels in Bulk and in Model Vesicle-Based Artificial Cells," *Methods in Enzymology*, vol. 550, pp. 187–214, 2015. Cited on page 32.

[148] D. Blanken, P. van Nies, and C. Danelon, "Quantitative imaging of gene-expressing liposomes reveals rare favorable phenotypes," *Physical Biology*, vol. 16, no. 4, p. 045002, 2019. Cited on pages 33, 73, 76, 78, 79, 82, and 84.

[149] C. E. Aitken, R. A. Marshall, and J. D. Puglisi, "An Oxygen Scavenging System for Improvement of Dye Stability in Single-Molecule Fluorescence Experiments," *Biophysical Journal*, vol. 94, no. 5, pp. 1826–1835, 2008. Cited on page 34.

[150] S. Havrylenko, P. Noguera, M. Abou-Ghali, J. Manzi, F. Faqir, A. Lamora, C. Guérin, L. Blanchoin, and J. Plastino, "WAVE binds Ena/VASP for enhanced Arp2/3 complex–based actin assembly," *Molecular Biology of the Cell*, vol. 26, no. 1, pp. 55–65, 2015. Cited on page 34.

[151] N. J. Gaut and K. P. Adamala, "Reconstituting Natural Cell Elements in Synthetic Cells," *Advanced Biology*, vol. 5, no. 3, p. 2000188, 2021. Cited on page 46.

[152] L. Van de Cauter, L. van Buren, G. H. Koenderink, and K. A. Ganzinger, "Exploring Giant Unilamellar Vesicle Production for Artificial Cells – Current Challenges and Future Directions," *Small Methods*, vol. 7, no. 12, p. 2300416, 2023. Cited on pages 46 and 93.

[153] L. Sercombe, T. Veerati, F. Moheimani, S. Y. Wu, A. K. Sood, and S. Hua, "Advances and Challenges of Liposome Assisted Drug Delivery," *Frontiers in Pharmacology*, vol. 6, 2015. Cited on page 46.

[154] T. M. Allen and P. R. Cullis, "Liposomal drug delivery systems: From concept to clinical applications," *Advanced Drug Delivery Reviews*, vol. 65, no. 1, pp. 36–48, 2013. Cited on page 46.

[155] P. J. Beltramo, L. Scheidegger, and J. Vermant, "Toward Realistic Large-Area Cell Membrane Mimics: Excluding Oil, Controlling Composition, and Including Ion Channels," *Langmuir*, vol. 34, no. 20, pp. 5880–5888, 2018. Cited on page 46.

[156] V. R. Ardham, V. Zoni, S. Adamowicz, P. Campomanes, and S. Vanni, "Accurate Estimation of Membrane Capacitance from Atomistic Molecular Dynamics Simulations of Zwitterionic Lipid Bilayers," *The Journal of Physical Chemistry B*, vol. 124, no. 38, pp. 8278–8286, 2020. Cited on page 46.

[157] L. Van de Cauter, F. Fanalista, L. van Buren, N. De Franceschi, E. Godino, S. Bouw, C. Danelon, C. Dekker, G. H. Koenderink, and K. A. Ganzinger, "Optimized cDICE for efficient reconstitution of biological systems in giant unilamellar vesicles," *ACS Synthetic Biology*, vol. 10, no. 7, pp. 1690–1702, 2021. Cited on pages 46, 47, 49, 50, 52, 54, 56, 58, 60, 73, 75, 76, 78, 79, 80, 81, 82, 83, 84, 86, 102, and 105.

[158] P. B. Umbanhowar, V. Prasad, and D. A. Weitz, "Monodisperse Emulsion Generation via Drop Break Off in a Coflowing Stream," *Langmuir*, vol. 16, no. 2, pp. 347–351, 2000. Cited on pages 47, 49, and 50.

[159] D. Barkley and R. D. Henderson, "Three-dimensional Floquet stability analysis of the wake of a circular cylinder," *Journal of Fluid Mechanics*, vol. 322, pp. 215–241, 1996. Cited on page 49.

[160] H. A. Stone, "Dynamics of Drop Deformation and Breakup in Viscous Fluids," *Annu. Rev. Fluid Mech.*, vol. 26, pp. 65–102, 1994. Cited on page 51.

[161] P. J. A. Janssen and P. D. Anderson, "Boundary-integral method for drop deformation between parallel plates," *Physics of Fluids*, vol. 19, no. 4, p. 043602, 2007. Cited on page 52.

[162] A. Komrakova, O. Shardt, D. Eskin, and J. Derksen, "Lattice Boltzmann simulations of drop deformation and breakup in shear flow," *International Journal of Multiphase Flow*, vol. 59, pp. 24–43, 2014. Cited on page 52.

[163] S. E. May and J. V. Maher, "Capillary-wave relaxation for a meniscus between miscible liquids," *Physical Review Letters*, vol. 67, no. 15, pp. 2013–2016, 1991. Cited on page 52.

[164] K. A. Ganzinger, A. Merino-Salomón, D. A. García-Soriano, A. N. Butterfield, T. Litschel, F. Siedler, and P. Schwille, "FtsZ reorganization facilitates deformation of giant vesicles in microfluidic traps," *Angewandte Chemie International Edition*, vol. 59, no. 48, pp. 21372–21376, 2020. Cited on pages 52, 79, 80, 82, 84, and 100.

[165] M. Tjahjadi, H. A. Stone, and J. M. Ottino, "Satellite and subsatellite formation in capillary breakup," *Journal of Fluid Mechanics*, vol. 243, pp. 297–317, 1992. Cited on page 53.

[166] P. K. Notz and O. A. Basaran, "Dynamics and breakup of a contracting liquid filament," *Journal of Fluid Mechanics*, vol. 512, pp. 223–256, 2004. Cited on page 53.

[167] S. G. Baldursdottir, M. S. Fullerton, S. H. Nielsen, and L. Jorgensen, "Adsorption of proteins at the oil/water interface-Observation of protein adsorption by interfacial shear stress measurements," *Colloids and Surfaces B: Biointerfaces*, vol. 79, no. 1, pp. 41–46, 2010. Cited on page 53.

[168] V. Mitropoulos, A. Mütze, and P. Fischer, "Mechanical properties of protein adsorption layers at the air/water and oil/water interface: A comparison in light of the thermodynamical stability of proteins," *Advances in Colloid and Interface Science*, vol. 206, pp. 195–206, 2014. Cited on page 53.

[169] C. Gicquaud, J.-P. Chauvet, G. Grenier, P. Tancrède, and G. Coulombe, "Adsorption of actin at the air-water interface: A monolayer study," *Biopolymers*, vol. 70, no. 3, pp. 289–296, 2003. Cited on page 53.

[170] C. Gicquaud, J. P. Chauvet, and P. Tancrède, "Surface film pressure of actin: interactions with lipids in mixed monolayers," *Biochemical and Biophysical Research Communications*, vol. 308, no. 4, pp. 995–1000, 2003.

[171] C. F. E. Schroer, L. Baldauf, L. van Buren, T. A. Wassenaar, M. N. Melo, G. H. Koenderink, and S. J. Marrink, "Charge-dependent interactions of monomeric and filamentous actin with lipid bilayers," *Proceedings of the National Academy of Sciences*, vol. 117, no. 11, pp. 5861–5872, 2020. Cited on page 53.

[172] J. Magnaudet and M. J. Mercier, "Particles, Drops, and Bubbles Moving Across Sharp Interfaces and Stratified Layers," *Annual Review of Fluid Mechanics*, vol. 52, no. 1, pp. 61–91, 2020. Cited on page 56.

[173] G. J. Amador, D. van Dijk, R. Kieffer, M.-E. Aubin-Tam, and D. Tam, "Hydrodynamic shear dissipation and transmission in lipid bilayers," *Proceedings of the National Academy of Sciences*, vol. 118, no. 21, p. e2100156118, 2021. Cited on page 56.

[174] L. Baldauf, F. Frey, M. Arribas Perez, T. Idema, and G. H. Koenderink, "Branched actin cortices reconstituted in vesicles sense membrane curvature," *Biophysical*

Journal, vol. 122, no. 11, pp. 2311–2324, 2023. Cited on pages 57, 65, 66, 75, 76, 79, 80, 81, 82, 83, 84, 93, 94, 97, and 106.

[175] G. F. Christopher, N. N. Noharuddin, J. A. Taylor, and S. L. Anna, "Experimental observations of the squeezing-to-dripping transition in T-shaped microfluidic junctions," *Physical Review E*, vol. 78, no. 3, p. 036317, 2008. Cited on page 57.

[176] M. De Menech, P. Garstecki, F. Jousse, and H. A. Stone, "Transition from squeezing to dripping in a microfluidic T-shaped junction," *Journal of Fluid Mechanics*, vol. 595, pp. 141–161, 2008. Cited on page 57.

[177] J. Schindelin, I. Arganda-Carreras, E. Frise, V. Kaynig, M. Longair, T. Pietzsch, S. Preibisch, C. Rueden, S. Saalfeld, B. Schmid, J.-Y. Tinevez, D. J. White, V. Hartenstein, K. Eliceiri, P. Tomancak, and A. Cardona, "Fiji: an open-source platform for biological-image analysis," *Nature Methods*, vol. 9, no. 7, pp. 676–682, 2012. Cited on page 59.

[178] H. Zwart, "From primal scenes to synthetic cells," *eLife*, vol. 8, p. e46518, 2019. Cited on page 68.

[179] J. W. Szostak, D. P. Bartel, and P. L. Luisi, "Synthesizing life," *Nature*, vol. 409, 2001. Cited on page 68.

[180] O. Staufer, J. A. De Lora, E. Bailoni, A. Bazrafshan, A. S. Benk, K. Jahnke, Z. A. Manzer, L. Otrin, T. Díez Pérez, J. Sharon, J. Steinkühler, K. P. Adamala, B. Jacobson, M. Dogterom, K. Göpfrich, D. Stefanovic, S. R. Atlas, M. Grunze, M. R. Lakin, A. P. Shreve, J. P. Spatz, and G. P. López, "Building a community to engineer synthetic cells and organelles from the bottom-up," *eLife*, vol. 10, p. e73556, 2021. Cited on page 68.

[181] "fabriCELL." (Online: https://www.imperial.ac.uk/a-z-research/fabricell/; accessed 2023-01-25). Cited on page 68.

[182] D. G. Gibson, J. I. Glass, C. Lartigue, V. N. Noskov, R.-Y. Chuang, M. A. Algire, G. A. Benders, M. G. Montague, L. Ma, M. M. Moodie, C. Merryman, S. Vashee, R. Krishnakumar, N. Assad-Garcia, C. Andrews-Pfannkoch, E. A. Denisova, L. Young, Z.-Q. Qi, T. H. Segall-Shapiro, C. H. Calvey, P. P. Parmar, C. A. Hutchison, H. O. Smith, and J. C. Venter, "Creation of a bacterial cell controlled by a chemically synthesized genome," *Science*, vol. 329, no. 5987, pp. 52–56, 2010. Cited on page 68.

[183] J. F. Pelletier, L. Sun, K. S. Wise, N. Assad-Garcia, B. J. Karas, T. J. Deerinck, M. H. Ellisman, A. Mershin, N. Gershenfeld, R.-Y. Chuang, J. I. Glass, and E. A. Strychalski, "Genetic requirements for cell division in a genomically minimal cell," *Cell*, vol. 184, no. 9, pp. 2430–2440.e16, 2021. Cited on page 68.

[184] I. Ezkurdia, D. Juan, J. M. Rodriguez, A. Frankish, M. Diekhans, J. Harrow, J. Vazquez, A. Valencia, and M. L. Tress, "Multiple evidence strands suggest that there may be as few as 19 000 human protein-coding genes," *Human Molecular Genetics*, vol. 23, no. 22, pp. 5866–5878, 2014. Cited on page 68.

[185] R. Milo, "What is the total number of protein molecules per cell volume? a call to rethink some published values," *BioEssays*, vol. 35, no. 12, pp. 1050–1055, 2013. Cited on page 68.

[186] A. P. Liu and D. A. Fletcher, "Biology under construction: in vitro reconstitution of cellular function," *Nature Reviews Molecular Cell Biology*, vol. 10, no. 9, pp. 644–650, 2009. Cited on page 68.

[187] M. Bedau, "The power and the pitfalls," *Nature*, vol. 465, 2010. Cited on page 69.

[188] S. Ausländer, D. Ausländer, and M. Fussenegger, "Synthetic biology-the synthesis of biology," *Angewandte Chemie International Edition*, vol. 56, no. 23, pp. 6396–6419, 2017. Cited on page 69.

[189] D. Fletcher, "Which biological systems should be engineered?," *Nature*, vol. 563, no. 7730, pp. 177–179, 2018. Cited on page 69.

[190] F. Lussier, O. Staufer, I. Platzman, and J. P. Spatz, "Can bottom-up synthetic biology generate advanced drug-delivery systems?," *Trends in Biotechnology*, vol. 39, no. 5, pp. 445–459, 2021. Cited on page 69.

[191] W. K. Spoelstra, S. Deshpande, and C. Dekker, "Tailoring the appearance: what will synthetic cells look like?," *Current Opinion in Biotechnology*, vol. 51, pp. 47–56, 2018. Cited on page 69.

[192] M. H. M. E. van Stevendaal, L. Vasiukas, N. A. Yewdall, A. F. Mason, and J. C. M. van Hest, "Engineering of biocompatible coacervate-based synthetic cells," *ACS Applied Materials & Interfaces*, vol. 13, no. 7, pp. 7879–7889, 2021. Cited on page 69.

[193] D. E. Discher and F. Ahmed, "POLYMERSOMES," *Annual Review of Biomedical Engineering*, vol. 8, no. 1, pp. 323–341, 2006. Cited on page 69.

[194] E. Rideau, R. Dimova, P. Schwille, F. R. Wurm, and K. Landfester, "Liposomes and polymersomes: a comparative review towards cell mimicking," *Chemical Society Reviews*, vol. 47, no. 23, pp. 8572–8610, 2018. Cited on page 69.

[195] M. Ugrinic, A. Zambrano, S. Berger, S. Mann, T.-Y. D. Tang, and A. de Mello, "Microfluidic formation of proteinosomes," *Chemical Communications*, vol. 54, no. 3, pp. 287–290, 2018. Cited on page 69.

[196] A. O. Robinson, O. M. Venero, and K. P. Adamala, "Toward synthetic life: Biomimetic synthetic cell communication," *Current Opinion in Chemical Biology*, vol. 64, pp. 165–173, 2021. Cited on page 69.

[197] Z. Abil and C. Danelon, "Roadmap to building a cell: An evolutionary approach," *Frontiers in Bioengineering and Biotechnology*, vol. 8, p. 927, 2020. Cited on page 69.

[198] S. Kumar, M. Karmacharya, and Y. Cho, "Bridging the gap between nonliving matter and cellular life," *Small*, vol. 19, no. 13, p. 2202962, 2022. Cited on page 69.

[199] M. E. Allen, J. W. Hindley, D. K. Baxani, O. Ces, and Y. Elani, "Hydrogels as functional components in artificial cell systems," *Nature Reviews Chemistry*, vol. 6, no. 8, pp. 562–578, 2022. Cited on page 69.

[200] J. Lombard, P. López-García, and D. Moreira, "The early evolution of lipid membranes and the three domains of life," *Nature Reviews Microbiology*, vol. 10, no. 7, pp. 507–515, 2012. Cited on page 69.

[201] M. Edidin, "Lipids on the frontier: a century of cell-membrane bilayers," *Nature Reviews Molecular Cell Biology*, vol. 4, no. 5, pp. 414–418, 2003. Cited on page 69.

[202] W. M. Śmigiel, P. Lefrançois, and B. Poolman, "Physicochemical considerations for bottom-up synthetic biology," *Emerging Topics in Life Sciences*, vol. 3, no. 5, pp. 445–458, 2019. Cited on page 70.

[203] A. Shevchenko and K. Simons, "Lipidomics: coming to grips with lipid diversity," *Nature Reviews Molecular Cell Biology*, vol. 11, no. 8, pp. 593–598, 2010. Cited on page 70.

[204] T. Harayama and H. Riezman, "Understanding the diversity of membrane lipid composition," *Nature Reviews Molecular Cell Biology*, vol. 19, no. 5, pp. 281–296, 2018. Cited on page 70.

[205] S. M. Gruner, "Intrinsic curvature hypothesis for biomembrane lipid composition: a role for nonbilayer lipids," *Proceedings of the National Academy of Sciences*, vol. 82, no. 11, 1985. Cited on page 70.

[206] D. Marsh, "Intrinsic curvature in normal and inverted lipid structures and in membranes," *Biophysical Journal*, vol. 70, no. 5, pp. 2248–2255, 1996. Cited on page 70.

[207] J. E. Vance and R. Steenbergen, "Metabolism and functions of phosphatidylserine," *Progress in Lipid Research*, vol. 44, no. 4, pp. 207–234, 2005. Cited on page 70.

[208] B. H. Falkenburger, J. B. Jensen, E. J. Dickson, B.-C. Suh, and B. Hille, "SYMPOSIUM REVIEW: Phosphoinositides: lipid regulators of membrane proteins: Phosphoinositides instruct membrane proteins," *The Journal of Physiology*, vol. 588, no. 17, pp. 3179–3185, 2010. Cited on page 70.

[209] J. P. Sáenz, D. Grosser, A. S. Bradley, T. J. Lagny, O. Lavrynenko, M. Broda, and K. Simons, "Hopanoids as functional analogues of cholesterol in bacterial membranes," *Proceedings of the National Academy of Sciences*, vol. 112, no. 38, pp. 11971–11976, 2015. Cited on page 70.

[210] Y. Barenholz, "Cholesterol and other membrane active sterols: from membrane evolution to "rafts"," *Progress in Lipid Research*, vol. 41, no. 1, pp. 1–5, 2002. Cited on page 70.

[211] O. G. Mouritsen and M. J. Zuckermann, "What's so special about cholesterol?," *Lipids*, vol. 39, no. 11, pp. 1101–1113, 2004. Cited on page 70.

[212] L. Limozin, M. Bärmann, and E. Sackmann, "On the organization of self-assembled actin networks in giant vesicles," *The European Physical Journal E*, vol. 10, no. 4, pp. 319–330, 2003. Cited on page 70.

[213] M. Aleksanyan, A. Grafmüller, F. Crea, V. N. Georgiev, J. Heberle, and R. Dimova, "Modulating membrane shape and mechanics of minimal cells by light: area increase, softening and interleaflet coupling of membrane models doped with azobenzene-lipid photoswitches," preprint, *bioRxiv*, 2023. Cited on page 70.

[214] M. Doktorova, J. L. Symons, and I. Levental, "Structural and functional consequences of reversible lipid asymmetry in living membranes," *Nature Chemical Biology*, vol. 16, no. 12, pp. 1321–1330, 2020. Cited on page 70.

[215] N. Sapay, W. F. D. Bennett, and D. P. Tieleman, "Thermodynamics of flip-flop and desorption for a systematic series of phosphatidylcholine lipids," *Soft Matter*, vol. 5, no. 17, pp. 3295–3302, 2009. Cited on page 70.

[216] J. Steinkühler, P. De Tillieux, R. L. Knorr, R. Lipowsky, and R. Dimova, "Charged giant unilamellar vesicles prepared by electroformation exhibit nanotubes and transbilayer lipid asymmetry," *Scientific Reports*, vol. 8, no. 1, p. 11838, 2018. Cited on pages 70 and 76.

[217] H.-G. Döbereiner, O. Selchow, and R. Lipowsky, "Spontaneous curvature of fluid vesicles induced by trans-bilayer sugar asymmetry," *European Biophysics Journal*, vol. 28, no. 2, pp. 174–178, 1999. Cited on page 70.

[218] M. Karimi, J. Steinkühler, D. Roy, R. Dasgupta, R. Lipowsky, and R. Dimova, "Asymmetric ionic conditions generate large membrane curvatures," *Nano Letters*, vol. 18, no. 12, pp. 7816–7821, 2018. Cited on page 70.

[219] J. Steinkühler, R. L. Knorr, Z. Zhao, T. Bhatia, S. M. Bartelt, S. Wegner, R. Dimova, and R. Lipowsky, "Controlled division of cell-sized vesicles by low densities of membrane-bound proteins," *Nature Communications*, vol. 11, no. 1, p. 905, 2020. Cited on page 70.

[220] D. W. Deamer and J. Bramhall, "Permeability of lipid bilayers to water and ionic solutes," *Chemistry and Physics of Lipids*, vol. 40, no. 2, pp. 167–188, 1986. Cited on page 71.

[221] E. Awoonor-Williams and C. N. Rowley, "Molecular simulation of nonfacilitated membrane permeation," *Biochimica et Biophysica Acta (BBA) - Biomembranes*, vol. 1858, no. 7, pp. 1672–1687, 2016. Cited on page 71.

[222] J. Frallicciardi, J. Melcr, P. Siginou, S. J. Marrink, and B. Poolman, "Membrane thickness, lipid phase and sterol type are determining factors in the permeability of membranes to small solutes," *Nature Communications*, vol. 13, no. 1, p. 1605, 2022. Cited on page 71.

[223] B. Hille, "Ionic channels in excitable membranes. current problems and biophysical approaches," *Biophysical Journal*, vol. 22, no. 2, pp. 283–294, 1978. Cited on page 71.

[224] S. Wilkens, "Structure and mechanism of ABC transporters," *F1000Prime Rep*, vol. 7, no. 14, 2015. Cited on page 71.

[225] T. Litschel and P. Schwille, "Protein reconstitution inside giant unilamellar vesicles," *Annual Review of Biophysics*, vol. 50, no. 1, pp. 100620–114132, 2021. Cited on pages 71, 77, and 81.

[226] N. H. Wubshet and A. P. Liu, "Methods to mechanically perturb and characterize GUV-based minimal cell models," *Computational and Structural Biotechnology Journal*, vol. 21, pp. 550–562, 2023. Cited on page 72.

[227] E. Rideau, F. R. Wurm, and K. Landfester, "Self-assembly of giant unilamellar vesicles by film hydration methodologies," *Advanced Biosystems*, vol. 3, no. 6, p. 1800324, 2019. Cited on pages 72, 73, 76, 78, 79, 81, 84, and 85.

[228] W. Rawicz, K. Olbrich, T. McIntosh, D. Needham, and E. Evans, "Effect of chain length and unsaturation on elasticity of lipid bilayers," *Biophysical Journal*, vol. 79, no. 1, pp. 328–339, 2000. Cited on page 72.

[229] D. Needham and R. Nunn, "Elastic deformation and failure of lipid bilayer membranes containing cholesterol," *Biophysical Journal*, vol. 58, no. 4, pp. 997–1009, 1990. Cited on page 72.

[230] D. Scherfeld, N. Kahya, and P. Schwille, "Lipid dynamics and domain formation in model membranes composed of ternary mixtures of unsaturated and saturated phosphatidylcholines and cholesterol," *Biophysical Journal*, vol. 85, no. 6, pp. 3758–3768, 2003. Cited on page 72.

[231] P. Cicuta, S. L. Keller, and S. L. Veatch, "Diffusion of liquid domains in lipid bilayer membranes," *The Journal of Physical Chemistry B*, vol. 111, no. 13, pp. 3328–3331, 2007. Cited on page 72.

[232] S. L. Veatch and S. L. Keller, "Separation of liquid phases in giant vesicles of ternary mixtures of phospholipids and cholesterol," *Biophysical Journal*, vol. 85, no. 5, pp. 3074–3083, 2003. Cited on page 72.

[233] Y. Tamba and M. Yamazaki, "Single giant unilamellar vesicle method reveals effect of antimicrobial peptide magainin 2 on membrane permeability," *Biochemistry*, vol. 44, no. 48, pp. 15823–15833, 2005. Cited on page 72.

[234] Z. Boban, I. Mardešić, W. K. Subczynski, and M. Raguz, "Giant unilamellar vesicle electroformation: What to use, what to avoid, and how to quantify the results," *Membranes*, vol. 11, no. 11, p. 860, 2021. Cited on pages 73, 78, 79, 84, and 85.

[235] Z. Boban, I. Mardešić, W. K. Subczynski, D. Jozić, and M. Raguz, "Optimization of giant unilamellar vesicle electroformation for phosphatidyl-

choline/sphingomyelin/cholesterol ternary mixtures," *Membranes*, vol. 12, no. 5, p. 525, 2022-05. Cited on pages 73 and 76.

[236] R. B. Lira, R. Dimova, and K. A. Riske, "Giant unilamellar vesicles formed by hybrid films of agarose and lipids display altered mechanical properties," *Biophysical Journal*, vol. 107, no. 7, pp. 1609–1619, 2014. Cited on pages 73 and 78.

[237] Z. Nourian, W. Roelofsen, and C. Danelon, "Triggered gene expression in fed-vesicle microreactors with a multifunctional membrane," *Angewandte Chemie International Edition*, vol. 51, no. 13, pp. 3114–3118, 2012. Cited on pages 73, 79, 82, and 84.

[238] V. Girish, J. Pazzi, A. Li, and A. B. Subramaniam, "Fabrics of diverse chemistries promote the formation of giant vesicles from phospholipids and amphiphilic block copolymers," *Langmuir*, vol. 35, no. 28, pp. 9264–9273, 2019. Cited on page 73.

[239] J. Pazzi, M. Xu, and A. B. Subramaniam, "Size distributions and yields of giant vesicles assembled on cellulose papers and cotton fabric," *Langmuir*, vol. 35, no. 24, pp. 7798–7804, 2019. Cited on page 73.

[240] K. M. Kresse, M. Xu, J. Pazzi, M. García-Ojeda, and A. B. Subramaniam, "Novel application of cellulose paper as a platform for the macromolecular self-assembly of biomimetic giant liposomes," *ACS Applied Materials & Interfaces*, vol. 8, no. 47, pp. 32102–32107, 2016. Cited on page 73.

[241] J. Pazzi and A. B. Subramaniam, "Nanoscale curvature promotes high yield spontaneous formation of cell-mimetic giant vesicles on nanocellulose paper," *ACS Applied Materials & Interfaces*, vol. 12, no. 50, pp. 56549–56561, 2020. Cited on page 73.

[242] S. Pautot, B. J. Frisken, and D. A. Weitz, "Production of unilamellar vesicles using an inverted emulsion," *Langmuir*, vol. 19, no. 7, pp. 2870–2879, 2003. Cited on pages 73, 79, and 84.

[243] S. Pautot, B. J. Frisken, and D. A. Weitz, "Engineering asymmetric vesicles," *Proceedings of the National Academy of Sciences*, vol. 100, no. 19, pp. 10718–10721, 2003. Cited on pages 73 and 77.

[244] Y. Elani, S. Purushothaman, P. J. Booth, J. M. Seddon, N. J. Brooks, R. V. Law, and O. Ces, "Measurements of the effect of membrane asymmetry on the mechanical properties of lipid bilayers," *Chemical Communications*, vol. 51, no. 32, pp. 6976–6979, 2015. Cited on pages 73 and 77.

[245] N. Yandrapalli, J. Petit, O. Bäumchen, and T. Robinson, "Surfactant-free production of biomimetic giant unilamellar vesicles using PDMS-based microfluidics," *Communications Chemistry*, vol. 4, no. 1, p. 100, 2021. Cited on pages 73, 75, 78, 79, 81, 82, and 84.

[246] S.-Y. Teh, R. Khnouf, H. Fan, and A. P. Lee, "Stable, biocompatible lipid vesicle generation by solvent extraction-based droplet microfluidics," *Biomicrofluidics*, vol. 5, no. 4, p. 044113, 2011.

[247] S. Matosevic and B. M. Paegel, "Stepwise synthesis of giant unilamellar vesicles on a microfluidic assembly line," *Journal of the American Chemical Society*, vol. 133, no. 9, pp. 2798–2800, 2011.

[248] R. Ushiyama, K. Koiwai, and H. Suzuki, "Plug-and-play microfluidic production of monodisperse giant unilamellar vesicles using droplet transfer across water–oil interface," *Sensors and Actuators B: Chemical*, vol. 355, p. 131281, 2022.

[249] N.-N. Deng, M. Yelleswarapu, and W. T. S. Huck, "Monodisperse uni- and multicompartment liposomes," *Journal of the American Chemical Society*, vol. 138, no. 24, pp. 7584–7591, 2016. Cited on page 73.

[250] K. Nishimura, H. Suzuki, T. Toyota, and T. Yomo, "Size control of giant unilamellar vesicles prepared from inverted emulsion droplets," *Journal of Colloid and Interface Science*, vol. 376, no. 1, pp. 119–125, 2012. Cited on page 73.

[251] G. Zhang and J. Sun, "Lipid in chips: A brief review of liposomes formation by microfluidics," *International Journal of Nanomedicine*, vol. Volume 16, pp. 7391–7416, 2021. Cited on pages 73 and 75.

[252] C. Martino and A. J. deMello, "Droplet-based microfluidics for artificial cell generation: a brief review," *Interface Focus*, vol. 6, no. 4, p. 20160011, 2016. Cited on pages 73 and 75.

[253] Y. Bashirzadeh, N. Wubshet, T. Litschel, P. Schwille, and A. P. Liu, "Rapid encapsulation of reconstituted cytoskeleton inside giant unilamellar vesicles," *Journal of Visualized Experiments*, no. 177, p. 63332, 2021. Cited on pages 75, 79, 80, 84, 93, and 94.

[254] T. Litschel, C. F. Kelley, D. Holz, M. Adeli Koudehi, S. K. Vogel, L. Burbaum, N. Mizuno, D. Vavylonis, and P. Schwille, "Reconstitution of contractile actomyosin rings in vesicles," *Nature Communications*, vol. 12, no. 1, p. 2254, 2021. Cited on pages 75, 79, 81, and 84.

[255] N. H. Wubshet, Y. Bashirzadeh, and A. P. Liu, "Fascin-induced actin protrusions are suppressed by dendritic networks in GUVs," *Molecular Biology of the Cell*, vol. 32, no. 18, pp. 1611–1791, 2021.

[256] L. Baldauf, F. Frey, M. A. Perez, M. Mladenov, M. Way, T. Idema, and G. H. Koenderink, "Biomimetic actin cortices shape cell-sized lipid vesicles," preprint, *bioRxiv*, 2023. Cited on pages 75, 79, 80, 81, 84, 93, and 104.

[257] K. Göpfrich, B. Haller, O. Staufer, Y. Dreher, U. Mersdorf, I. Platzman, and J. P. Spatz, "One-pot assembly of complex giant unilamellar vesicle-based synthetic cells," *ACS Synthetic Biology*, vol. 8, no. 5, pp. 937–947, 2019. Cited on pages 75, 76, 77, 78, 79, 81, and 84.

[258] O. M. Venero, W. Sato, J. M. Heili, C. Deich, and K. P. Adamala, "Liposome preparation by 3d-printed microcapillary-based apparatus," in *Cell-Free Gene Expression:*

Methods and Protocols (A. S. Karim and M. C. Jewett, eds.), Methods in Molecular Biology, pp. 227–235, Springer US, 2022. Cited on pages 75, 79, 81, 82, and 84.

[259] K. Kamiya, R. Kawano, T. Osaki, K. Akiyoshi, and S. Takeuchi, "Cell-sized asymmetric lipid vesicles facilitate the investigation of asymmetric membranes," *Nature Chemistry*, vol. 8, no. 9, pp. 881–889, 2016. Cited on pages 75 and 77.

[260] M. Armstrong, M. D. Vahey, T. P. Hunt, and D. A. Fletcher, "Forming and loading giant unilamellar vesicles with acoustic jetting," *Biomicrofluidics*, vol. 14, no. 6, p. 064105, 2020. Cited on page 75.

[261] S. Deshpande and C. Dekker, "On-chip microfluidic production of cell-sized liposomes," *Nature Protocols*, vol. 13, no. 5, pp. 856–874, 2018. Cited on pages 75, 79, and 84.

[262] L. Bagatolli, E. Gratton, T. K. Khan, and P. L.-G. Chong, "Two-photon fluorescence microscopy studies of bipolar tetraether giant liposomes from thermoacidophilic archaebacteria sulfolobus acidocaldarius," *Biophysical Journal*, vol. 79, no. 1, pp. 416–425, 2000. Cited on page 76.

[263] S. Rezelj, M. Kozorog, T. Švigelj, N. P. Ulrih, N. Žnidaršič, M. Podobnik, and G. Anderluh, "Cholesterol enriched archaeosomes as a molecular system for studying interactions of cholesterol-dependent cytolysins with membranes," *The Journal of Membrane Biology*, vol. 251, no. 3, pp. 491–505, 2018. Cited on page 76.

[264] A. Yoshida, S. Kohyama, K. Fujiwara, S. Nishikawa, and N. Doi, "Regulation of spatiotemporal patterning in artificial cells by a defined protein expression system," *Chemical Science*, vol. 10, no. 48, pp. 11064–11072, 2019. Cited on pages 76, 79, 80, and 84.

[265] A. Shimomura, S. Ina, M. Oki, and G. Tsuji, "Effects of charged lipids on giant unilamellar vesicle fusion and inner content mixing via freeze-thawing," *ChemBioChem*, vol. 23, no. 24, p. e202200550, 2022. Cited on pages 76, 79, and 84.

[266] T. Hamada, Y. Miura, Y. Komatsu, Y. Kishimoto, M. Vestergaard, and M. Takagi, "Construction of asymmetric cell-sized lipid vesicles from lipid-coated water-in-oil microdroplets," *The Journal of Physical Chemistry B*, vol. 112, no. 47, pp. 14678–14681, 2008. Cited on page 77.

[267] I. L. Jørgensen, G. C. Kemmer, and T. G. Pomorski, "Membrane protein reconstitution into giant unilamellar vesicles: a review on current techniques," *European Biophysics Journal*, vol. 46, no. 2, pp. 103–119, 2017. Cited on page 77.

[268] H. Stein, S. Spindler, N. Bonakdar, C. Wang, and V. Sandoghdar, "Production of isolated giant unilamellar vesicles under high salt concentrations," *Frontiers in Physiology*, vol. 8, no. 63, 2017. Cited on page 78.

[269] H. A. Faizi, A. Tsui, R. Dimova, and P. M. Vlahovska, "Bending rigidity, capacitance, and shear viscosity of giant vesicle membranes prepared by spontaneous swelling,

electroformation, gel-assisted, and phase transfer methods: A comparative study," *Langmuir*, vol. 38, no. 34, pp. 10548–10557, 2022. Cited on page 78.

[270] S. M. Bartelt, J. Steinkühler, R. Dimova, and S. V. Wegner, "Light-guided motility of a minimal synthetic cell," *Nano Letters*, vol. 18, no. 11, pp. 7268–7274, 2018. Cited on pages 79 and 84.

[271] E. Godino and C. Danelon, "Gene-directed FtsZ ring assembly generates constricted liposomes with stable membrane necks," *Advanced Biology*, vol. 7, no. 3, p. 2200172, 2023. Cited on pages 79, 81, and 84.

[272] E. Godino, J. N. López, I. Zarguit, A. Doerr, M. Jimenez, G. Rivas, and C. Danelon, "Cell-free biogenesis of bacterial division proto-rings that can constrict liposomes," *Communications Biology*, vol. 3, no. 1, p. 539, 2020. Cited on page 81.

[273] E. Godino, J. N. López, D. Foschepoth, C. Cleij, A. Doerr, C. F. Castellà, and C. Danelon, "De novo synthesized min proteins drive oscillatory liposome deformation and regulate FtsA-FtsZ cytoskeletal patterns," *Nature Communications*, vol. 10, no. 1, p. 4969, 2019. Cited on page 81.

[274] J. Kattan, A. Doerr, M. Dogterom, and C. Danelon, "Shaping liposomes by cell-free expressed bacterial microtubules," *ACS Synthetic Biology*, vol. 10, no. 10, pp. 2447–2455, 2021. Cited on page 81.

[275] D. Blanken, D. Foschepoth, A. C. Serrão, and C. Danelon, "Genetically controlled membrane synthesis in liposomes," *Nature Communications*, vol. 11, no. 1, p. 4317, 2020. Cited on pages 79, 81, and 84.

[276] F. Yuan, H. Alimohamadi, B. Bakka, A. N. Trementozzi, K. J. Day, N. L. Fawzi, P. Rangamani, and J. C. Stachowiak, "Membrane bending by protein phase separation," *Proceedings of the National Academy of Sciences*, vol. 118, no. 11, p. e2017435118, 2021. Cited on pages 79 and 84.

[277] H. Chaudhary, V. Subramaniam, and M. M. A. E. Claessens, "Direct visualization of model membrane remodeling by alpha-synuclein fibrillization," *ChemPhysChem*, vol. 18, no. 12, pp. 1620–1626, 2017.

[278] T. Abele, T. Messer, K. Jahnke, M. Hippler, M. Bastmeyer, M. Wegener, and K. Göpfrich, "Two-Photon 3D Laser Printing Inside Synthetic Cells," *Advanced Materials*, p. 2106709, 2021. Cited on page 86.

[279] Y. Dreher, K. Jahnke, E. Bobkova, J. P. Spatz, and K. Göpfrich, "Division and regrowth of phase-separated giant unilamellar vesicles," *Angewandte Chemie International Edition*, vol. 60, no. 19, pp. 10661–10669, 2021.

[280] Y. Dreher, K. Jahnke, M. Schröter, and K. Göpfrich, "Light-triggered cargo loading and division of DNA-containing giant unilamellar lipid vesicles," *Nano Letters*, vol. 21, no. 14, pp. 5952–5957, 2021. Cited on page 86.

[281] C. Herold, G. Chwastek, P. Schwille, and E. P. Petrov, "Efficient electroformation of supergiant unilamellar vesicles containing cationic lipids on ITO-coated electrodes," *Langmuir*, vol. 28, no. 13, pp. 5518–5521, 2012.

[282] Q. Li, X. Wang, S. Ma, Y. Zhang, and X. Han, "Electroformation of giant unilamellar vesicles in saline solution," *Colloids and Surfaces B: Biointerfaces*, vol. 147, pp. 368–375, 2016. Cited on pages 79 and 84.

[283] B. Peter, A. Levrier, and P. Schwille, "Spatiotemporal propagation of a minimal catalytic RNA network in GUV protocells by temperature cycling and phase separation," *Angewandte Chemie International Edition*, vol. 62, no. 17, p. e202218507, 2023. Cited on pages 79, 80, and 84.

[284] M. Hayashi, M. Nishiyama, Y. Kazayama, T. Toyota, Y. Harada, and K. Takiguchi, "Reversible morphological control of tubulin-encapsulating giant liposomes by hydrostatic pressure," *Langmuir*, vol. 32, no. 15, pp. 3794–3802, 2016. Cited on page 80.

[285] S. Berhanu, T. Ueda, and Y. Kuruma, "Artificial photosynthetic cell producing energy for protein synthesis," *Nature Communications*, vol. 10, no. 1, p. 1325, 2019. Cited on page 80.

[286] S. Krishnan, D. Ziegler, V. Arnaut, T. G. Martin, K. Kapsner, K. Henneberg, A. R. Bausch, H. Dietz, and F. C. Simmel, "Molecular transport through large-diameter DNA nanopores," *Nature Communications*, vol. 7, no. 1, p. 12787, 2016.

[287] S. Majumder, J. Garamella, Y.-L. Wang, M. DeNies, V. Noireaux, and A. P. Liu, "Cell-sized mechanosensitive and biosensing compartment programmed with DNA," *Chemical Communications*, vol. 53, no. 53, pp. 7349–7352, 2017. Cited on page 80.

[288] A. Merino-Salomón, J. Schneider, L. Babl, J.-H. Krohn, M. Sobrinos-Sanguino, T. Schäfer, J. R. Luque-Ortega, C. Alfonso, M. Jiménez, M. Jasnin, G. Rivas, and P. Schwille, "Crosslinking by ZapD drives the assembly of short, discontinuous FtsZ filaments into ring-like structures in solution," preprint, *bioRxiv*, 2023. Cited on page 80.

[289] S. Kohyama, A. Merino-Salomón, and P. Schwille, "In vitro assembly, positioning and contraction of a division ring in minimal cells," *Nature Communications*, vol. 13, no. 1, p. 6098, 2022. Cited on page 80.

[290] S. Kohyama, K. Fujiwara, N. Yoshinaga, and N. Doi, "Conformational equilibrium of MinE regulates the allowable concentration ranges of a protein wave for cell division," *Nanoscale*, vol. 12, no. 22, pp. 11960–11970, 2020. Cited on page 80.

[291] G. Zubaite, J. W. Hindley, O. Ces, and Y. Elani, "Dynamic reconfiguration of subcompartment architectures in artificial cells," *ACS Nano*, vol. 16, no. 6, pp. 9389–9400, 2022.

[292] D. Garenne and V. Noireaux, "Analysis of cytoplasmic and membrane molecular

crowding in genetically programmed synthetic cells," *Biomacromolecules*, vol. 21, no. 7, pp. 2808–2817, 2020. Cited on page 80.

[293] J. Garamella, D. Garenne, and V. Noireaux, "Chapter nine - TXTL-based approach to synthetic cells," in *Methods in Enzymology* (C. Schmidt-Dannert and M. B. Quin, eds.), vol. 617 of *Metabolons and Supramolecular Enzyme Assemblies*, pp. 217–239, Academic Press, 2019. Cited on page 80.

[294] A. Fink, C. R. Doll, A. Yagüe Relimpio, Y. Dreher, J. P. Spatz, K. Göpfrich, and E. A. Cavalcanti-Adam, "Extracellular cues govern shape and cytoskeletal organization in giant unilamellar lipid vesicles," *ACS Synthetic Biology*, vol. 12, no. 2, pp. 369–374, 2023. Cited on pages 79 and 84.

[295] Y. Bashirzadeh, N. H. Wubshet, and A. P. Liu, "Confinement geometry tunes fascin-actin bundle structures and consequently the shape of a lipid bilayer vesicle," *Frontiers in Molecular Biosciences*, vol. 7, p. 610277, 2020. Cited on pages 79, 81, and 84.

[296] N. H. Wubshet, B. Wu, S. Veerapaneni, and A. P. Liu, "Differential regulation of GUV mechanics via actin network architectures," *Biophysical Journal*, vol. 122, no. 11, pp. 2068–2081, 2022. Cited on page 80.

[297] Y. Bashirzadeh, H. Moghimianavval, and A. P. Liu, "Encapsulated actomyosin patterns drive cell-like membrane shape changes," *iScience*, vol. 25, no. 5, p. 104236, 2022. Cited on pages 79, 80, 84, and 93.

[298] F. Lussier, M. Schröter, N. J. Diercks, K. Jahnke, C. Weber, C. Frey, I. Platzman, and J. P. Spatz, "pH-triggered assembly of endomembrane multicompartments in synthetic cells," *ACS Synthetic Biology*, vol. 11, no. 1, p. 366–382, 2021. Cited on pages 79, 81, and 84.

[299] M. P. Tran, R. Chatterjee, Y. Dreher, J. Fichtler, K. Jahnke, L. Hilbert, V. Zaburdaev, and K. Göpfrich, "A DNA segregation module for synthetic cells," *Small*, vol. 19, no. 13, p. 2202711, 2023. Cited on page 81.

[300] O. Staufer, M. Schröter, I. Platzman, and J. P. Spatz, "Bottom-up assembly of functional intracellular synthetic organelles by droplet-based microfluidics," *Small*, vol. 16, no. 27, p. 1906424, 2020.

[301] K. Jahnke, V. Huth, U. Mersdorf, N. Liu, and K. Göpfrich, "Bottom-up assembly of synthetic cells with a DNA cytoskeleton," *ACS Nano*, vol. 16, no. 5, pp. 7233–7241, 2022. Cited on pages 79, 81, and 84.

[302] C. Deich, N. J. Gaut, W. Sato, A. E. Engelhart, and K. P. Adamala, "New *Aequorea* fluorescent proteins for cell-free bioengineering," preprint, *bioRxiv*, 2022. Cited on pages 79, 81, and 84.

[303] R. Tivony, M. Fletcher, and U. F. Keyser, "Quantifying proton-induced membrane polarization in single biomimetic giant vesicles," *Biophysical Journal*, vol. 121, no. 12, pp. 2223–2232, 2022. Cited on pages 79 and 84.

[304] D. T. Gonzales, N. Yandrapalli, T. Robinson, C. Zechner, and T.-Y. D. Tang, "Cell-free gene expression dynamics in synthetic cell populations," *ACS Synthetic Biology*, vol. 11, no. 1, pp. 205–215, 2022. Cited on pages 79, 81, and 84.

[305] F. Urban and P. A. Shaffer, "THE ACIDIC PROPERTY OF SUGARS," *Journal of Biological Chemistry*, vol. 94, no. 3, pp. 697–715, 1932. Cited on page 80.

[306] S. Malerz, K. Mudryk, L. Tomaník, D. Stemer, U. Hergenhahn, T. Buttersack, F. Trinter, R. Seidel, W. Quevedo, C. Goy, I. Wilkinson, S. Thürmer, P. Slavíček, and B. Winter, "Following in emil fischer's footsteps: A site-selective probe of glucose acid–base chemistry," *The Journal of Physical Chemistry A*, vol. 125, no. 32, pp. 6881–6892, 2021. Cited on page 80.

[307] K. Kajii, A. Shimomura, M. T. Higashide, M. Oki, and G. Tsuji, "Effects of sugars on giant unilamellar vesicle preparation, fusion, PCR in liposomes, and pore formation," *Langmuir*, vol. 38, no. 29, pp. 8871–8880, 2022. Cited on page 80.

[308] K. Carvalho, F.-C. Tsai, E. Lees, R. Voituriez, G. H. Koenderink, and C. Sykes, "Cell-sized liposomes reveal how actomyosin cortical tension drives shape change," *Proceedings of the National Academy of Sciences*, vol. 110, no. 41, pp. 16456–16461, 2013. Cited on page 81.

[309] R. Lopes dos Santos and C. Campillo, "Studying actin-induced cell shape changes using giant unilamellar vesicles and reconstituted actin networks," *Biochemical Society Transactions*, vol. 50, no. 5, pp. 1527–1539, 2022. Cited on page 81.

[310] P. Supramaniam, Z. Wang, S. Chatzimichail, C. Parperis, A. Kumar, V. Ho, O. Ces, and A. Salehi-Reyhani, "Measuring encapsulation efficiency in cell-mimicking giant unilamellar vesicles," *ACS Synthetic Biology*, 2023. Cited on page 82.

[311] L. M. Dominak, D. M. Omiatek, E. L. Gundermann, M. L. Heien, and C. D. Keating, "Polymeric crowding agents improve passive biomacromolecule encapsulation in lipid vesicles," *Langmuir*, vol. 26, no. 16, pp. 13195–13200, 2010. Cited on page 82.

[312] K. Jahnke, N. Ritzmann, J. Fichtler, A. Nitschke, Y. Dreher, T. Abele, G. Hofhaus, I. Platzman, R. R. Schröder, D. J. Müller, J. P. Spatz, and K. Göpfrich, "Proton gradients from light-harvesting e. coli control DNA assemblies for synthetic cells," *Nature Communications*, vol. 12, no. 1, p. 3967, 2021. Cited on page 86.

[313] Y. Zhou, C. K. Berry, P. A. Storer, and R. M. Raphael, "Peroxidation of polyunsaturated phosphatidyl-choline lipids during electroformation," *Biomaterials*, vol. 28, no. 6, pp. 1298–1306, 2007. Cited on page 86.

[314] M. Depierre, L. Jacquelin, and F. Niedergang, "Phagocytosis," in *Encyclopedia of Cell Biology (Second Edition)*, vol. 3, pp. 286–295, Elsevier, 2022. Cited on page 92.

[315] D. M. Underhill and H. S. Goodridge, "Information processing during phagocytosis," *Nature Reviews Immunology*, vol. 12, no. 7, pp. 492–502, 2012. Cited on page 92.

[316] D. Vorselen, Y. Wang, M. M. de Jesus, P. K. Shah, M. J. Footer, M. Huse, W. Cai, and J. A. Theriot, "Microparticle traction force microscopy reveals subcellular force exertion patterns in immune cell–target interactions," *Nature Communications*, vol. 11, no. 1, p. 20, 2020. Cited on pages 92 and 104.

[317] Q. Wang, M. Taschner, K. A. Ganzinger, C. Kelley, A. Villasenor, M. Heymann, P. Schwille, E. Lorentzen, and N. Mizuno, "Membrane association and remodeling by intraflagellar transport protein IFT172," *Nature Communications*, vol. 9, no. 1, p. 4684, 2018. Cited on pages 94, 100, and 107.

[318] L. Van de Cauter, Y. K. Jawale, D. Tam, L. Baldauf, L. v. Buren, G. H. Koenderink, M. Dogterom, and K. A. Ganzinger, "Uncovering the hidden mechanisms of giant unilamellar vesicle formation in cDICE," preprint, *bioRxiv*, 2023. Cited on page 94.

[319] J. A. Killian, I. Salemink, and D. V. Greathouse, "Induction of Nonbilayer Structures in Diacylphosphatidylcholine Model Membranes by Transmembrane R-Helical Peptides: Importance of Hydrophobic Mismatch and Proposed Role of Tryptophans," *Biochemistry*, vol. 35, no. 3, pp. 1037–1045, 1996. Cited on page 95.

[320] P. C. A. Van Der Wel, T. Pott, S. Morein, D. V. Greathouse, R. E. Koeppe, and J. A. Killian, "Tryptophan-Anchored Transmembrane Peptides Promote Formation of Nonlamellar Phases in Phosphatidylethanolamine Model Membranes in a Mismatch-Dependent Manner," *Biochemistry*, vol. 39, no. 11, pp. 3124–3133, 2000. Cited on page 95.

[321] T. M. Weiss, P. C. A. van der Wel, J. A. Killian, R. E. Koeppe, and H. W. Huang, "Hydrophobic Mismatch between Helices and Lipid Bilayers," *Biophysical Journal*, vol. 84, no. 1, pp. 379–385, 2003. Cited on page 95.

[322] M. R. R. de Planque, E. Goormaghtigh, D. V. Greathouse, R. E. Koeppe, J. A. W. Kruijtzer, R. M. J. Liskamp, B. de Kruijff, and J. A. Killian, "Sensitivity of Single Membrane-Spanning alpha-Helical Peptides to Hydrophobic Mismatch with a Lipid Bilayer: Effects on Backbone Structure, Orientation, and Extent of Membrane Incorporation," *Biochemistry*, vol. 40, no. 16, pp. 5000–5010, 2001. Cited on page 95.

[323] S. Morein, R. E. Koeppe II, G. Lindblom, B. de Kruijff, and J. Antoinette Killian, "The Effect of Peptide/Lipid Hydrophobic Mismatch on the Phase Behavior of Model Membranes Mimicking the Lipid Composition in Escherichia coli Membranes," *Biophysical Journal*, vol. 78, no. 5, pp. 2475–2485, 2000. Cited on page 95.

[324] K. A. Podolsky, T. Masubuchi, G. T. Debelouchina, E. Hui, and N. K. Devaraj, "*In Situ* Assembly of Transmembrane Proteins from Expressed and Synthetic Components in Giant Unilamellar Vesicles," *ACS Chemical Biology*, vol. 17, no. 5, pp. 1015–1021, 2022. Cited on pages 95 and 96.

[325] R. Jahn and R. H. Scheller, "SNAREs — engines for membrane fusion," *Nature Reviews Molecular Cell Biology*, vol. 7, no. 9, pp. 631–643, 2006. Cited on page 96.

[326] A. S. Lygina, K. Meyenberg, R. Jahn, and U. Diederichsen, "Transmembrane Domain Peptide/Peptide Nucleic Acid Hybrid as a Model of a SNARE Protein in Vesicle Fusion," *Angewandte Chemie International Edition*, vol. 50, no. 37, pp. 8597–8601, 2011. Cited on pages 96 and 105.

[327] D.-H. Kweon, C. S. Kim, and Y.-K. Shin, "Regulation of neuronal SNARE assembly by the membrane," *Nature Structural & Molecular Biology*, vol. 10, no. 6, pp. 440–447, 2003.

[328] D. Langosch, J. M. Crane, B. Brosig, A. Hellwig, L. K. Tamm, and J. Reed, "Peptide mimics of SNARE transmembrane segments drive membrane fusion depending on their conformational plasticity," *Journal of Molecular Biology*, vol. 311, no. 4, pp. 709–721, 2001. Cited on page 96.

[329] F. Schneider, D. Waithe, M. P. Clausen, S. Galiani, T. Koller, G. Ozhan, C. Eggeling, and E. Sezgin, "Diffusion of lipids and GPI-anchored proteins in actin-free plasma membrane vesicles measured by STED-FCS.," *Molecular biology of the cell*, vol. 28, pp. 1–22, 2017. Cited on page 97.

[330] J. M. Baskin, J. A. Prescher, S. T. Laughlin, N. J. Agard, P. V. Chang, I. A. Miller, A. Lo, J. A. Codelli, and C. R. Bertozzi, "Copper-free click chemistry for dynamic *in vivo* imaging," *Proceedings of the National Academy of Sciences*, vol. 104, no. 43, pp. 16793–16797, 2007. Cited on page 98.

[331] D. P. Nair, M. Podgórski, S. Chatani, T. Gong, W. Xi, C. R. Fenoli, and C. N. Bowman, "The Thiol-Michael Addition Click Reaction: A Powerful and Widely Used Tool in Materials Chemistry," *Chemistry of Materials*, vol. 26, no. 1, pp. 724–744, 2014. Cited on page 98.

[332] C. S. Theile, M. D. Witte, A. E. M. Blom, L. Kundrat, H. L. Ploegh, and C. P. Guimaraes, "Site-specific N-terminal labeling of proteins using sortase-mediated reactions," *Nature Protocols*, vol. 8, no. 9, pp. 1800–1807, 2013. Cited on pages 98 and 107.

[333] G. S. Fiorini and D. T. Chiu, "Disposable microfluidic devices: fabrication, function, and application," *BioTechniques*, vol. 38, no. 3, pp. 429–446, 2005. Cited on page 100.

[334] D. J. Beebe, G. A. Mensing, and G. M. Walker, "Physics and Applications of Microfluidics in Biology," *Annual Review of Biomedical Engineering*, vol. 4, no. 1, pp. 261–286, 2002. Cited on page 100.

[335] Y. Xia, J. J. McClelland, R. Gupta, D. Qin, X.-M. Zhao, L. L. Sohn, R. J. Celotta, and G. M. Whitesides, "Replica molding using polymeric materials: A practical step toward nanomanufacturing," *Advanced Materials*, vol. 9, no. 2, pp. 147–149, 1997. Cited on page 100.

[336] R. Dimova, "Recent developments in the field of bending rigidity measurements on membranes," *Advances in Colloid and Interface Science*, vol. 208, pp. 225–234, 2014. Cited on page 101.

[337] M. Heinrich, A. Tian, C. Esposito, and T. Baumgart, "Dynamic sorting of lipids and proteins in membrane tubes with a moving phase boundary," *Proceedings of the National Academy of Sciences*, vol. 107, no. 16, pp. 7208–7213, 2010. Cited on page 102.

[338] P. Ramesh, Y. F. Baroji, S. N. S. Reihani, D. Stamou, L. B. Oddershede, and P. M. Bendix, "FBAR Syndapin 1 recognizes and stabilizes highly curved tubular membranes in a concentration dependent manner," *Scientific Reports*, vol. 3, no. 1, p. 1565, 2013.

[339] A. K. Cada, M. R. Pavlin, J. P. Castillo, A. B. Tong, K. P. Larsen, X. Ren, A. L. Yokom, F.-C. Tsai, J. V. Shiah, P. M. Bassereau, C. J. Bustamante, and J. H. Hurley, "Friction-driven membrane scission by the human ESCRT-III proteins CHMP1B and IST1," *Proceedings of the National Academy of Sciences*, vol. 119, no. 29, p. e2204536119, 2022. Cited on page 102.

[340] S. Aimon, A. Callan-Jones, A. Berthaud, M. Pinot, G. E. S. Toombes, and P. Bassereau, "Membrane Shape Modulates Transmembrane Protein Distribution," *Developmental Cell*, vol. 28, no. 2, pp. 212–218, 2014. Cited on page 102.

[341] B.-M. Chen, T.-L. Cheng, and S. R. Roffler, "Polyethylene Glycol Immunogenicity: Theoretical, Clinical, and Practical Aspects of Anti-Polyethylene Glycol Antibodies," *ACS Nano*, vol. 15, no. 9, pp. 14022–14048, 2021. Cited on page 102.

[342] A. Tian and T. Baumgart, "Sorting of Lipids and Proteins in Membrane Curvature Gradients," *Biophysical Journal*, vol. 96, no. 7, pp. 2676–2688, 2009. Cited on page 102.

[343] C. A. de Oliveira and B. Mantovani, "Latrunculin A is a potent inhibitor of phagocytosis by macrophages," *Life Sciences*, vol. 43, no. 22, pp. 1825–1830, 1988. Cited on page 104.

[344] C. van der Wel, A. Vahid, A. Šarić, T. Idema, D. Heinrich, and D. J. Kraft, "Lipid membrane-mediated attraction between curvature inducing objects," *Scientific Reports*, vol. 6, no. 1, p. 32825, 2016. Cited on page 104.

[345] A. Azadbakht, B. Meadowcroft, T. Varkevisser, A. Šarić, and D. J. Kraft, "Wrapping Pathways of Anisotropic Dumbbell Particles by Giant Unilamellar Vesicles," *Nano Letters*, vol. 23, no. 10, pp. 4267–4273, 2023. Cited on page 104.

[346] N. Araki, T. Hatae, A. Furukawa, and J. A. Swanson, "Phosphoinositide-3-kinase-independent contractile activities associated with Fcgamma-receptor-mediated phagocytosis and macropinocytosis in macrophages," *Journal of Cell Science*, vol. 116, no. Pt 2, pp. 247–257, 2003. Cited on page 104.

[347] B. Chen, Z. Wu, M. Tian, T. Feng, C. Yuanwei, and X. Luo, "Effect of surface morphology change of polystyrene microspheres through etching on protein corona and phagocytic uptake," *Journal of Biomaterials Science, Polymer Edition*, vol. 31, no. 18, pp. 2381–2395, 2020. Cited on page 104.

[348] J. Agudo-Canalejo and R. Lipowsky, "Adhesive Nanoparticles as Local Probes of Membrane Curvature," *Nano Letters*, vol. 15, no. 10, pp. 7168–7173, 2015. Cited on page 104.

[349] D. Paul, S. Achouri, Y.-Z. Yoon, J. Herre, C. E. Bryant, and P. Cicuta, "Phagocytosis Dynamics Depends on Target Shape," *Biophysical Journal*, vol. 105, no. 5, pp. 1143–1150, 2013. Cited on page 104.

[350] D. Vorselen, S. R. Barger, Y. Wang, W. Cai, J. A. Theriot, N. C. Gauthier, and M. Krendel, "Phagocytic 'teeth' and myosin-II 'jaw' power target constriction during phagocytosis," *eLife*, vol. 10, p. e68627, 2021. Cited on page 104.

[351] R. Lopes dos Santos, M. Malo, and C. Campillo, "Spatial Control of Arp2/3-Induced Actin Polymerization on Phase-Separated Giant Unilamellar Vesicles," *ACS Synthetic Biology*, vol. 12, no. 11, pp. 3267–3274, 2023. Cited on page 104.

[352] S. Razavi, F. Wong, B. Abubaker-Sharif, H. T. Matsubayashi, H. Nakamura, E. Sandoval, D. N. Robinson, B. Chen, J. Liu, P. A. Iglesias, and T. Inoue, "Synthetic control of actin polymerization and symmetry breaking in active protocells," preprint, *bioRxiv*, 2023. Cited on page 104.

[353] A. B. Søgaard, A. B. Pedersen, K. B. Løvschall, P. Monge, J. H. Jakobsen, L. Džabbarova, L. F. Nielsen, S. Stevanovic, R. Walther, and A. N. Zelikin, "Transmembrane signaling by a synthetic receptor in artificial cells," *Nature Communications*, vol. 14, no. 1, p. 1646, 2023. Cited on page 104.

[354] D. G. Andersen, A. B. Pedersen, M. H. Jørgensen, M. C. Montasell, A. B. Søgaard, G. Chen, A. Schroeder, G. R. Andersen, and A. N. Zelikin, "Chemical Zymogens and Transmembrane Activation of Transcription in Synthetic Cells," *Advanced Materials*, p. 2309385, 2023. Cited on page 104.

[355] K. Jahnke, M. Illig, M. Scheffold, M. P. Tran, U. Mersdorf, and K. Göpfrich, "DNA Origami Signaling Units Transduce Chemical and Mechanical Signals in Synthetic Cells," *Advanced Functional Materials*, p. 2301176, 2023. Cited on page 104.

[356] A. J. García-Sáez, D. C. Carrer, and P. Schwille, "Fluorescence Correlation Spectroscopy for the Study of Membrane Dynamics and Organization in Giant Unilamellar Vesicles," in *Liposomes: Methods and Protocols, Volume 2: Biological Membrane Models* (V. Weissig, ed.), Methods in Molecular Biology™, pp. 493–508, Totowa, NJ: Humana Press, 2010. Cited on page 105.

[357] L. Freiburger, M. Sonntag, J. Hennig, J. Li, P. Zou, and M. Sattler, "Efficient segmental isotope labeling of multi-domain proteins using Sortase A," *Journal of Biomolecular NMR*, vol. 63, no. 1, pp. 1–8, 2015. Cited on page 107.

[358] K. Y. Wan, "Life through the fluid dynamics lens," *Nature Physics*, vol. 19, no. 12, pp. 1744–1745, 2023. Cited on page 114.

[359] T. Sanchis, "Strategies for multidisciplinary research," *Nature Physics*, vol. 19, no. 12, pp. 1736–1737, 2023. Cited on page 114.

[360] E. K. Paluch, "After the Greeting: Realizing the Potential of Physical Models in Cell Biology," *Trends in Cell Biology*, vol. 25, no. 12, pp. 711–713, 2015.

[361] X. Trepat and R. Alert, "How to bridge the gap between theory and experiments in biological physics," *Nature Physics*, vol. 19, no. 12, pp. 1738–1739, 2023. Cited on page 114.

Part v

Appendix

Curriculum Vitæ

Lori Van de Cauter

04 – 10 – 1996 born in Leuven, Belgium

Education

2014 – 2017 Bachelor of Science in Biochemistry and Biotechnology
University of Leuven, Belgium

2017 – 2019 Master of Science in Biochemistry and Biotechnology
University of Leuven, Belgium

2019 – 2024 PhD in biophysics
AMOLF, The Netherlands
Delft University of Technology, The Netherlands

List of Publications

Related to this thesis

- L. Van de Cauter, Y. K. Jawale, D. Tam, L. Baldauf, L. van Buren, G. H. Koenderink, M. Dogterom, and K. A. Ganzinger, "High-speed imaging of giant unilamellar vesicle formation in cDICE", preprint, *bioRxiv*, 2023. (*currently under review at ACS Omega*)
- L. Van de Cauter, L. van Buren, G. H. Koenderink, and K. A. Ganzinger, "Exploring Giant Unilamellar Vesicle Production for Artificial Cells - Current Challenges and Future Directions", *Small Methods*, vol. 7, no. 12, 2300416, 2023.
- L. Van de Cauter, F. Fanalista, L. van Buren, N. De Franceschi, E. Godino, S. Bouw, C. Danelon, C. Dekker, G. H. Koenderink, and K. A. Ganzinger, "Optimized cDICE for Efficient Reconstitution of Biological Systems in Giant Unilamellar Vesicles", *ACS Synthetic Biology*, vol. 10, no. 7, pp. 1690–1702, 2021.

Other publications

- G. Wackers, T. Putzeys, M. Peeters, L. Van de Cauter, P. Cornelis, M. Wübbenhorst, J. Tack, F. Troost, N. Verhaert, T. Doll, and P. Wagner, "Towards a catheter-based impedimetric sensor for the assessment of intestinal histamine levels in IBS patients", *Biosensors and Bioelectronics*, vol. 158, 112152, 2020.